

AD-A248 942



PL-TR-91-2252

DTIC
S **ELECTE** **D**
c
APR 4 1992

(2)

**THE INTERPLANETARY HEAVY ION ENVIRONMENT FOR BOTH
GALACTIC COSMIC RAYS AND SOLAR ENERGETIC PARTICLES
DURING THE CRRES MISSION**

John P. Wefel
T. Gregory Guzik

Louisiana State University
Nicholson Hall
Baton Rouge, LA 70803-4001

18 October 1991

Scientific Report No. 1

APPROVED FOR PUBLIC RELEASE; DISTRIBUTION UNLIMITED



**PHILLIPS LABORATORY
AIR FORCE SYSTEMS COMMAND
HANSCOM AIR FORCE BASE, MASSACHUSETTS 01731-5000**

92-09503

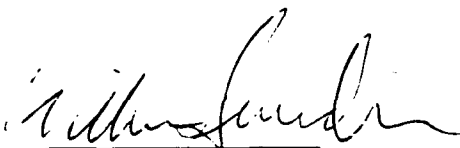


92 4 13 077

"This technical report has been reviewed and is approved for publication"


KEVIN P. RAY, LT, USAF
Contract Manager


E. G. MULLEN
Branch Chief


WILLIAM SWIDER
Deputy Director

This document has been reviewed by the ESD Public Affairs Office (PA) and is releasable to the National Technical Information Service (NTIS).

Qualified requestors may obtain additional copies from the Defense Technical Information Center. All others should apply to the National Technical Information Service.

If your address has changed, or if you wish to be removed from the mailing list, or if the addressee is no longer employed by your organization, please notify PL/TSI, Hanscom AFB, MA 01731. This will assist us in maintaining a current mailing list.

Do not return copies of this report unless contractual obligations or notices on a specific document requires that it be returned.

REPORT DOCUMENTATION PAGE			Form Approved OMB No. 0704-0188	
<small>Public reporting burden for this collection of information is estimated to average 1 hour per response, including the time for reviewing instructions, searching existing data sources, gathering and maintaining the data needed, and completing and reviewing the collection of information. Send comments regarding this burden estimate or any other aspect of this collection of information, including suggestions for reducing this burden, to Washington Headquarters Service, Directorate for Information Operations and Reports, 1215 Jefferson Davis Highway, Suite 1204, Arlington, VA 22202-4302, and to the Office of Management and Budget, Paperwork Reduction Project (0704-0188), Washington, DC 20503.</small>				
1. AGENCY USE ONLY (leave blank)		2. REPORT DATE 18 October 1991		3. REPORT TYPE AND DATES COVERED Scientific Report No. 1
4. TITLE AND SUBTITLE The Interplanetary Heavy Ion Environment for Both Galactic Cosmic Rays and Solar Energetic Particles During the CRRES Mission			5. FUNDING NUMBERS PE 621(1F) PR 7601 TA 22 WU LS Contract F19628-90-K-0026	
6. AUTHOR(S) John P. Wefel T. Gregory Guzik				
7. PERFORMING ORGANIZATION NAME(S) AND ADDRESS(ES) Louisiana State University Nicholson Hall Baton Rouge, LA 70803-4001			8. PERFORMING ORGANIZATION REPORT NUMBER	
9. SPONSORING / MONITORING AGENCY NAME(S) AND ADDRESS(ES) Phillips Laboratory Hanscom AFB, MA 01731-5000 Contract Manager: Lt Kevin Ray/PHP			10. SPONSORING / MONITORING AGENCY REPORT NUMBER PL-TR-91-2252	
11. SUPPLEMENTARY NOTES				
12a. DISTRIBUTION / AVAILABILITY STATEMENT Approved for public release; Distribution unlimited			12b. DISTRIBUTION CODE	
13. ABSTRACT (Maximum 200 words) A calculational model of the Interplanetary Heavy Ion Environment is being developed for the CRRES mission to include both galactic cosmic rays (GCR) and solar energetic particles (SEP). Data from the ONR-604 experiment on CRRES plus results from other experiments/spacecraft are being combined to evaluate the heavy ion radiation environment in near-Earth space in the 1990-1991 epoch. The modeling effort is described along with the operation and performance of the ONR-604 experiment, including prelaunch accelerator calibrations and on-orbit response. The status of the data system development for this effort is summarized, along with its use for the initial analysis of the data and the modeling effort. The preliminary "working" environment for the period 9/1/90-2/28/91 is characterized by a high level of solar modulation and correspondingly low flux of GCR and no significant component from SEP's. Both particle flux and LET spectra have been calculated. The limitations and uncertainties inherent in this "working" model are presented, along with the effort to be undertaken to understand and reduce the uncertainties.				
14. SUBJECT TERMS Radiation effects Space radiation environment Cosmic rays		15. NUMBER OF PAGES 90		16. PRICE CODE
17. SECURITY CLASSIFICATION OF REPORT Unclassified	18. SECURITY CLASSIFICATION OF THIS PAGE Unclassified	19. SECURITY CLASSIFICATION OF ABSTRACT Unclassified	20. LIMITATION OF ABSTRACT SAR	

CONTENTS

List of Figures.....	iv
List of Tables.....	viii
1. INTRODUCTION.....	1
2. THE "HEAVY ION MODEL" PROJECT.....	2
a. Rationale.....	2
b. Technique.....	3
c. Heavy Ion Components.....	4
i. Galactic Cosmic Rays.....	4
ii. Solar Energetic Particles.....	8
iii. The Anomalous Component.....	10
d. Distribution of Effort.....	11
3. THE ONR-604 EXPERIMENT.....	13
a. Instrument Description and Operation.....	13
b. Pre-launch Calibration.....	19
c. Launch and On-Orbit Checkout.....	35
d. Post-Launch Performance.....	40
4. DATA SYSTEM DEVELOPMENT.....	42
a. Reduction and Processing.....	44
b. Ancillary Databases.....	47
5. THE HEAVY ION ENVIRONMENT IN LATE 1990-EARLY 1991.....	49
a. Overview.....	49
b. Solar Modulation.....	55
c. Galactic Cosmic Rays.....	61
d. Preliminary Predictions.....	69
6. SUMMARY.....	72
7. BIBLIOGRAPHY.....	78



Accession For	
NTIS GRA&I	<input checked="" type="checkbox"/>
DTIC TAB	<input type="checkbox"/>
Unannounced	<input type="checkbox"/>
Justification	
By	
Distribution/	
Availability Codes	
Dist	Avail and/or Special
A-1	

LIST OF FIGURES

Figure 1.	Relative event rates for GCR Heavy Ions at solar minimum. The lines connect the different isotopes of the elements.	5
Figure 2.	Measured energy spectra for C, O, Ne, Mg and Si from IMP-8.	5
Figure 3.	Compiled data for the energy spectra of the elements Hydrogen, Helium, Carbon and Iron in the galactic cosmic rays. (See Simpson, 1983 for references to the data points.)	7
Figure 4:	Differential energy spectra for cosmic-ray protons (left) and helium nuclei (right) measured in 1987 (filled circles for LEAP, open circles for IMP 8) along with the previous balloon measurements (see Seo et al., 1991 for references to the data). The dashed curves represent the local interstellar and modulated spectra with different amounts of modulation indicated by the parameter ϕ : (a) local interstellar spectra (no modulation); (b) $\phi = 200$ MV; (c) $\phi = 400$ MV; (d) $\phi = 500$ MV; (e) $\phi = 600$ MV; (f) $\phi = 800$ MV; (g) $\phi = 1000$ MV.	8
Figure 5:	Solar flare energy spectra.	9
Figure 6:	GCR energy spectra showing the presence of anomalous Nitrogen and Oxygen at low energies.	10
Figure 7:	Data flow for the modeling effort.	12
Figure 8:	The ONR-604 Telescope and its Position Sensing Detectors.	14
Figure 9.	ONR-604 energy ranges for selected isotopes.	16
Figure 10a:	ONR-604 Priority Counting Rates and Command State.	20
Figure 10b:	ONR-604 Singles Counting Rates.	21
Figure 10c:	ONR-604 Coincidence Counting Rates, D1-D5.	22
Figure 10d:	ONR-604 Coincidence Counting Rates, K1-K4.	23
Figure 10e:	ONR-604 Coincidence Counting Rates, K5-A.	24

Figure 11:	Raw Fe and Ne calibration data from the Bevalac25 showing the intensity variations with energy.
Figure 12:	Accelerator calibration data from Iron (top), Neon27 (center) and Helium (bottom) runs.
Figure 13:	Bevalac Neon data showing all events (top) and priority28 2+3 events only (bottom). A stopping radius cut has been applied to the data.
Figure 14:	Iron + Neon data in K1 vs K2-8. The lower plot shows29 only P1 events.
Figure 15:	D1 + D2 versus D3-K8 for Helium events showing the31 effects of the normal mode command (top) and the P2-P3 division (bottom).
Figure 16:	D1-D6 versus K1-K8 matrix for Iron beam events with32 NO source (top) and WITH source (bottom).
Figure 17:	K1 versus K2-K8 matrix for Iron beam events with NO33 source (top) and WITH source (bottom).
Figure 18:	Charge histograms for events observed in iron runs with34 NO source (top) and WITH source (bottom).
Figure 19:	Energy deposits in D1 (top), D2 (middle) and D3 (bottom)36 versus K1-K8 for iron events taken WITH the radioactive source.
Figure 20:	GSE Run 530, IFC Run at CSTC. Deviations of the points37 for each amplifier from a straight line as a function of calibration step.
Figure 21:	One of the first full orbits of data from ONR-604. Plotted38 is the P3 counting rate versus the Vehicle Time Code Word (VTCW) for the Apogee and Perigee portions of the orbit (GSE Run 515).
Figure 22:	P3 and P2 rates versus VTCW for a full orbit of ONR-60439 data in proton mode (GSE Run 521).
Figure 23:	Expanded plot of the P3 and D2 counting rates for an outer belt41 pass approaching Apogee (GSE Run 508) showing the spin modulation in the rates.

Figure 24.	Comparison of the K1 versus K2-K8 matrix for P1 events43 from flight data (top) and accelerator calibration data (bottom).
Figure 25.	Data Flow through the current LSU Processing System.45
Figure 26.	Auxillary databases established as part of the modeling effort.48
Figure 27.	Four solar cycles of neutron monitor data from Climax50 (courtesy University of Chicago) and McMurdo (courtesy Bartol Research Institute) are shown on top. An Expansion of the latter half of 1990 and the first part of 1991 is given in the bottom plot.
Figure 28.	Comparison of ONR-604 CRRES rates with GOES and51 neutron monitor data.
Figure 29.	IMP-8 quiet time (clear areas) determined from six different52 channels.
Figure 30.	The number of P1 events as a function of orbit number (top)53 and the L distribution of P1 events (bottom).
Figure 31.	Charge distribution (top) and energy <u>vs</u> charge plot (bottom)54 for P1 events.
Figure 32.	The modulation parameter Φ (MV) for 1974-1980 determined57 by Evenson et al. (1983) from the flux of 70-95 MeV/nucleon Helium compared to the Climax Neutron Monitor rate.
Figure 33.	Energy dependent geometry factors for Ne and Fe events (left)58 and the geomagnetic transmission function (right).
Figure 34.	Calculated priority counting rates for ONR-604 (left) and60 comparison of the calculations to the data (right).
Figure 35.	Oxygen energy spectra from IMP-8 for different time periods 62 (top) and modulation fits to the IMP=8 data for 1978 and 1990-91 (bottom).
Figure 36.	Comparison of calculated P1, P1* and P2* rates for different63 local interstellar spectra.
Figure 37.	Measurements of GCR He, C and Fe flux from the baseline65 database along with predictions (solid curve) of the initial GCR Model.

Figure 38.	Measurements of B/C with Model predictions using67 different PLDs.
Figure 39.	Measurements of Sub-Fe/Fe with Model predictions67 using different PLDs (see text).
Figure 40.	Spectra predicted by the GCR Model for different PLDs68 (see text).
Figure 41.	Predicted energy spectra for GCR nuclei H, He, O and Fe70 for the late '90-early '91 time period.
Figure 42.	Integral number of particles with LET greater than threshold,71 LO, as a function of LO. The curves are labeled with the thickness of Aluminum shielding (in mils) assumed in the calculation.

LIST OF TABLES

Table 1:	ONR-604 Counting Rates.....	18
Table 2:	Calculated galactic cosmic ray spectra for $Z = 1$ to 28 and $E = 50$ to over 60,000 MeV/nucleon.	74
Table 3:	Integral LET spectra for aluminum shields of thickness ranging from 50 mils to 1600 mils of aluminum.	77

1. INTRODUCTION

Air Force Contract F19628-90-K-0026 was established June 29, 1990 at Louisiana State University to support work leading to a model of the heavy ion environment encountered by the CRRES (Combined Release and Radiation Effects Satellite) spacecraft. Such a model is needed to support the Microelectronics Package data analysis and to understand, quantitatively, the effects of the near-Earth space environment on electronic devices. The overall effort involves work by three laboratories; The University of Chicago (J. A. Simpson and M. Garcia-Munoz, lead investigators), The Lockheed Palo Alto Research Laboratory (D. L. Chenette, lead investigator) and Louisiana State University (J. P. Wefel and T. G. Guzik, lead investigators). The principal source of data on high energy, heavy ions on-board CRRES is The University of Chicago Experiment, ONR-604, (J. A. Simpson, PI; M. Garcia-Munoz and J. P. Wefel, Co-I's) which was designed specifically to measure the charge, mass and energy of particles from Hydrogen through Nickel that come to rest in the instrument. Other sensors on CRRES provide detailed measurements of protons and electrons.

The overall goal of this effort is to provide a numerical model of the high energy (≥ 10 MeV/nucleon) interplanetary heavy ion environment, which is operationally interchangeable with the existing, widely-used computer model CREME (see Adams et al., 1981; 1982). This new model will be updated periodically using data from the charged particle sensors on the CRRES satellite. The effort involves (a) modifications to existing computer codes to include time dependent parameters that can be adjusted to reproduce the measured data, (b) timely processing, reduction and analysis of the data, including uncertainty estimates, from selected CRRES sensors, (c) comparison of the experimental results to the model predictions and adjustment of the model parameters and (d) preparation and dissemination of periodic reports giving the analysis results and the refined model parameters to the user community.

This approach to the assessment of the heavy ion environment provides both consistency in technique for the user groups, especially during the analyses of the CRRES Microelectronics data, and current, accurate information on the heavy ion environment deduced from instruments on-board the same spacecraft, which will be consistent with the accumulated body of experimental data on interplanetary heavy ions.

The project, "The Interplanetary Heavy Ion Environment for both Galactic Cosmic Rays and Solar Energetic Particles during the CRRES Mission," is a multi-year effort. This Technical Progress Report covers the first 15 months of effort, ~1 July 90 - 30 September 91. The first model release is now scheduled for Fall, 1991 in the mid-November to early December time-frame.

2. THE "HEAVY ION MODEL" PROJECT

a. Rationale

The heavy ion radiation environment encountered in near-Earth space consists of three major components: (a) galactic cosmic rays (GCR), (b) solar energetic particles (SEP), and (c) trapped magnetospheric particles. The first two of these arrive at the earth from outside our immediate geospace environment and are termed "interplanetary" while the last resides within the Earth's magnetosphere, and is termed a "local" component. The interplanetary particles encompass a wide range in both energy ($E > 500$ keV) and charge ($1 \leq Z \leq 92$). Some of these particles penetrate the Earth's magnetic field and form part of the radiation environment in which spacecraft must operate.

For electronic components located within a spacecraft, there is a large radiation dose (depending upon the actual orbit) contributed by protons and electrons plus radiation effects due to the heavy ion component. This latter is particularly important because of the ability of a single heavy nucleus to affect ("upset") microelectronic circuitry (Binder et al., 1975) particularly low power memory chips (Kolasinski, et al., 1979). Even though the relative abundance of heavy ions is small, compared to protons, the heavy ion efficiency is high since the effects are caused directly by the passage of the particle through the device. The major concern for the future lies in the decreasing feature size of the electronic systems being designed or proposed, since as the feature size decreases, the sensitivity of these systems to disruption by individual particles increases (see, for example Iverson, 1979).

An important objective of the CRRES program is to investigate the effects of the space radiation environment on the modern microelectronic components that will be used in future spacecraft. One of these effects is the ability of single, intensely-ionizing particles to upset the logical state of a single bit in a digital microcircuit, causing a single event upset (SEU). The MicroElectronics Package (MEP) onboard the CRRES satellite is measuring SEU rates in a large sample of digital components.

The data from the CRRES particle sensors provides simultaneous measurements to characterize the environment being sampled by the engineering experiments. However, detailed characterization requires significant amounts of analysis effort and extended periods of time, thereby affecting the ability of the engineering experiments to complete their analysis schedule. An accurate model of the heavy ion radiation environment is required for the analysis of the single-event upset data from the CRRES Microelectronics Package and to support the other engineering experiments on the CRRES mission. Of longer range concern is the ability of ground testing and calculations to predict, accurately, the effects of the space radiation environment on satellite systems and instrumentation. One of the important goals of the MEP program is to develop such methods for spacecraft electronic systems. An essential part of such calculations is an accurate model of the

space radiation environment that is responsible for the SEU's, particularly the heavy ion component. Thus, the predictive model being developed under this contract will retain its usefulness long after the CRRES mission is completed.

b. Technique

A computer model of the Interplanetary Heavy Ion Radiation Environment, calibrated and adjusted with the actual CRRES flight data from a number of different particle sensors, which is updated at regular intervals throughout the CRRES mission lifetime, can provide the data needed for the interpretation of the CRRES Engineering experiments, particularly the Microelectronics package, while maintaining faithfulness to the actual conditions encountered by the CRRES spacecraft. The model under development is an analytic description of the flux of each ion species as a function of energy and time. It will include the two major sources of heavy ion flux in the interplanetary medium: galactic cosmic rays and solar energetic particles. The model will cover the energy range above ~10 MeV/nucleon and will describe all elements including estimates for those elements that are not well measured. Once developed, the model will have a minimum number of parameters needed to describe the overall environment. To keep the model accurate and to insure that time variations do not become large, periodic updates, approximately semi-annually throughout the CRRES mission will be issued. These updates will be keyed to the model parameters and will provide the information necessary for a user to update his calculations for the particular period under consideration. Following termination of the CRRES mission, a final model release may be made along with the techniques necessary to utilize and update the model software for future time periods. Such a new predictive model will supplement the products of the Microelectronics test package, so as to produce a standard method of estimating SEU rates for future space missions.

It might, at first, seem best to employ the measurements from the particle sensors on CRRES directly to determine the radiation environment. This is not practical for several reasons: (1) the total flux of particles is so low that accurate measurements of all particle species will take a long time to accumulate; (2) a thorough analysis of the data to determine accurate abundances of each individual element will be time-consuming; (3) the CRRES sensors can only measure about half of the integral flux during quiet periods because they do not measure all of the highest energy particles; and most importantly, (4) the scientific research in cosmic ray physics over the past 30 years has established, accurately, relative abundances and energy spectra for most of the elements. The best GCR model should take full advantage of this accumulated knowledge and use contemporary measurements most efficiently to accurately define the cosmic ray intensities over the energy ranges where temporal variations are large and not easily predicted in detail.

For these reasons, a different approach, is undertaken, namely a description based on the well-established physical principles of propagation and solar modulation that control and determine the time- and energy-dependent GCR

intensity at earth. This model will incorporate observations obtained over the past several decades of space research. Even when complete, the CRRES particle sensor datasets are unlikely to be a significant improvement over the existing GCR database in terms of composition, characteristics of energy spectra, or range of intensity variation. Thus, the CRRES particle data sets will not provide information that would change the known qualitative features of the interplanetary high energy heavy ion environment model, but are of crucial importance in obtaining quantitative agreement between the model and the exact conditions during the period of the CRRES mission.

Quantitative values of parameters in any heavy ion computer model have a significant range of variation with time. These variations are dominated by solar phenomena and the changing levels of solar activity. While the solar cycle period and phase are known, active solar processes are sufficiently random that short term effects cannot be accurately predicted in advance. CRRES data will be analyzed on, at least, monthly time scales and will be subject to such fluctuations. In addition, for a 3-5 year mission, CRRES should sample conditions from solar maximum through solar minimum, and a viable model must be able to describe the full range of solar cycle conditions. Precise values for the parameters of the model must depend upon contemporary measurements of the heavy ion environment. Particle flux measurements from sensors aboard CRRES are thus required to normalize the model as well as to describe the conditions following solar energetic particle (SEP) events. The most accurate and effective way to merge the CRRES particle sensor datasets with the environment model will be to use the data to define key parameters of the model. For the galactic cosmic ray (GCR) component these key parameters will describe the level of solar modulation and presence of any "anomalous" components. For the solar flare component these key parameters will define the occurrence of the flare, its peak flux, total fluence, composition characteristics, and the form of its energy spectrum.

c. Heavy Ion Components

The model will provide a description of the flux of each ion species as a function of energy and time, focusing on the two major sources of heavy ions, GCR and SEP. The model addresses the energy range above ~10 MeV/nucleon and will describe all elements, including estimates for the rare species that are not well measured.

i. Galactic Cosmic Rays

Figure 1 shows the relative event rate for each of the elements $Z > 2$ in the galactic cosmic rays, with the points connected by lines within each element giving the relative abundance of the isotopes of that element. The point to note here is that the heavy ion flux is dominated by the major species, C, O, Ne, Mg, Si, Fe, but the other elements, taken together, still constitute a significant part of the total flux. The analysis of CRRES particle

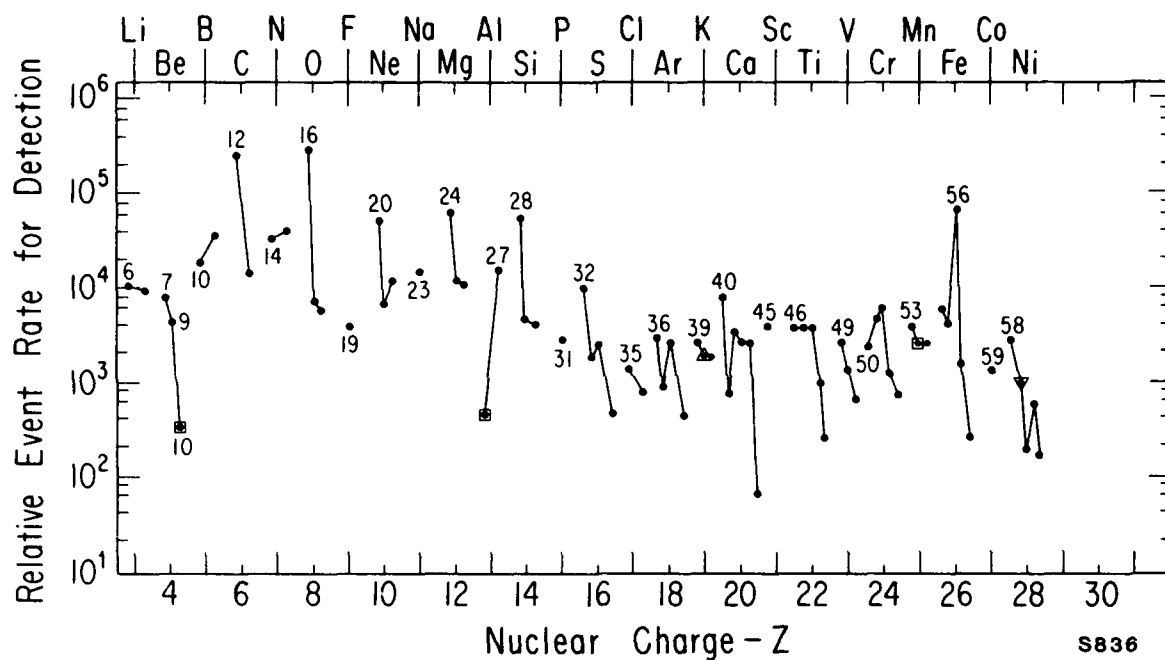


Figure 1. Relative event rates for GCR Heavy Ions at solar minimum. The lines connect the different isotopes of the elements.

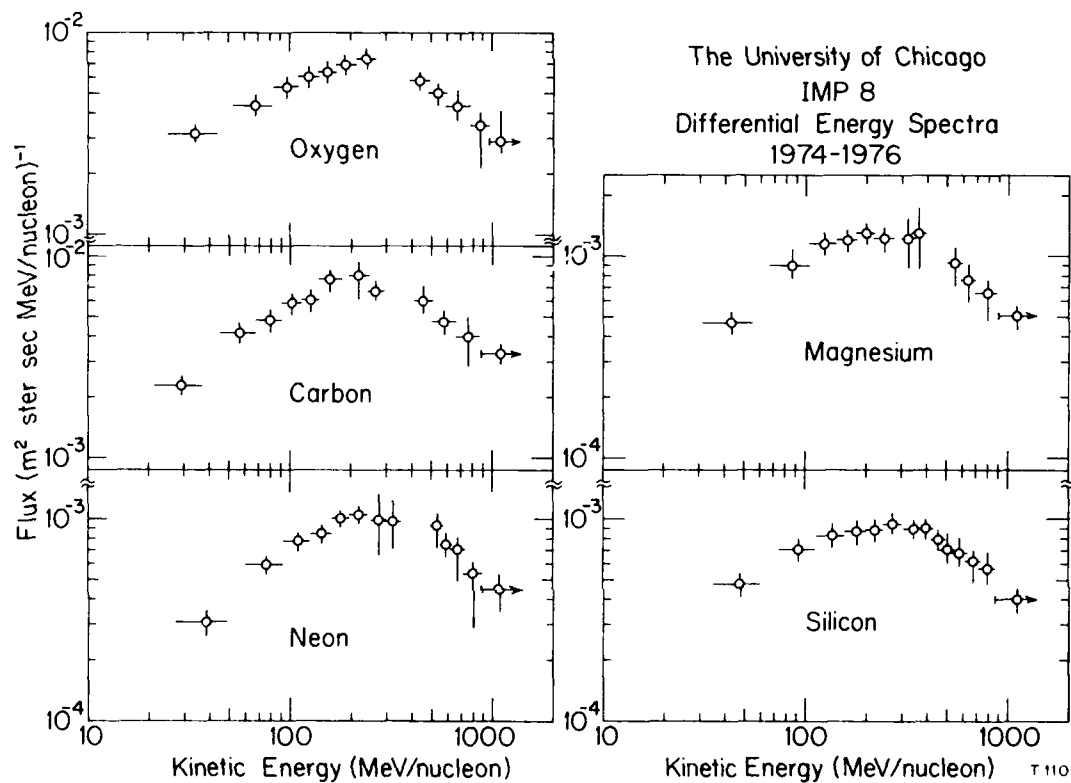


Figure 2. Measured energy spectra for C, O, Ne, Mg and Si from IMP-8.

sensor data will focus, initially, on the most abundant species (H, He, C, O, Ne, Si, Ca, and Fe). The data reduction efforts will produce fluxes for each of these in energy intervals as appropriate and convenient for each of the sensors, with attention paid to instrument calibrations and backgrounds in order to obtain accurate flux normalizations.

Figure 2 shows an example of measured GCR heavy ion spectra for the major species, C, O, Ne, Mg, Si from below 100 MeV/nucleon to about 1 GeV/nucleon taken at solar minimum modulation conditions (Garcia-Munoz et al., 1977). The spectra peak at several hundred MeV/nucleon and fall off on both the higher and lower energy sides due to the nature of the energy (rigidity) spectrum and, at low energies, the effect of solar modulation. The basic shape of the individual element spectra are similar, however, the shape of the spectra do vary with the level of solar modulation.

The cosmic rays diffuse into the Heliosphere against the outward flowing solar wind. In this solar modulation process, the cosmic rays lose energy to the expanding field (adiabatic deceleration) and their energy spectra are modified. Thus, the spectra observed at Earth are not the same as the spectra outside the Heliosphere in local interstellar space (LIS). In addition, the observed spectra vary with time as conditions change within the Heliosphere. The time scales for significant changes in the intensities of the GCR flux are typically months. Thus a model of the galactic cosmic ray component can be kept accurate and up-to-date with only periodic changes to its parameters. (Solar modulation is described in more detail in a subsequent section.)

Figure 3 shows a compilation of data (Simpson, 1983) for the energy spectra of Hydrogen, Helium, Carbon and Iron. Above 1-10 GeV/nucleon (depending upon the element), the spectra are power laws. Below these energies the spectral shape varies with the modulation level. The CRRES sensors measure below ~1 GeV/nucleon, and, therefore, the flux for the highest energy particles must be calculated from the "known" characteristics of the spectra.

Figure 4 shows a set of recent measurements (1987) on the spectra of protons and helium nuclei (Seo et al., 1991). The dashed curves show the results of calculations for different levels of solar modulation, which demonstrate the degree of variability introduced into the spectra by changing Heliospheric conditions. In all of the calculations, the assumed spectra in Local Interstellar Space remained constant.

Thus, predicting the intensity of GCR's at Earth requires knowledge of

- The Local Interstellar Spectra for each element
- The level of solar modulation applicable to the time period under consideration.

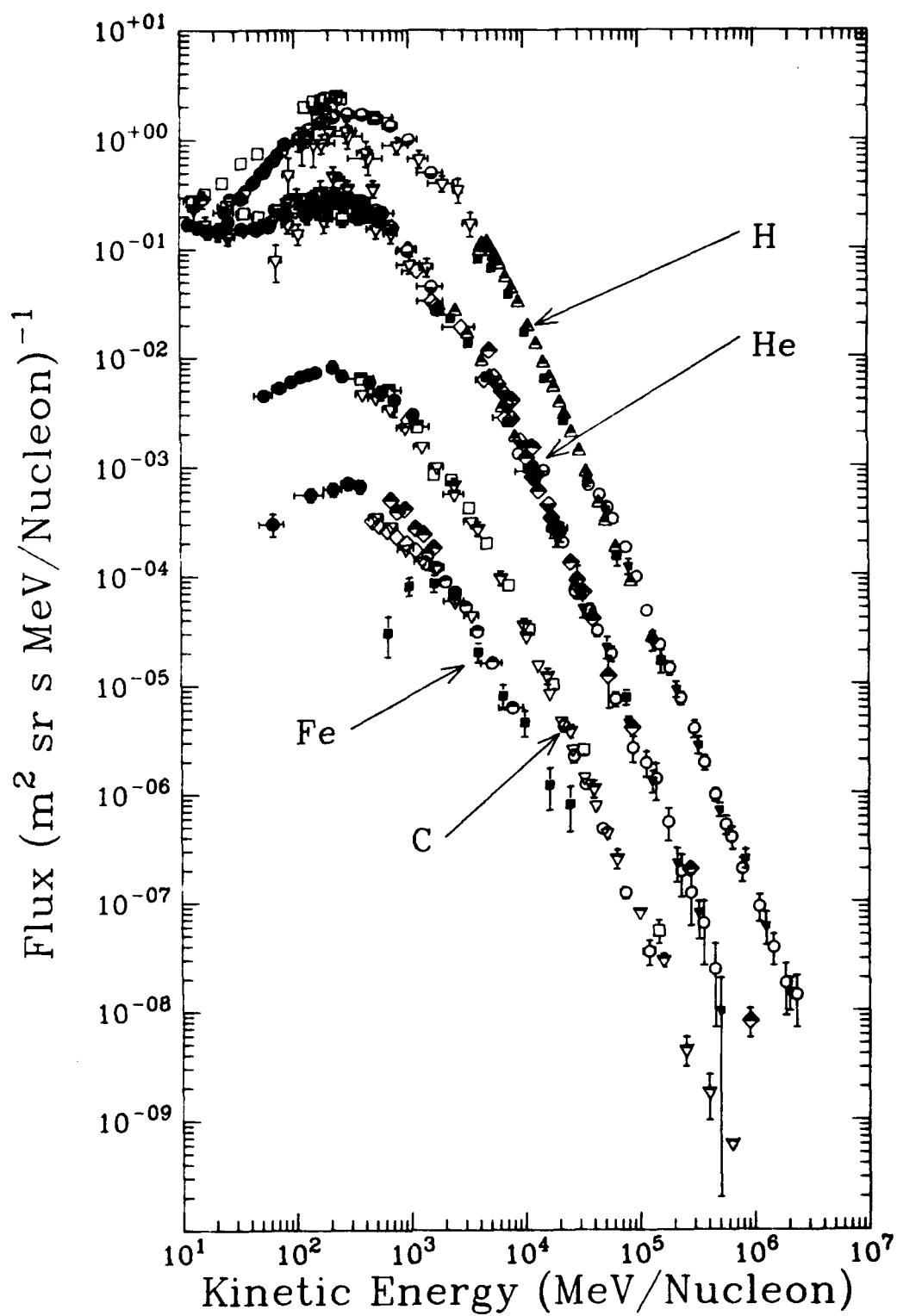


Figure 3. Compiled data for the energy spectra of the elements Hydrogen, Helium, Carbon and Iron in the galactic cosmic rays. (See Simpson, 1983 for references to the data points.)

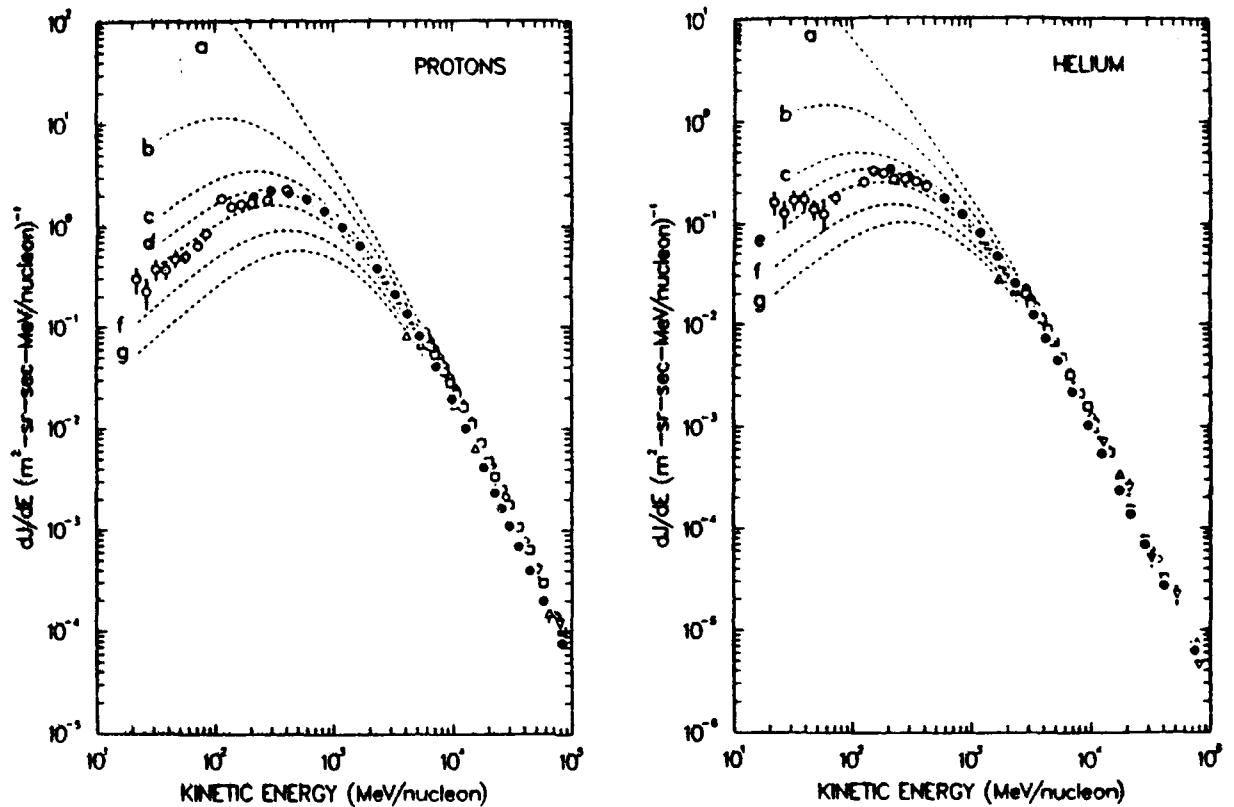


Figure 4: Differential energy spectra for cosmic-ray protons (left) and helium nuclei (right) measured in 1987 (filled circles for LEAP, open circles for IMP 8) along with the previous balloon measurements (see Seo et al., 1991 for references to the data). The dashed curves represent the local interstellar and modulated spectra with different amounts of modulation indicated by the parameter ϕ : a, local interstellar spectra (no modulation); b, $\phi = 200$ MV; c, $\phi = 400$ MV; d, $\phi = 500$ MV; e, $\phi = 600$ MV; f, $\phi = 800$ MV, g, $\phi = 1000$ MV.

Determining these two parameters has been the focus of much of our analytical work during the past year.

ii. Solar Energetic Particles

Solar flare events are semi-random in occurrence. The flare activity peaks near solar maximum in the cycle, but there are events scattered throughout the full solar cycle. Flares also vary widely from event to event, and this requires SEP events to be described individually. Data from the particle sensors onboard the CRRES satellite and from other sources detect SEP events, each of which will be fit to a SEP model. The results are then added to the galactic cosmic ray component to obtain a complete description of the heavy ion environment, at a reasonable minimum level of data

reduction and analysis effort. Even at the maximum of solar activity, there will be only a few flares per month that will produce significant fluxes of heavy ions at the energies of interest here. Based on these considerations, semi-annual updates should suffice to review the solar flare component. However, for particularly active periods (e.g. the late March-June 1991 interval) more frequent data presentation may be desirable.

There have been a number of efforts over the years to model SEP spectra. These have resulted in the use of power laws in kinetic energy (Dietrich and Simpson, 1978; Cook et al., 1984) exponential functions in magnetic rigidity (Freier and Webber, 1963), exponential functions in momentum/nucleon (Mewaldt et al., 1984) and Bessel function fits (McGuire and von Rosenvinge, 1984) to the spectra. The exact form to apply seems to depend upon the individual flare, the energy range of the fit and the species being considered. Figure 5, from Mewaldt et al. (1984), shows the fits obtained, for one flare, to the major heavy ion species from carbon to silicon. In this particular case, the exponential form appears to give a good representation of the data.

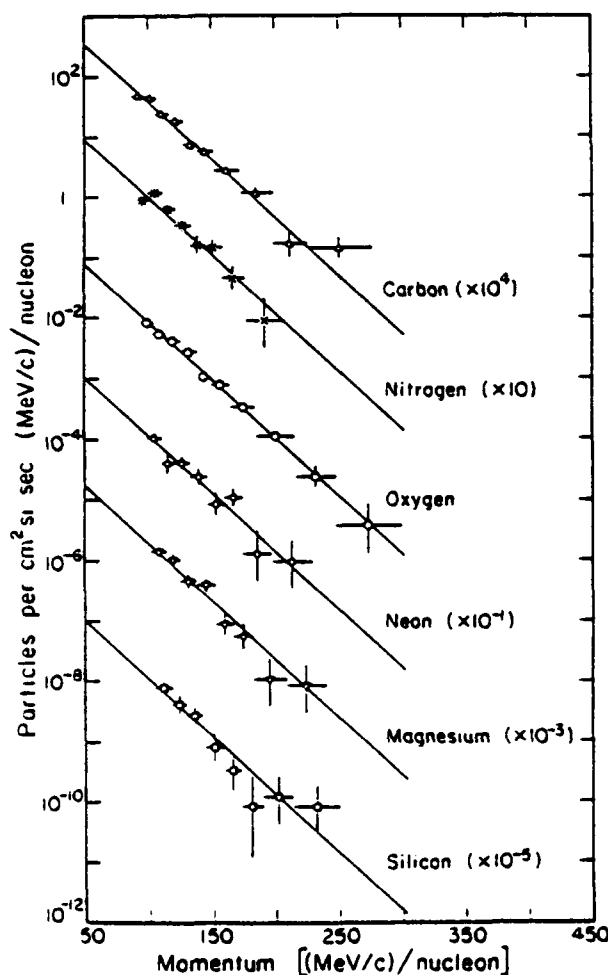


Figure 5. Solar flare energy spectra.

The heavy ions, such as are shown on Figure 5, are often enhanced (relative to normal solar system abundances) in solar flares. Often the enhancement is a function of charge, Z . For heavy nuclei such as iron, potentially the most important for the SEU problem, the abundances can be enhanced by over an order of magnitude relative to oxygen.

The heavy ion enrichment in flares of varying sizes has been the subject of numerous studies (McGuire et al., 1985; Meyer, 1985a; 1985b; Breneman and Stone, 1985; Mason et al., 1986; Guzik, 1988), and these models, as well as others, must be examined to select a representation for SEP events that describes the contributions of these events to the various heavy ion abundances and spectra. The parameters of such a representation will have to be determined from the CRRES data for each SEP event. However, since not all SEP's will be large enough to determine all of the parameters of the model, we will rely on published data for earlier SEP events to define typical values that can be adopted for such events.

The elements above the iron peak, $Z > 28$, are potentially more damaging to microelectronic circuitry than even the iron peak elements. These nuclei are found in both solar flares and in the galactic cosmic rays and could contribute to a few isolated events. However, the normal abundance of the $Z > 28$ elements is quite low and even in a heavy ion enhanced flare, the expected numbers of such nuclei are only a few tenths of a percent of the iron flux. A similar situation applies to the GCR (Binns et al., 1981) where Zinc is only 10^{-3} of iron and the heavier elements are at the $<10^{-4}$ level.

Solar energetic particle events are unpredictable, and identification of SEP events, especially small flares, is not easy with the ONR-604 sensor data, over a limited period of time. It will be necessary to use data from other sensors, external to the CRRES program, to unambiguously identify the SEP events. The monitoring provided by the GOES geostationary satellites and by the IMP-8 interplanetary spacecraft are important sources of SEP information.

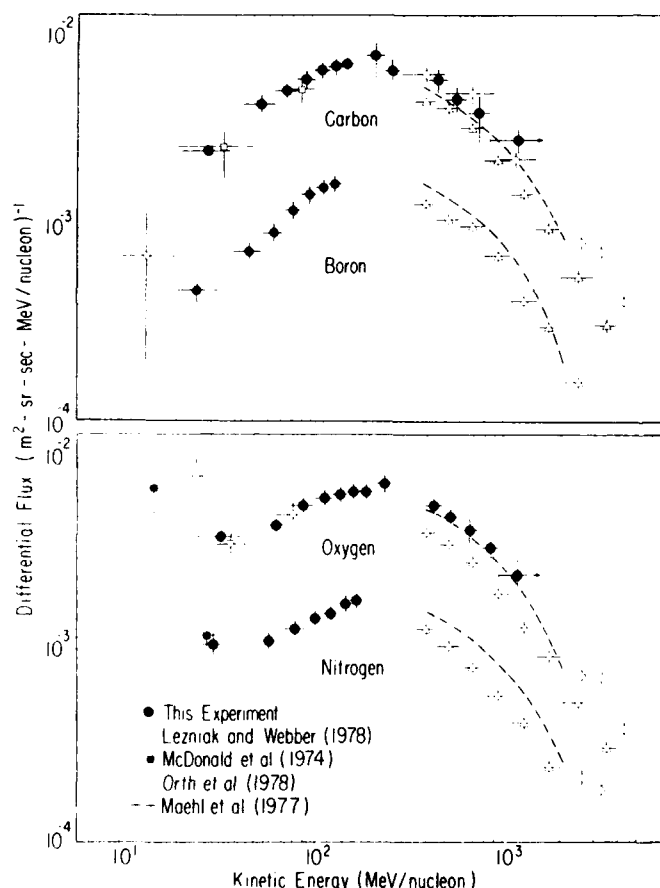


Figure 6: GCR energy spectra showing the presence of anomalous Nitrogen and Oxygen at low energies.

iii. The Anomalous Component

This anomalous component is prominent under solar minimum modulation conditions, at energies below ~ 50 MeV/nucleon at Earth, and appears to involve only high ionization potential elements, He, N, O, Ne and Ar. Figure 6 (from Garcia-Munoz et al., 1979) shows the energy spectra for B, C, N and O for energies above ~ 10 MeV/nucleon compiled from a number of different experiments. From the peaks of the spectra, the B and C show a steady decrease in flux with decreasing energy as expected from the spectrum and solar modulation models. The O and N spectra, however, show a flattening and a turn-up at energies below ~ 40 MeV/nucleon. This is due to the presence of the so-called "anomalous" component contributing to the spectrum at low energies. For oxygen, the flux at 10-20 MeV/nucleon is actually greater than the peak flux at several

hundred MeV/nucleon. The anomalous component can be important for CRRES during times of solar minimum. At solar maximum, this component is largely absent, showing that it is affected strongly by the level of solar modulation. It will be necessary, therefore, to model and include the solar modulation dependence of the anomalous component in the interplanetary heavy ion model, once the CRRES mission enters the minimum phase of the current solar cycle.

d. Distribution of Effort

Developing the model described above involves a combination of modeling/calculation and data analysis/interpretation. The tasks involved include:

- Compilation of previous GCR and SEP data and reduction of this dataset.
- Development of a First-order model based upon the accumulated GCR and SEP dataset.
- Software development for the analysis of ONR-604 data including plotting software, background assessment, normalization programs, correlation routines and the like.
- Establish techniques to measure the level of solar modulation during the mission.
- Finalize SEP description for use in the models.
- Support launch and on-orbit operations of CRRES and monitoring of the ONR-604 instrument.
- Establish routine processing and analysis software for the CRRES data.
- Develop ancillary databases for comparison and use in the modeling effort.

Thus, the effort involves a combination of data processing and analysis with modeling and interpretation of both new and existing data. All aspects must be worked simultaneously, since there was no Air Force support for the planned pre-launch modeling activities.

The approximate distribution of effort among the collaborating institutions is shown schematically in Figure 7. The data flow begins at Phillips Laboratory (AFGL) with the production of Agency Tapes and proceeds to the right through processing at Chicago, analysis at LSU, model calculations at LPARL and back to the Working Groups at Phillips Laboratory in the form of model predictions of LET spectra and SEU estimates. Significant coordination is required for this program, but, during the first year of effort, this approach has worked reasonably well.

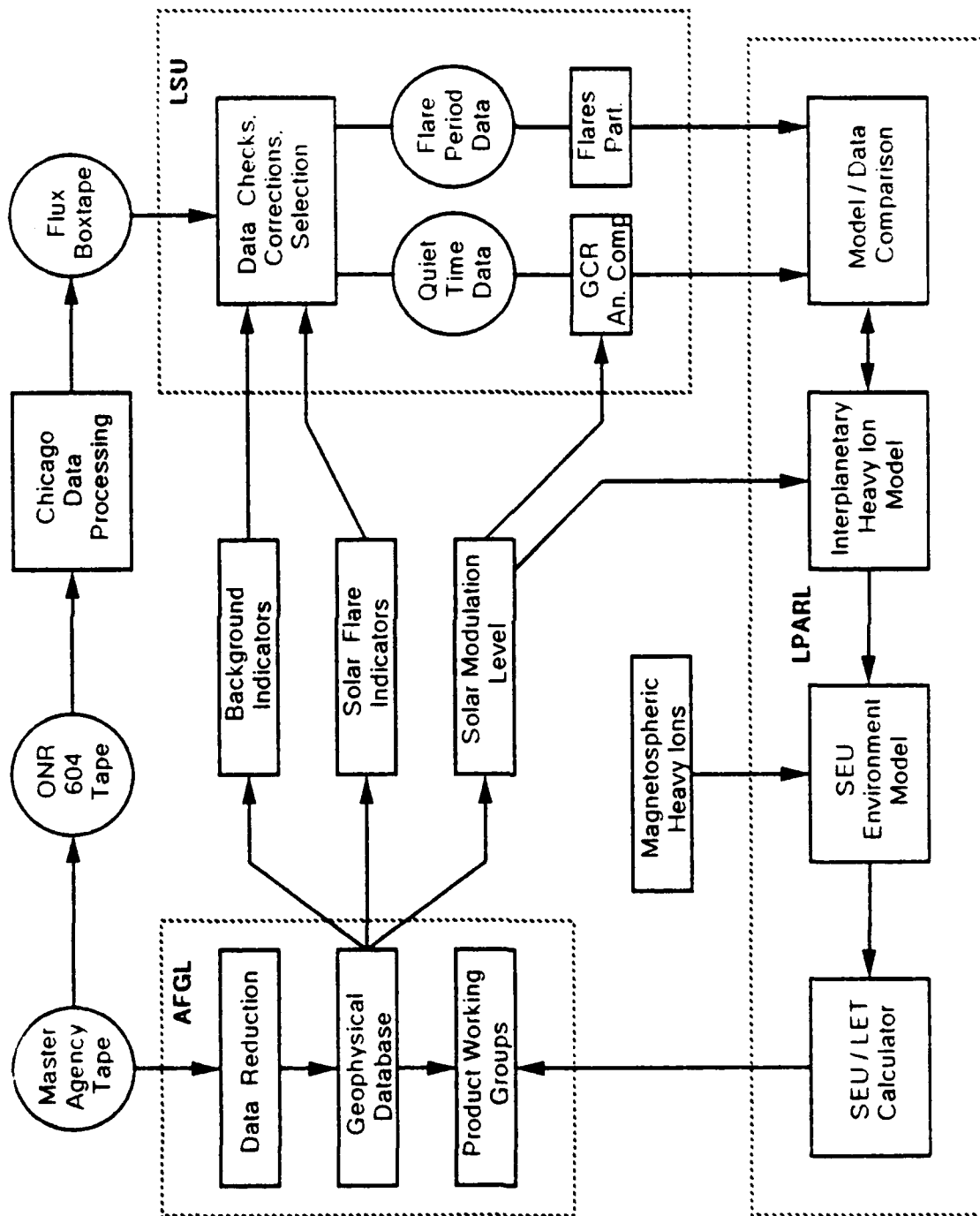


Figure 7. Data flow for the modeling effort.

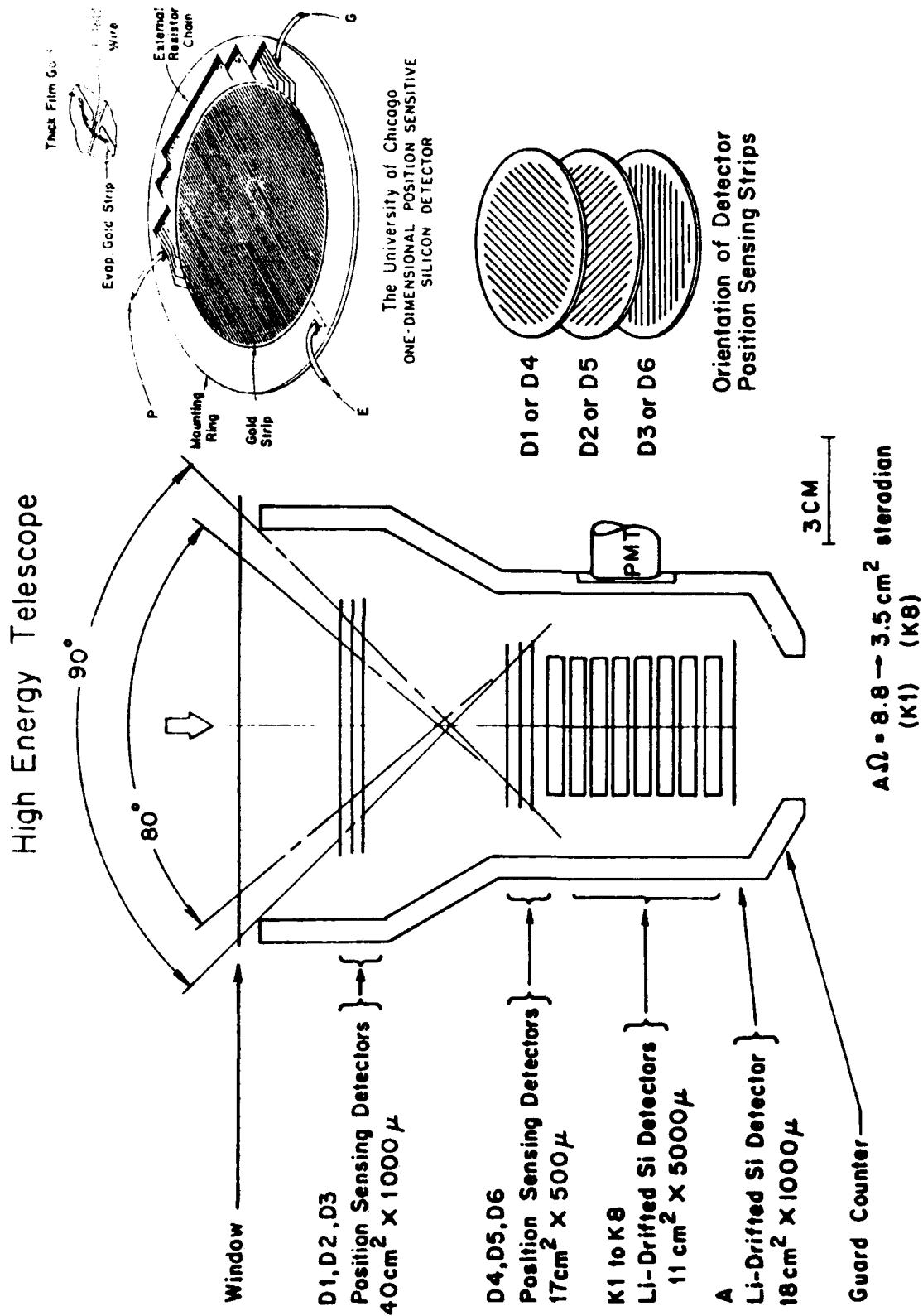
3. THE ONR-604 EXPERIMENT

The particle sensor data needed to refine the parameters of a heavy ion model are the flux and energy dependence of the major ion species, protons, helium nuclei and heavier elements. The intensities of the heavier elements are low, and obtaining a reliable estimate of their flux will require integrating over months, in broad energy intervals. In this analysis care must be taken to account for time dependent changes in sensor/electronic calibrations and/or backgrounds. It is prudent, therefore, to analyze elements chosen so as to be relevant to the model and to give reasonably accurate flux measurements over an approximately three-six month period, e.g. H, He, B, C, O, Ne, Si, Ca and Fe-Ni, analyzed over the energy ranges convenient for each species. The "key" experiment for this heavy ion analysis is the ONR-604 instrument built by the Laboratory for Astrophysics and Space Research at The University of Chicago under the direction of John A. Simpson. The experiment was constructed with NASA support from the CRIE project (M. Garcia-Munoz and J. P. Wefel, Co-Investigators) under contract NAS-2-24430 and sponsored for flight on-board CRRES by the Office of Naval Research.

a. Instrument Description and Operation

The ONR-604 investigation was designed to obtain new data on the elemental and isotopic composition of high energy, heavy ions to explore processes in solar flares, in the galaxy and within our Geospace environment. The instrument is optimized for studies of the heaviest ions, up through the iron peak. The single High Energy Telescope (HET), shown schematically in Figure 8 (Simpson et al., 1985), consists of a stack of fifteen silicon solid state detectors surrounded by a scintillation guard counter plus external passive shielding to reduce the effects of low energy background radiation. The stack contains six Position Sensitive Detectors (PSD) -- upper right -- used to determine the particle trajectory (Lamport et al., 1976) followed by eight 5 mm thick detectors which measure the particle energy loss and residual energy, allowing mass and charge identification by the ΔE -E technique. A 1000 micron thick penetration detector (A) is located at the bottom of the stack.

A unique feature of the instrument is the six PSD's, for which ONR-604 is the first space exposure of this new technology developed at Chicago. A schematic view of a PSD is shown at the top right of the figure. The upper surface consists of many parallel strips of gold each connected via a wire bond to a resistive divider network. By comparing the signal from the resistive divider network (P) to the full energy signal measured at the back surface (E), the strip nearest the point of incidence of the particle can be determined. From a fit to the positions in the six PSD's, the trajectory of the particle is determined with an angular accuracy of better than 1° , as validated by accelerator calibrations. The PSD's allow the incident trajectory of each event to be determined, providing corrections for the path length in the other detectors and point of incidence on the detector surface as well as allowing, for example, the particle pitch angle distribution to be studied.



The University of Chicago

Figure 8. The ONR-604 Telescope and its Position Sensing Detectors

For each event that is pulse height analyzed, the total energy deposited in each of the first 14 detectors is read out. This allows the particle range ("ID") to be used to subdivide the full energy interval. For high precision charge and mass identification, the particle must come to rest within the instrument, which determines the energy over which each type of particle can be studied. The entire stack is surrounded by a scintillator guard counter to eliminate out-of-geometry events and particles that exit from the side of the apparatus. The scintillator signal is not part of the trigger logic but is recorded (along with A) as a flag for each analyzed event. In addition, a ground-commandable operations mode is provided for the detailed analysis of proton and alpha particle flux levels.

Because the anti-coincidence scintillator guard subtends a large solid angle, it must be shielded from the high counting rates induced by electrons trapped in the magnetosphere. Passive shielding to eliminate <4 MeV electrons is provided by a magnesium shield and Tantalum collar. The lower part of the scintillator is located well within the instrument package and is surrounded on five sides by electronic modules which offer additional shielding. The backward moving particles are shielded additionally by the spacecraft structure.

In order to protect further against accumulated radiation damage to the detectors D1, D2, and D3 (where the average geometrical factor is $87 \text{ cm}^2\text{-sr}$), a 3 mm external aluminum window shield is placed over the telescope. This shield lowers the magnetospheric integrated proton and electron radiation doses for detectors D1, D2, and D3 below the tolerance threshold of these detectors while increasing, only slightly, the energy intervals for measurement of the heavy particles which are the main objective of the experiment.

Separating isotopes for elements as heavy as nickel, requires precision measurements of the energy deposits in the detectors. For this, exceptionally linear, highly stable electronic circuits to analyze the signals have been developed. Each analysis chain is individually calibrated preflight. The performance of each analysis chain is monitored during flight by an on-board calibrator which sends a sequence of 2000 pulses spanning the entire range of signal sizes. Further, in-flight calibration and normalization is provided by measurement of actual galactic cosmic ray events.

In addition to heavy particles, the instrument measures protons and alpha particles over the energy range 25-120 MeV/nucleon. In quiet regions of space, a priority system insures that the heavy nuclei are analyzed in preference to protons and alphas. In regions of high background radiation, a commandable heavy particle "normal mode" is invoked. This raises the thresholds on the detectors D1 through D6 to suppress the high firing rates induced by trapped protons and electrons while still permitting the rare heavy ions to be analyzed. In "normal mode," the "proton mode" thresholds of detectors D1 through D6 are increased by a factor of 5.8 and, as a consequence, the instrument becomes practically insensitive to protons.

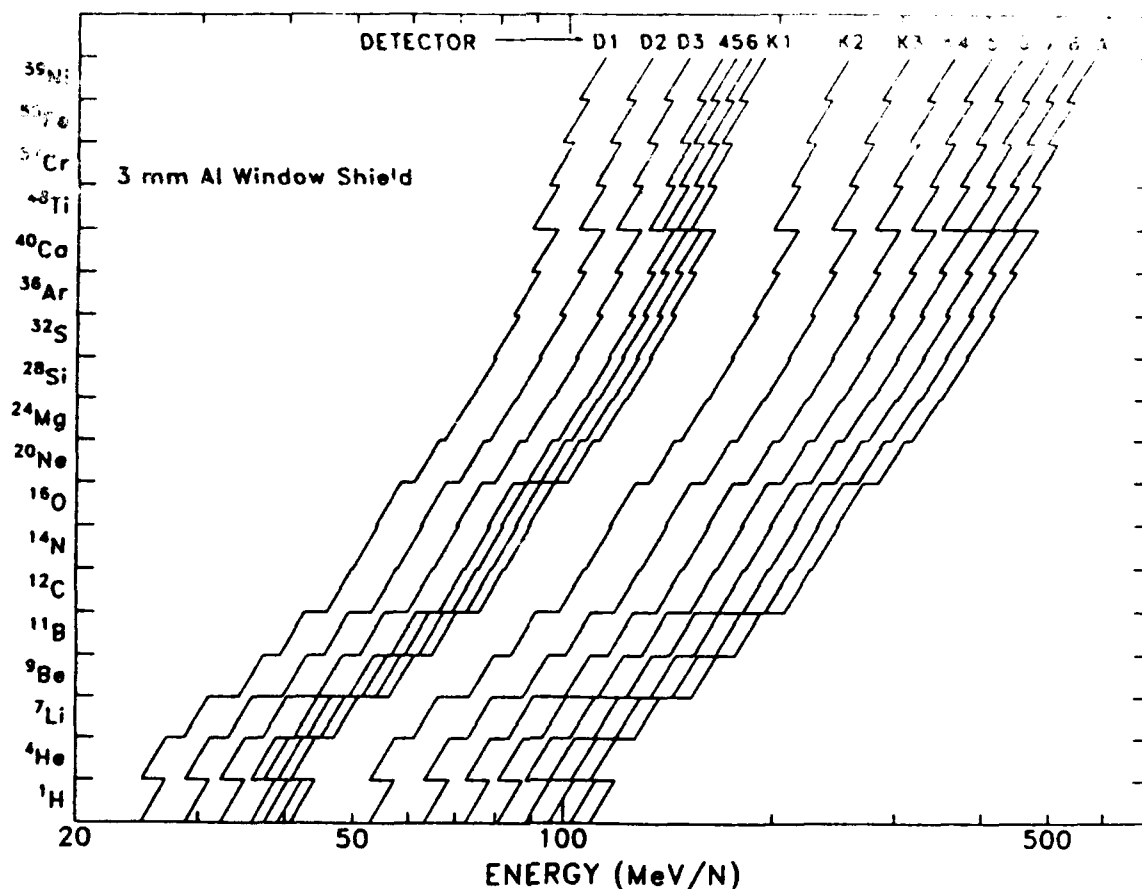


Figure 9. ONR-604 energy ranges for selected isotopes.

The energy ranges for triggering the different detectors for different species in the ONR-604 instrument are illustrated in Figure 9 for selected isotopes from H through Ni. The lines connect the incident energies for 0° and 30° angles of incident. Figure 9 indicates that H and He are studied over an approximate interval of 25-120 MeV/nucleon while Fe is measured over a range of ~100-550 MeV/nucleon. Comparison with Figure 3 shows that these intervals are just below the peak in the cosmic ray spectra.

The instrument acceptance is also a function of energy. For the lowest energy events, those that stop in D1 - D3, the geometrical factor is $>80 \text{ cm}^2\text{-sr}$ while for the highest energies (stopping in K8) the geometrical factor is only $\sim 3 \text{ cm}^2\text{-sr}$. This changing acceptance provides one of the principal normalization problems in deriving particle spectra.

The highest quality data is obtained for particles stopping in K2-K8. However the HET also measures particles that (1) stop in K1, (2) stop in D2 - D6 and (3) penetrate K8. For (1) and (2), it is necessary to use the signal from the E contact of the PSTs to provide energy loss information. For events stopping in D2 or D3, the

path length uncertainty is given by $\sec \theta$ where θ is the maximum angle through the window ($\sim 69^\circ$ for D2) which gives a spread of a factor of 2.8. Thus, D1, D2 and D3 analysis can separate protons and helium, but no heavier elements. For particles stopping in D4, the $\sec \theta$ spread is reduced to a factor of 1.44. Particles stopping in D5 - K1, have trajectory information available, and elemental separation is limited only by the quality of the E signals from the PSDs. Finally, the charge composition of events penetrating the entire stack can be studied over a limited energy interval.

The ONR-604 instrument incorporates a priority system for the pulse height analyzed events. Each particle is defined by the instrument logic hardware as either a P1, P2 or P3 event. P3 is the instrument trigger, defined by the logic condition

$$P3 = GC = D1D2D3\bar{S} + D1D2D3(K1 + K2).$$

Thus, allowed events must trigger the first three PSD's, and not go out the sides triggering the scintillator OR must trigger the first three detectors and one of either K1 or K2, independent of the scintillator. (Commands are available to allow any or all of detectors D1, D2, D3, K1, K2, S or A to be disabled in the logic.) P2 events add to P3 the requirement, $(K1M + K2M)\bar{A}$, i.e. the particle must stop in the stack and trigger the medium level discriminator threshold on detectors K1 or K2. Finally, P1 events add to P3 the requirement that one of the high discriminator thresholds on K1 - K8 must be triggered. Thus, considering the discriminator thresholds, P1 responds approximately to $\geq Ne$ (stopping or penetrating); P2 records He to $\sim Ne$ (stopping), and P3 encompasses everything else allowed by the trigger logic. When a high priority event is detected, it will cancel the pulse height analysis of a lower priority event. Thus a P1 will replace a P2 or P3 event, while a P2 will override a P3 event. (Discriminator patterns indicate when such an override has taken place.) This priority system ensures that a maximum number of P1 events will be analyzed and that the preponderance of H and He will not "swamp" the heavy ions. This is particularly important for obtaining heavy ion fluxes for the model, since for Iron, for example, over the energy range 180-535 MeV/nucleon, corresponding to IDK1 through IDK8 in ONR-604, the expected number of nuclei is only about a dozen per day!

The ONR-604 instrument returns both pulse height and count rate data, the latter involving both singles and coincidence rates, including the P1, P2 and P3 priority rates. The counting rates are important in their own right, provide a diagnostic for instrument performance and are used to normalize the pulse height readouts to obtain particle flux. The rates are accommodated for a fixed time period of 4.096 seconds and their readout is controlled by a commutation system. Logic rates are output continuously while detector singles counting rates are sub-computed so that singles rates are available less frequently. Table 1 gives the logic for the different rates as well as an indication of the approximate particle energy range sampled by the rate.

TABLE 1: ONR-604 Counting Rates

Rate No.	Detector Interval (Rate Name)	Rate Logic		Energy Interval of Rate in Proton Mode (MeV)	Particle Defining Energy Interval
1	D1	$D1\bar{D2}\bar{D3}$	$(\bar{S})_a$	24.8 - 44.5	Protons
2	D2	$D1D2\bar{D3}\bar{D4}$	$(\bar{S})_a$	28.3 - 48.2	"
3	D4	$D13D4\bar{D5}\bar{D6}$	$(\bar{S})_a$	35.1 - 43.9	"
4	D5	$D13D5\bar{D6}\bar{K1}$	$(\bar{S})_a$	36.6 - 45.5	"
5	K1	$D13K1\bar{K2}\bar{K3}$	$(\bar{S})_a$	40.0 - 59.4	"
6	K2	$D13K1K2\bar{K3}$	$(\bar{S})_a$	52.0 - 70.6	"
7	K3	$D13K1K3\bar{K4}$	$(\bar{S})_a$	62.1 - 79.9	"
8	K4	$D13K1K4\bar{K5}$	$(\bar{S})_a$	71.2 - 88.5	"
9	K5	$D13K1K5\bar{K6}$	$(\bar{S})_a$	79.3 - 96.5	"
10	K6	$D13K1K6\bar{K7}$	$(\bar{S})_a$	87.0 - 103.5	"
11	K7K8	$D13K1K7\bar{A}$	$(\bar{S})_a$	94.0 - 116.9	"
12	A	$D13K1K8A$	$(\bar{S})_a$	107.5 - 275	"
13	P3	$D13\bar{S}+D13(K1+K2)$		24.8 - 275	"
14	P2	$P3(K1M+K2M)\bar{A}$		42- 105	He ⁴
15	P1	$P3(K1H+K2H+K3H+K4H+K5H+K6H+K8H)$		127 - 352 (typical)	Mg ²⁴
16		Single's Rate Sub-com			

Notes: M = Medium Threshold; H = High Threshold; (Low Threshold is indicated by detector symbol)

S Scintillation guard counter

$(\bar{S})_a$ S term included every alternate readout.

P3 Pulse Height Analysis Gate Control (Priority No. 3 or low priority).

P2 Priority No. 2 or Medium Priority

P1 Priority No. 1 or High Priority

Figure 10 shows a sample plot of the rates for orbit 649, first part of day 108 of 1991. Figure 10a gives the three priority rates and the command state of the instrument. ONR-604 went into proton mode (PM) about 0615 and remained there until ~1115, corresponding to the apogee portion of the orbit. The P3 rate, for example, jumped about an order of magnitude when PM mode was on. Note the P1, P2 and P3 spike around 0900. This corresponds to a calibration period as indicated by the CAL (C) command, and must be removed from rate averages. There was also a data gap during this orbit from ~1145 - 1350. Just after the gap the P2 rate shows a tremendous "spike" for a single readout. These occur periodically and must also be eliminated to obtain clean data. Finally, one should note the P1 rate in which the individual particles can (almost) be counted, indicating the low intensity of the heavy ions.

Figure 10b displays the singles rates from the different detectors as ~1 minute averages, and Figures 10c-e show the coincidence rates listed in Table 1. In each plot of Figure 10c-e, the rate logic with the \bar{S} term is plotted as the solid line, while the rate without this term is given as the dashed line. Rate D1 and D2 are shown as 33 second averages while the remainder are displayed as 3 minute averages. In all cases, the peak between 0400 and 0500 corresponds to low-L values ($L = 1-3$) and shows the effect of magnetospheric particles on the ONR-604 counting rates. Note also that there is significant structure in the rates during a perigee pass (0400-0500) and into the "apogee" portion (0630, $L > 5$) of the orbit. Understanding this structure is one of the challenges for the ONR-604 data analysis.

b. Pre-launch Calibration

The ONR-604 instrument was calibrated in July, 1977, April, 1978, July, 1979, and again in February, 1989 with beams of He, C, Ne, Ar, and Fe particles (with energies such that the particles stopped in the telescope) at the Bevalac heavy ion accelerator at the Lawrence Berkeley Laboratory. These extensive calibrations demonstrated that ONR-604 can resolve isotopes of H to Ni, over the relevant energy ranges. In addition, these runs provided a means to check instrument operation, priorities, rates and thresholds. Finally, the use of a radioactive source during the Feb. 89 calibration provided a simulation of expected instrument performance in a high radiation background environment.

For the acceleration work, special interface electronics were constructed. This interface eliminated the slow synchronous readout of the instrument and replaced it with a fast asynchronous readout which allowed the accumulation of significant statistical samples of events from the accelerator beam. For final confirmation of performance, the CRRES S/C interface was re-installed and data were recorded in spacecraft mode. Significantly more heavy ion events were recorded during these accelerator runs than will be seen during the entire CRRES mission!

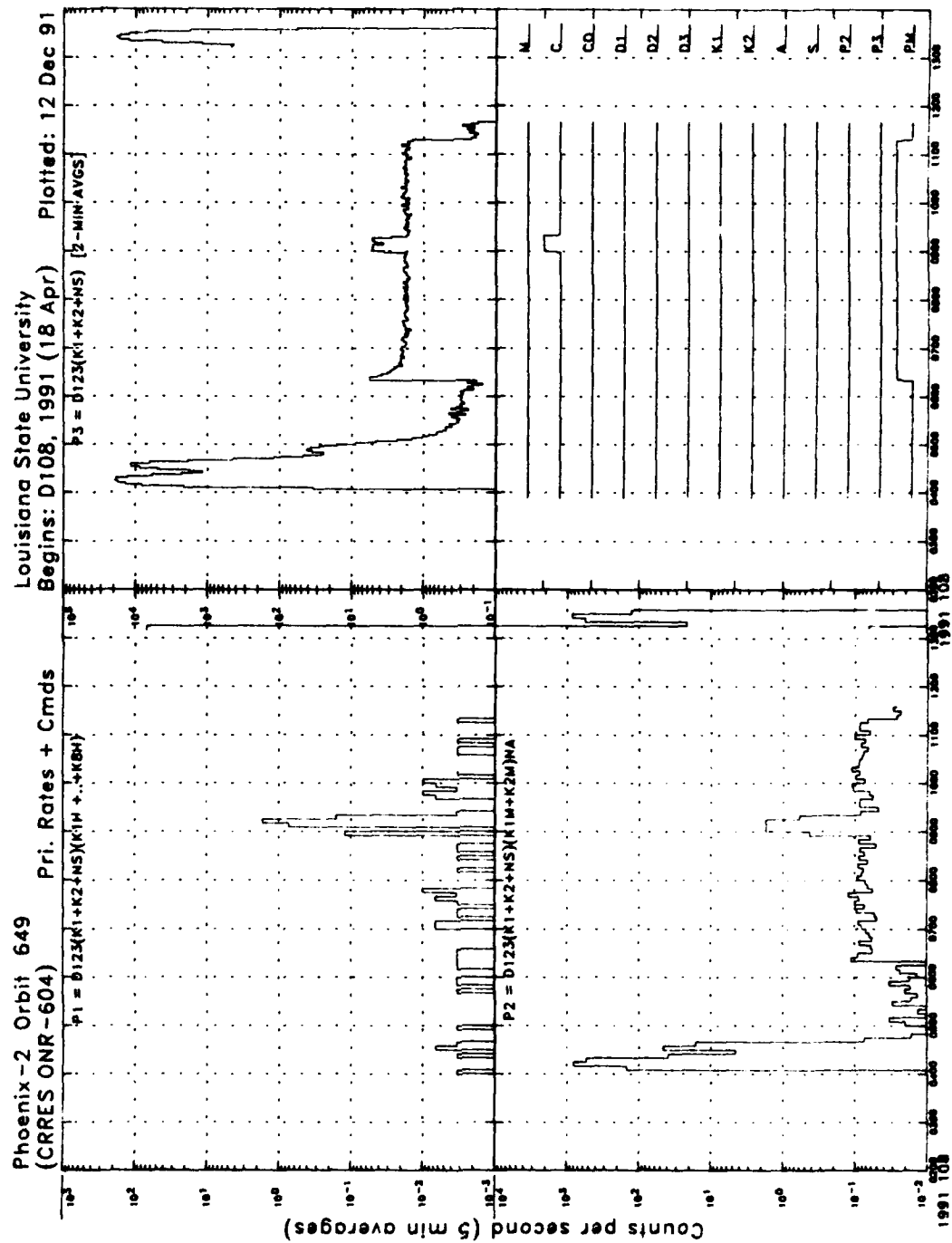
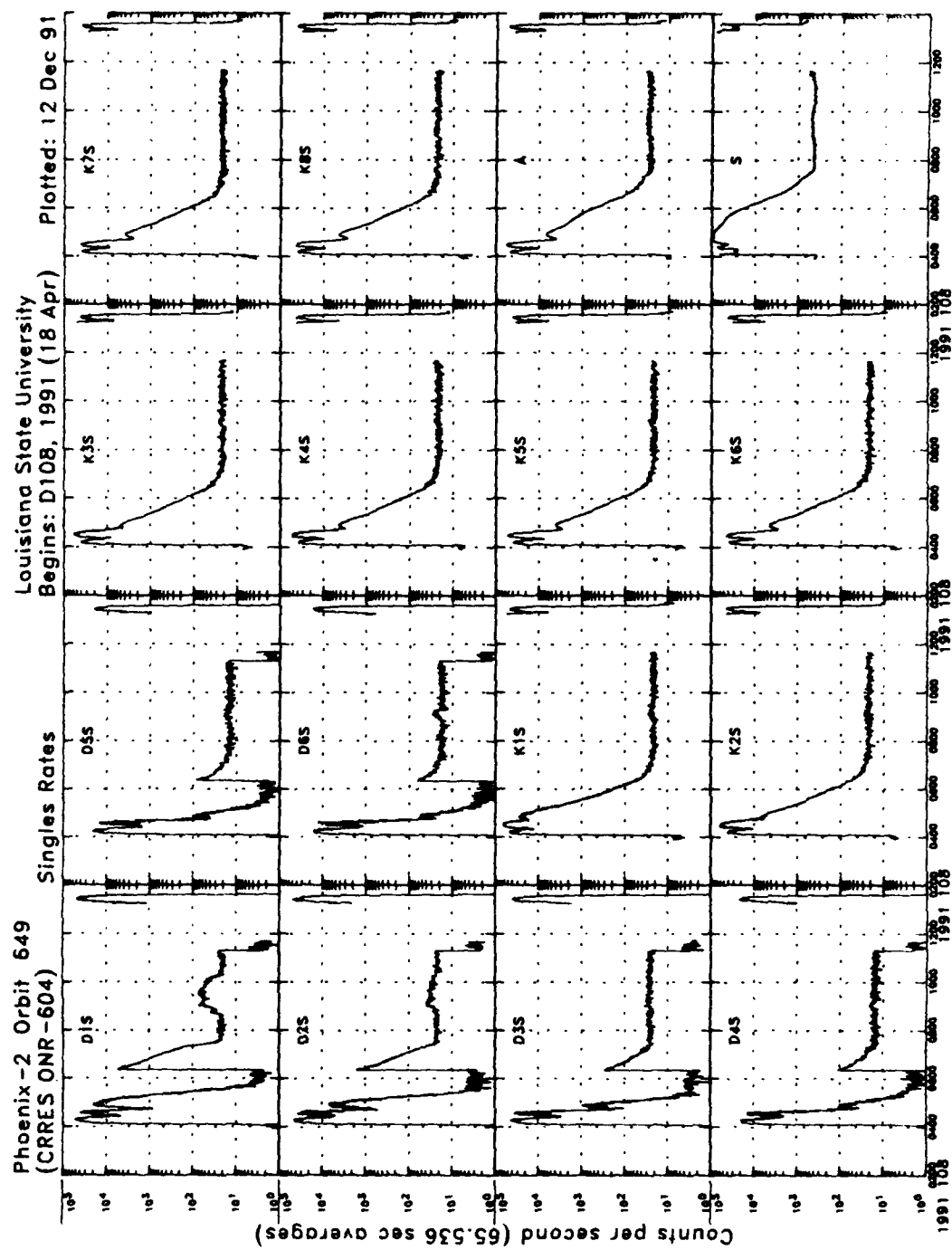


Figure 10a. ONR-604 Priority Counting Rates and Command State.



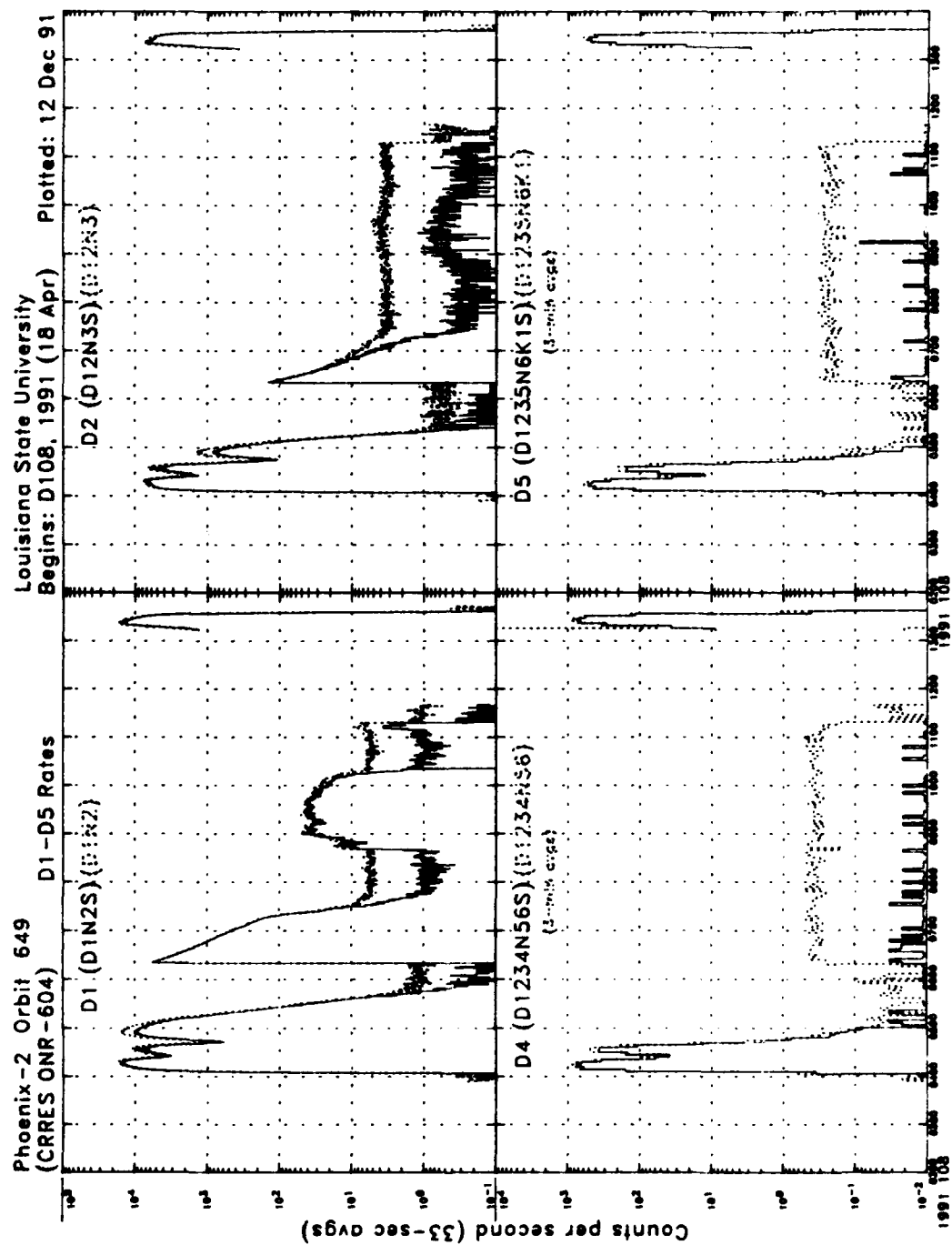


Figure 10c. Coincidence Counting Rates, D1-D5.

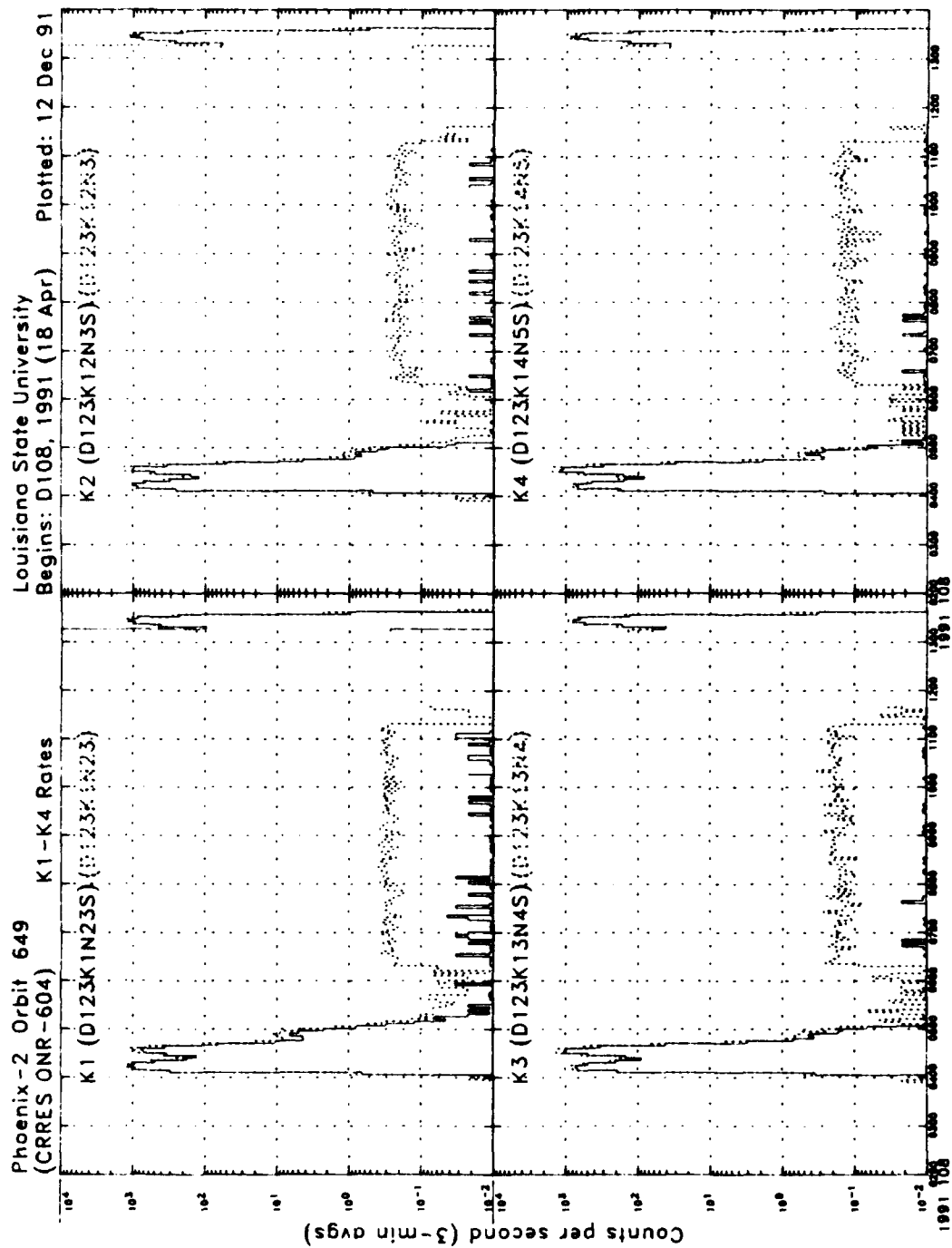


Figure 10d. Coincidence Counting Rates, K1-K4.

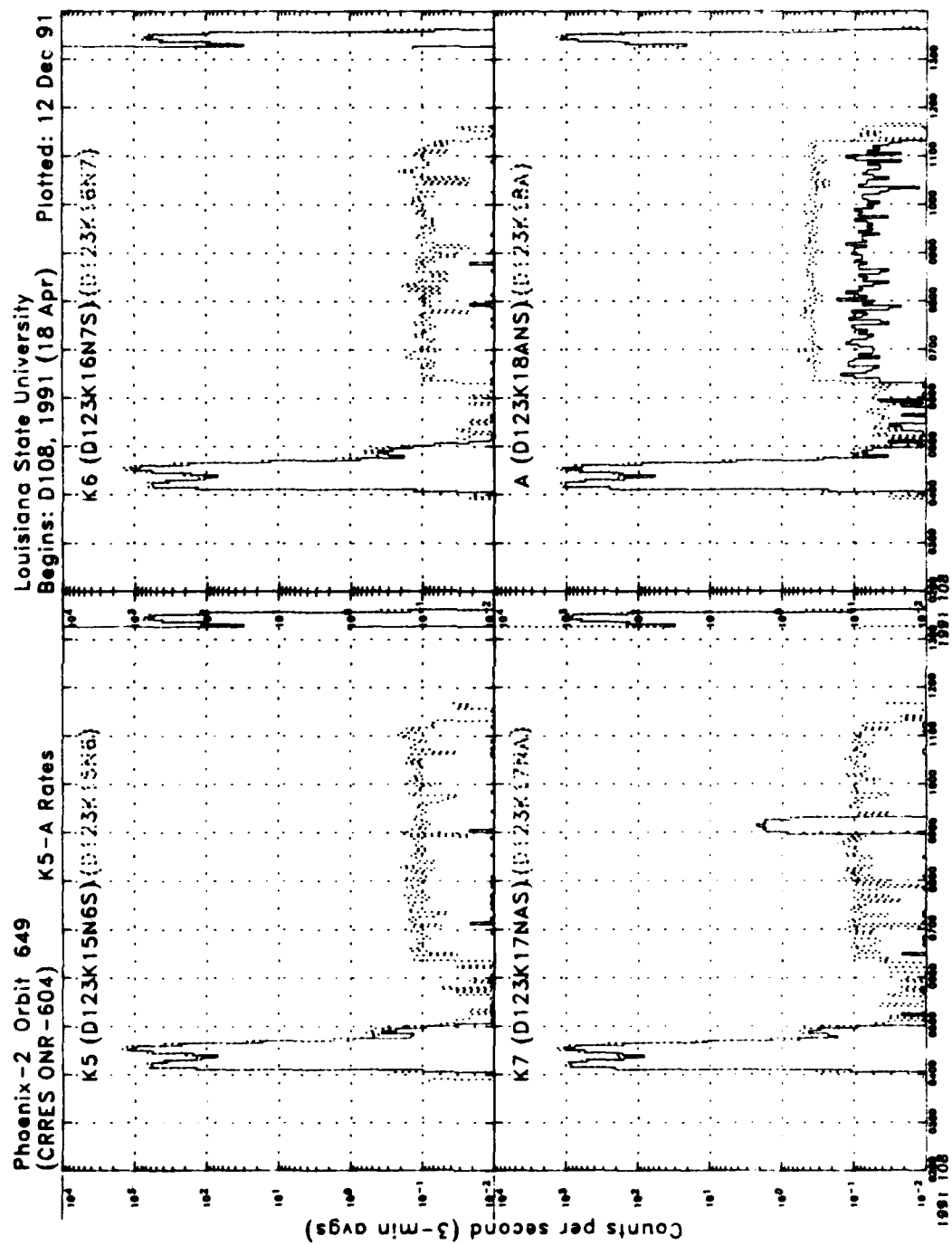


Figure 10e. Coincidence Counting Rates, K5-A

For the accelerator calibrations, the instrument was mounted in a gimballed cradle that allowed it to be rotated in two axes. This permitted the beam to enter the telescope at a variety of zenith and azimuth angles. Such angular variations allowed the performance of the PSD trajectory system to be checked over the full range of allowed particle incidence angles and permitted the study of "edge effects" for particles incident at the maximum possible angles.

The accelerator beams were first focussed at the instrument. Then, in front of the instrument was placed a polyethylene target (to fragment the beam into lower charge isotopes) and a rotatable aluminum wedge. The rotation of the wedge reduced the energy of the beam to provide events stopping throughout the detector stack. The beam was then defocussed, which expanded it from about 1 in² to ~ 4 in², to cover the full size of the front three detectors (see Figure 8). Small adjustments in beam energy were made by a remote controlled absorber system, in order to study events stopping in the PSD's or near the top and bottom surfaces of one of the K detectors.

For some runs it was necessary to generate the ion of interest, e.g. helium. This was done by putting a thick target in the beam upstream of the bending and focusing magnets. The isotope of interest was then focussed by the magnets onto the telescope (of course, all isotopes with the same rigidity are focussed as well, so these generated beams are not as clean). This allowed a specific charge range to be investigated in detail.

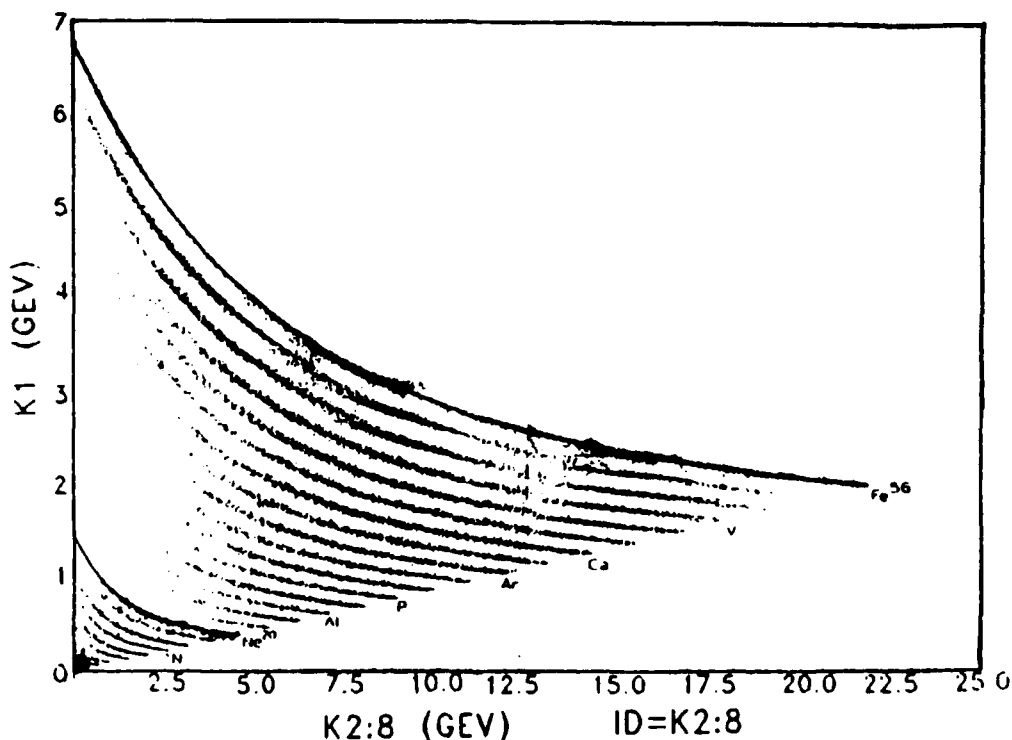


Figure 11: Raw Fe and Ne calibration data from the Bevalac showing the intensity variations with energy.

The energy coverage obtained with the wedge system was not uniform as shown in Figure 11 for Iron plus Neon data. The large black blobs correspond to concentrations of beam. Thus, in the analysis it was necessary to remove events to try to obtain as uniform a track coverage as possible, within the constraint of still maintaining ample statistics.

Figure 12 displays samples of the data from three separate "beams," Iron (top), Neon (center) and Helium (bottom). In all cases the plot shows the energy deposited in D1 + D2 vs the sum of the energy deposits in D3 through K8. For the Iron beam only priority 1 events are shown. By combining data from several beams it has been possible to populate the element "tracks" over the full matrix. Note the tracks that are almost vertical, labeled "R" on the Neon plot. These correspond to events that passed through D1 D2 D3 but missed the edge of D4 or events that passed through D1-D6 but missed the edge of K1. Recalling the geometry of Figure 8, the detector radii decrease between D1-3, D4-6 and K1-8, so such events are allowed. Some will pass into the scintillator guard counter (S), but others will stop in the structural materials before S. This is one source of "background" that must be eliminated from the flight data.

There is also a black horizontal track on the Neon plot which corresponds to events leaving the edge of the stopping detector and not penetrating to S. Such events can be eliminated by using the instrument trajectory system to require the particle to be incident upon the central 2 cm of the last detector triggered. The result of such a "clean-up" is shown in the top panel of Figure 13, and has already been applied to the Fe and He parts of Figure 12. Note also that one can begin to see separated isotopes for H and He and the fragments of Ne.

Figure 13 shows the high resolution data, events that stop in detectors K2-K8, as the energy deposited in K1 versus the sum of energies in K2-K8, for the Neon calibration. Note that distinct isotope tracks for the Neon fragments are visible. The lower portion of Figure 13 shows the data restricted to P2 and P3 events, i.e. P1 not triggered. The high discriminator thresholds on the K detectors (used to determine the P1-P2 division) cross the Neon energy deposit curve dividing this element between priority 1 and priority 2 as shown. Such a calibration allowed the KH discriminator thresholds to be checked and compared to the design values and calculated track structure.

Figure 14 shows a combination of the Ne and Fe datasets with the Iron track eliminated so that the fragment tracks can be observed. Over portions of the energy interval, separate isotope tracks can be discerned up into the sub-iron region. This demonstrates the intrinsic ability of the instrument to resolve heavy isotopes. In the lower portion of the figure, the data are restricted to only P1 events. The portions of the Neon track in P1 are apparent. Closer inspection shows that F and Na are also divided between P1 and P2 as predicted by the calculations.

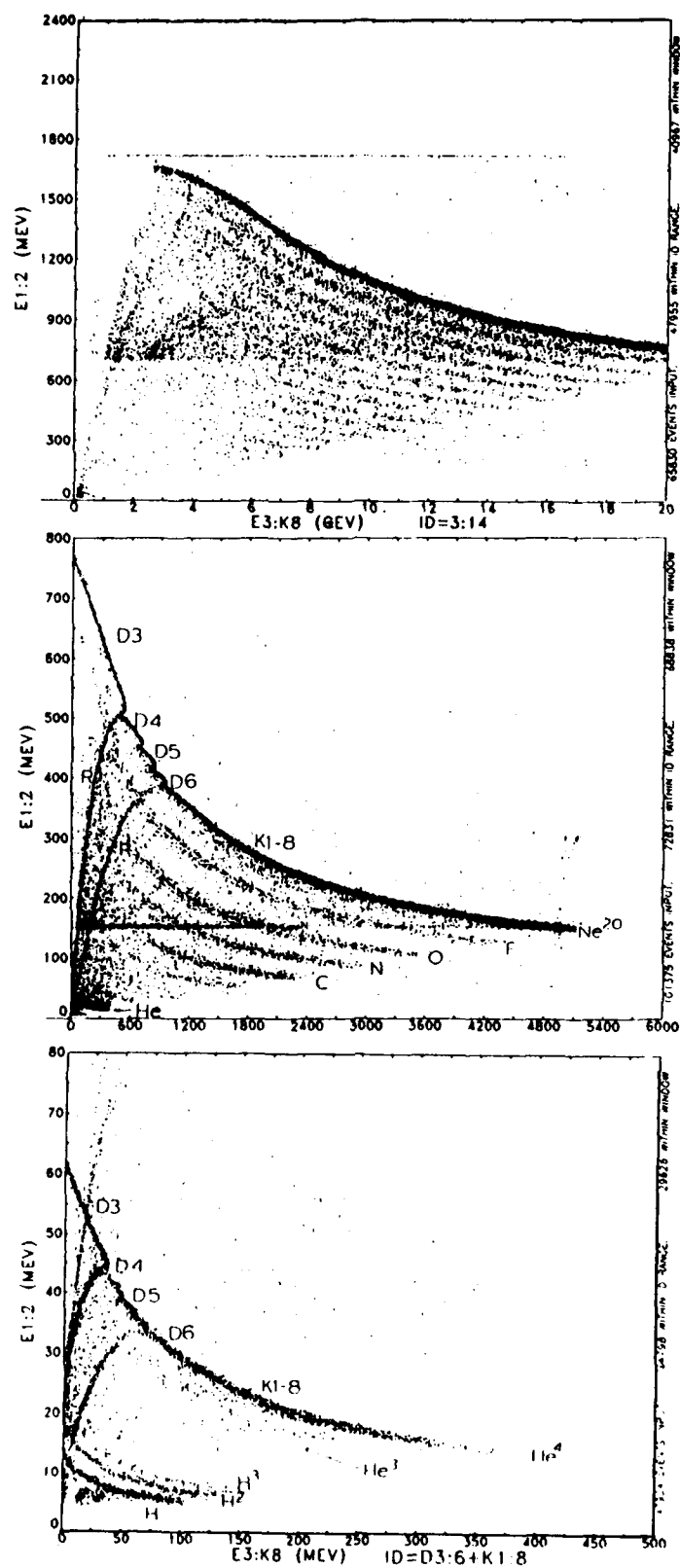


Figure 12: Accelerator calibration data from Iron (top), Neon (center) and Helium (bottom) runs.

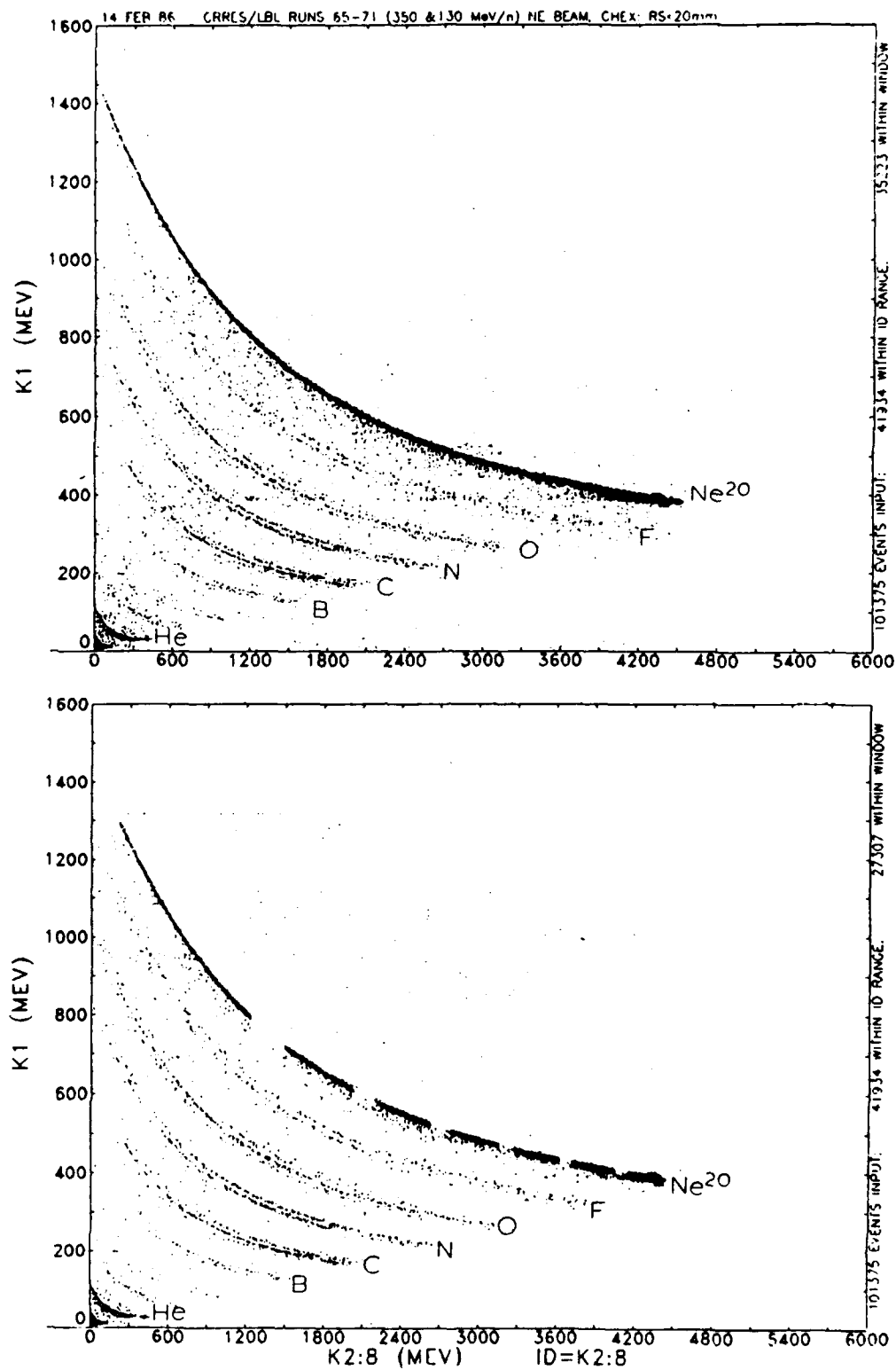


Figure 13. Bevalac Neon data showing all events (top) and priority 2+3 events only (bottom). A stopping radius cut has been applied to the data.

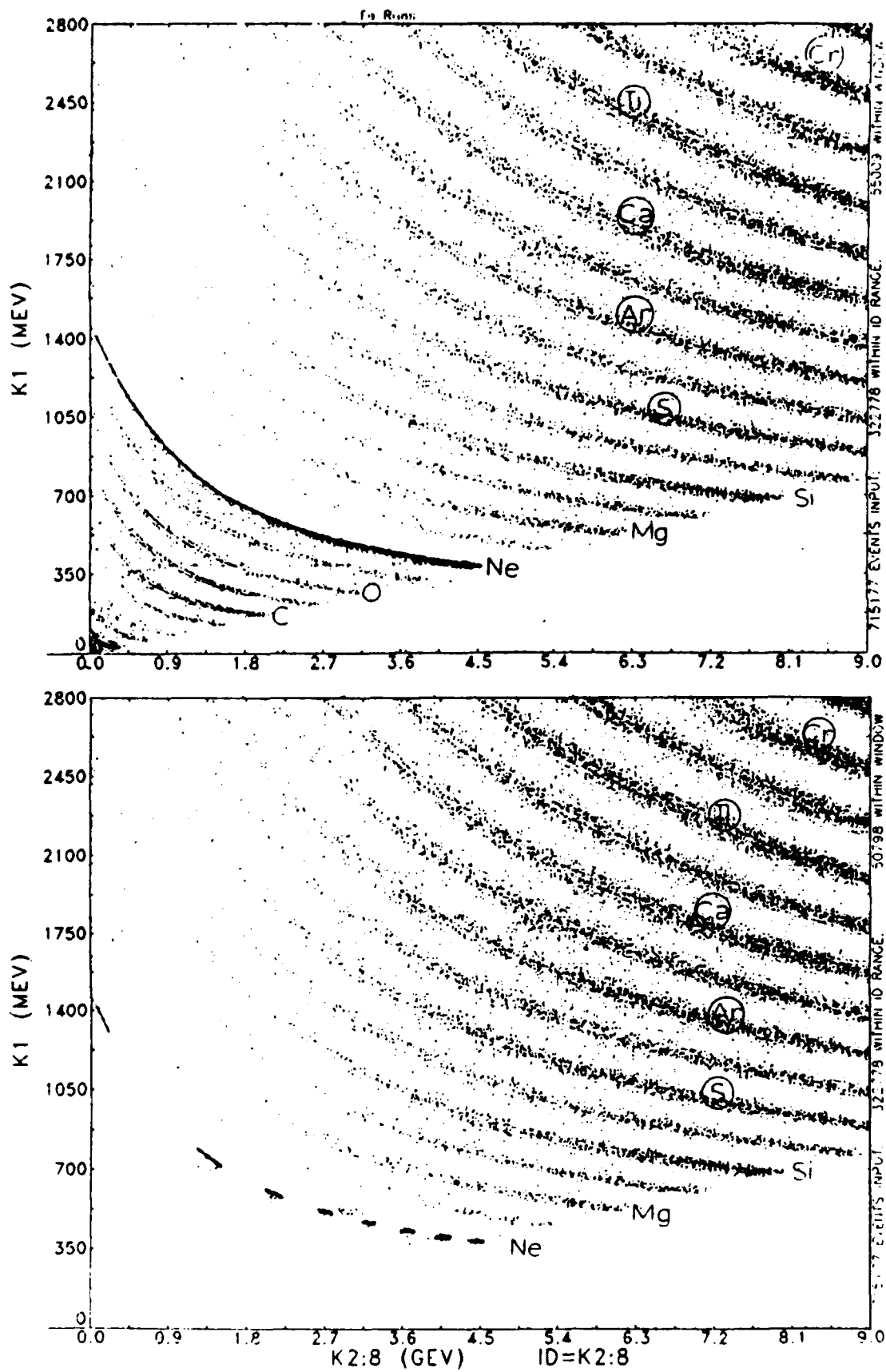


Figure 14. Iron + Neon data in K1 vs K2-8. The lower plot shows only P1 events.

Looking at the Helium events allows the P2-P3 transition to be investigated as well as the instrument command states. Figure 15 shows plots similar to Figure 12 (bottom). In the top panel the instrument is in its "normal" mode command state (i.e. high D thresholds to eliminate protons and electrons) to be compared to the "proton" mode state which was shown in Figure 12. Note that all of the hydrogen isotopes are eliminated by the normal (=heavy) mode command. The lower part of Figure 15 shows data restricted to P1 and P2 events (i.e. no P3 triggers). This indicates that the majority of the helium track lies in P2, but the lowest and highest energy helium events are found in the P3 priority state. Thus, reconstructing the Helium (Neon) energy spectrum will require normalizing the P3 (P1) priority readout to the P2 readout efficiency.

As part of the 1989 calibration, we investigated the operation of the instrument in a high radiation background provided by a specially purchased $^{144}\text{Ce} - ^{144}\text{Pr}$ radioactive source of strength 100 milli-curies. This isotope, half-life of 284 days, decays by beta emission to excited states of ^{144}Pr which transition quickly to the ground state emitting a gamma ray or themselves decay by beta emission. The maximum beta energy is just under 3 MeV with a 2.2 MeV γ -ray as the highest energy photon. The source was prepared on a type-A mount and inserted into a machined aluminum holder equipped with removeable brass shields, each of which had a different size hole machined into it. This allowed the intensity of the source to be varied with a minimum amount of handling and no direct exposure.

Data were taken with the source located at different distances from the instrument, using the full flight electronics. Individual electrons should not be able to trigger a P3 event, but 2 or 3-fold electron pile-up could. The observation of pulse height analyzed events produced with only the source near the instrument confirmed this prediction. Similar "events" will probably be observed in the inner magnetosphere or in the slot region.

A second question was what effect the presence of background radiation would have on heavy ions observed at the same time. To answer this question, the instrument was operated with the Iron beam on and with the radioactive source mounted at an angle exposing the front portion of the instrument. Figure 16 shows the result. Plotted is the energy deposit in D1-D6 versus the energy deposit in K1-K8 for an iron beam run without the source (top) and with the source (bottom). The bottom plot shows a second iron track, below the beam track, at an intensity $\sim 1/3$ of the normal track. The lowered track results from the D detector amplifiers being below baseline when the iron event occurred, due to the high firing rate of the front detectors from the source radiation. That this effect is limited to the PSD's is demonstrated in Figure 17 where the K1 vs K2-K8 matrix is shown for the same data. No second track appears in the lower (source "on") plot in Figure 17. This is as expected since the energies of the source radiation are insufficient to cause rapid firing of the K detectors. Figure 18 shows the charge histograms in the two cases

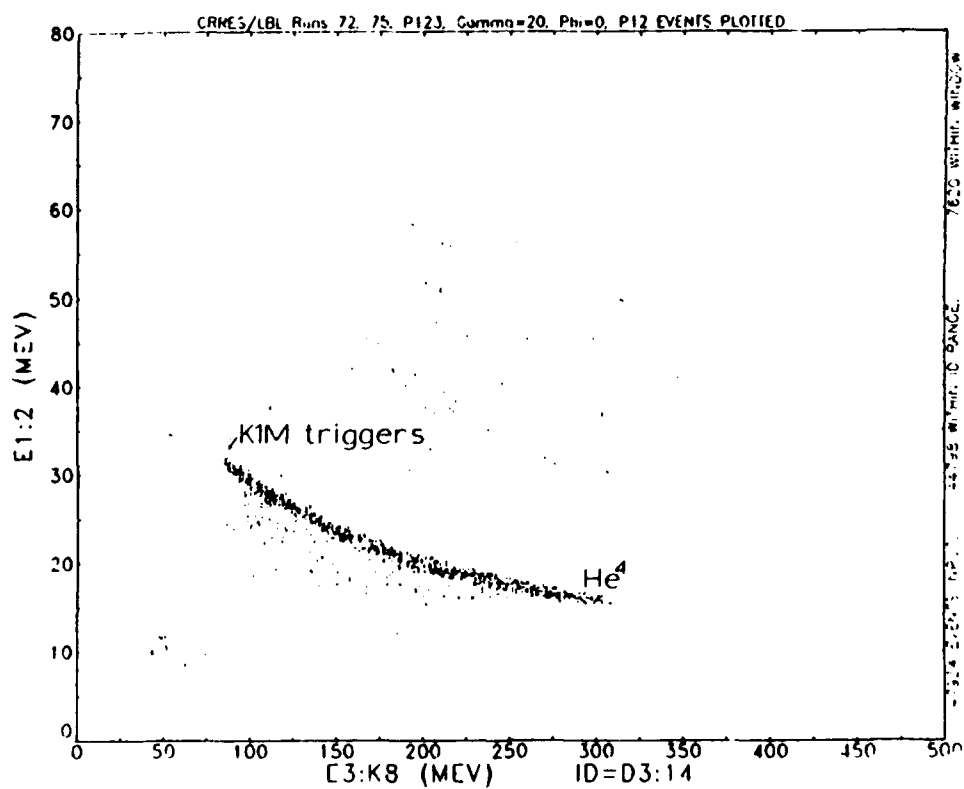
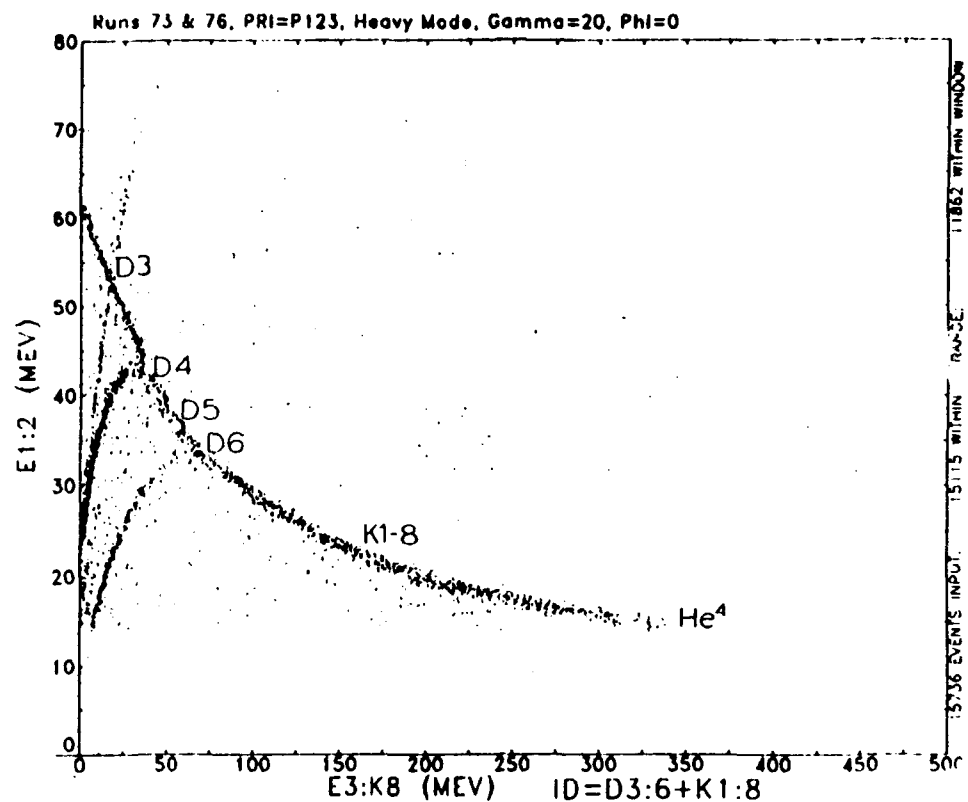


Figure 15. D1 + D2 versus D3-K8 for Helium events showing the effects of the normal mode command (top) and the P2-P3 division (bottom).

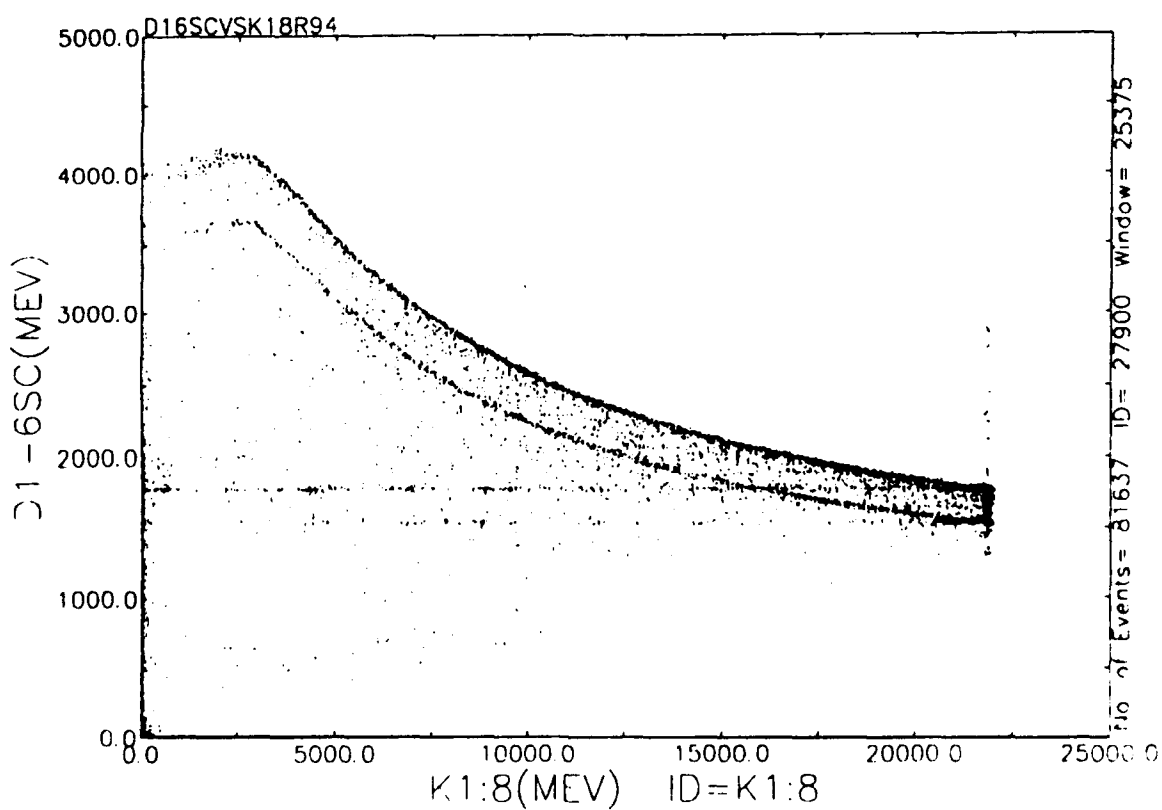
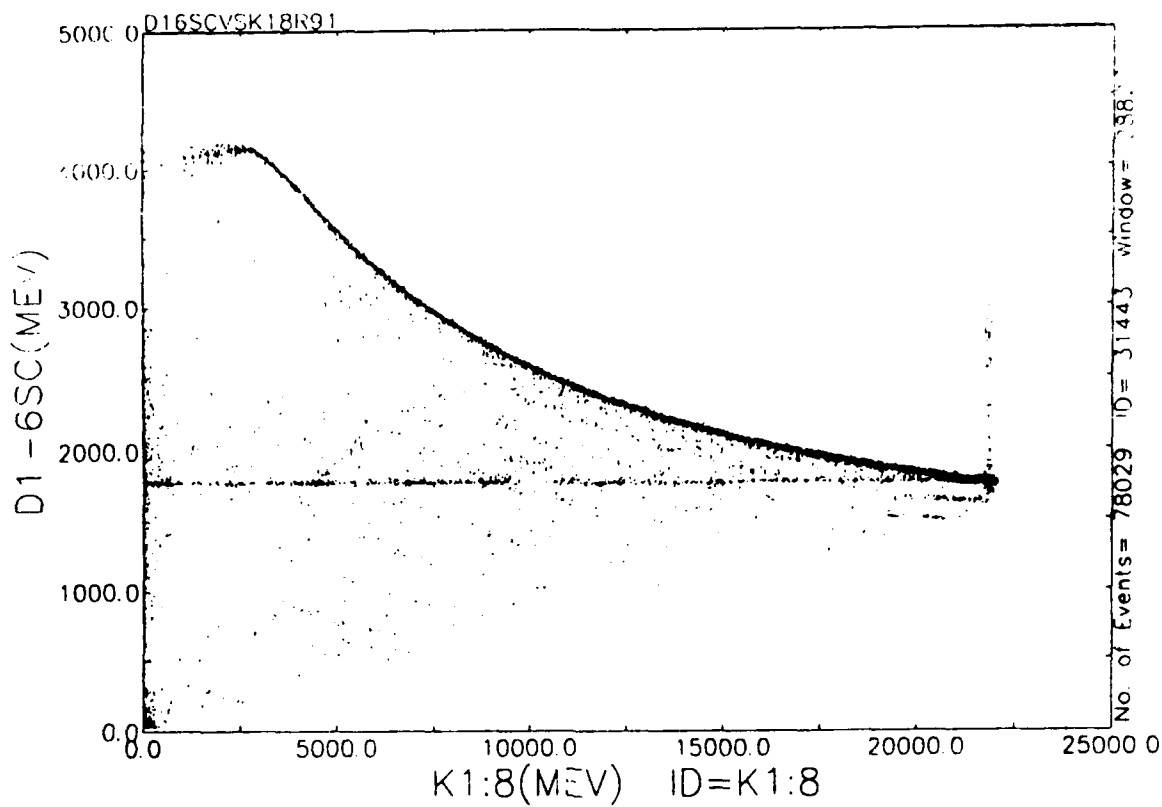


Figure 16. D1-D6 versus K1-K8 matrix for Iron beam events with NO source (top) and WITH source (bottom).

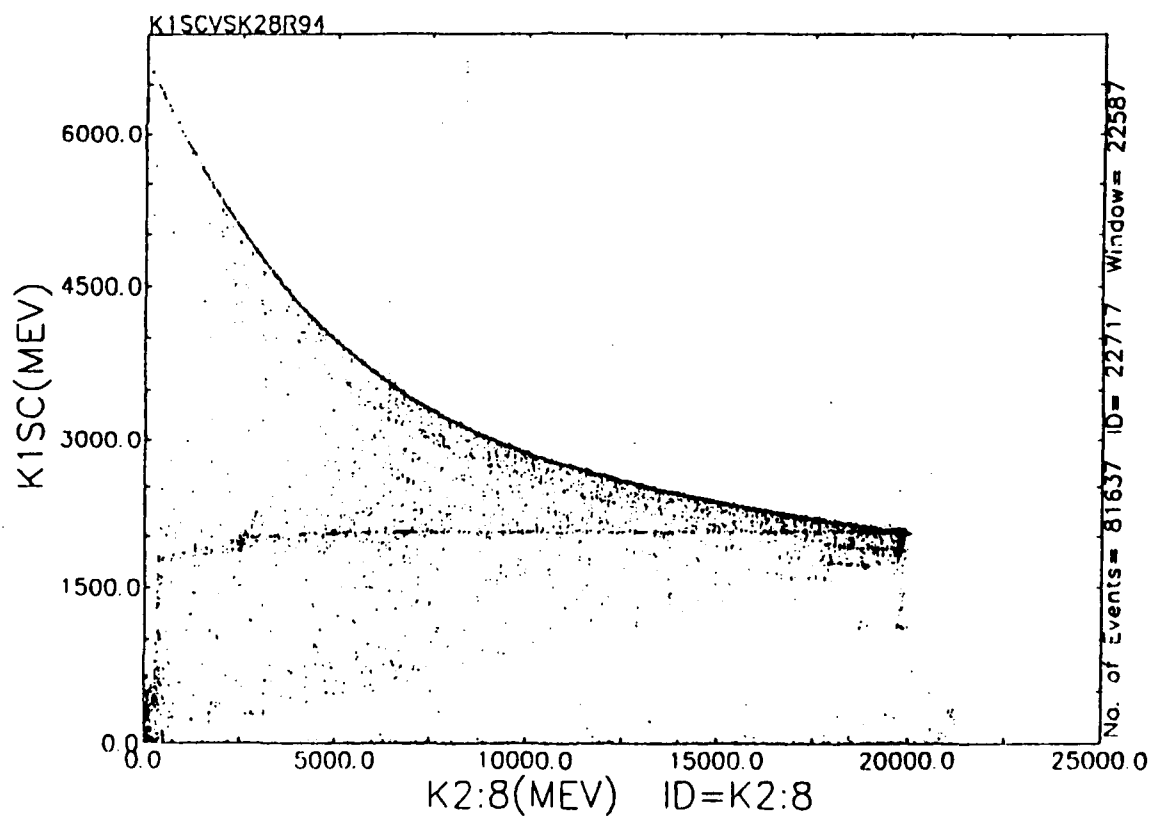
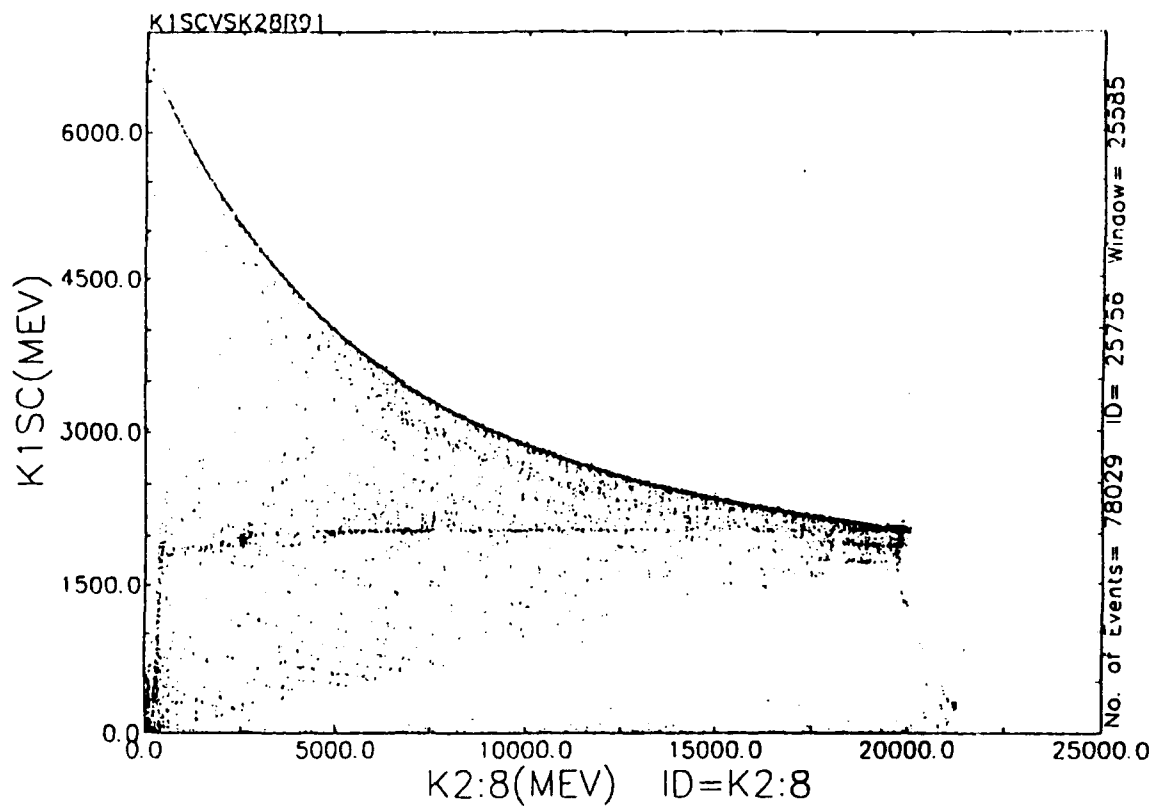


Figure 17. K1 versus K2-K8 matrix for Iron beam events with NO source (top) and WITH source (bottom).

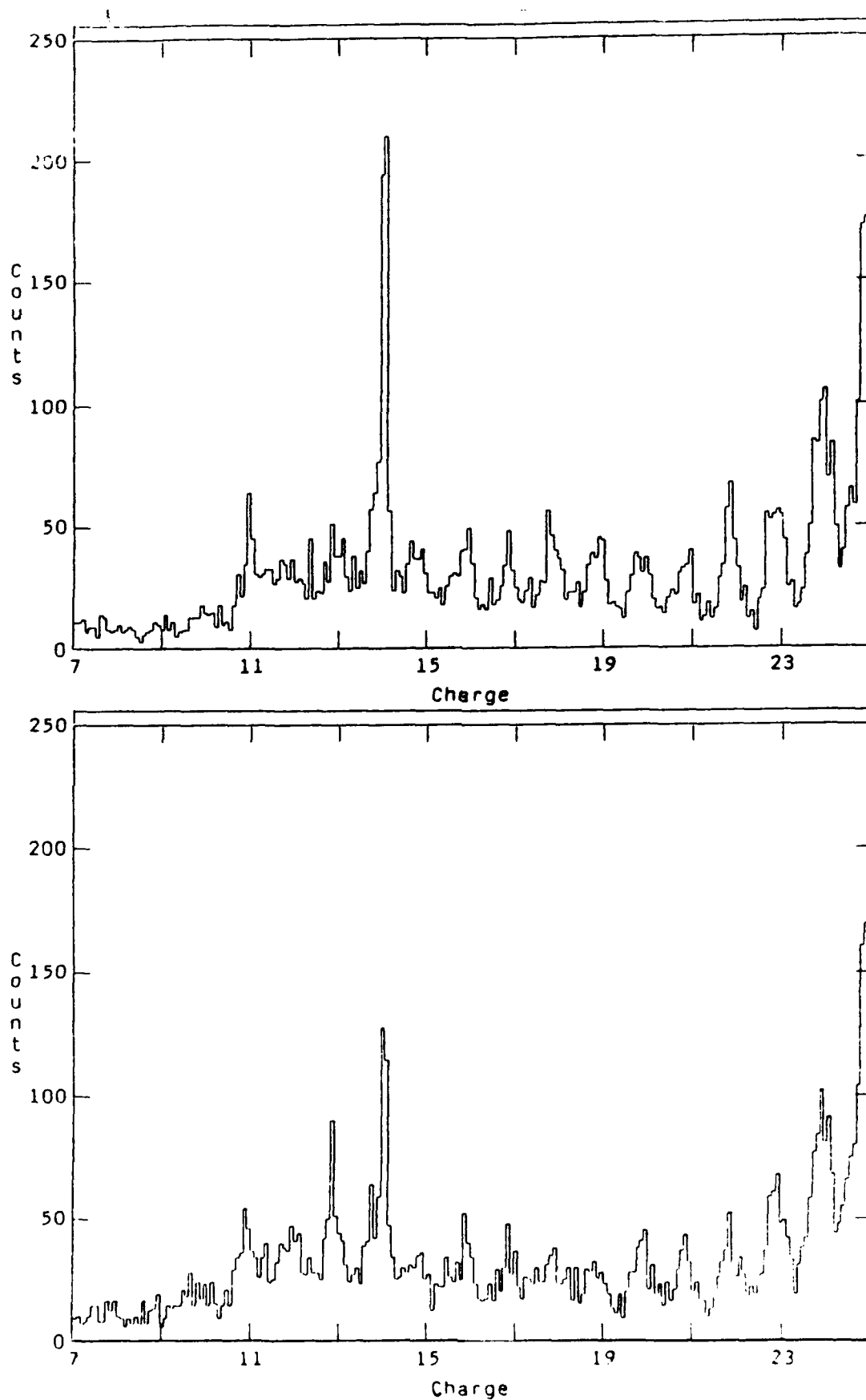


Figure 18. Charge histograms for events observed in iron runs with NO source (top) and WITH source (bottom).

shown in Figure 17, and there appears to be no discernible degradation in the charge resolution from the presence of the radioactive source. In addition, there is no discernible shift in the position of the Iron track between the two panels of Figure 17.

The majority of the source effect is confined to the first detector D1. This is illustrated in Figure 19 which shows plots of the energy deposited in D1 (top), D2 (middle) and D3 (bottom) versus K1-K8. Only in the top plot is the "second track" noticeable.

We expect such effects to occur during the CRRES mission, particularly near the outer belt. The flux and energy distribution of the background radiation in space will be different from that obtained in this source calibration, however the effects should be predictable. We expect that the K1-K8 events will be largely unaffected, but extracting the lower energies from the ONR-604 data will require very careful analysis.

C. Launch and On-Orbit Checkout

Much of the initial several months of effort under this contract was devoted to pre-launch preparations, rehearsals and training at CSTC, launch operations and instrument turn-on and initial operations planning for the experiment. The important questions for ONR-604 were the instrument calibration, the performance in various parts of the orbit in different command states and the development of a plan for routine operations of ONR-604 on CRRES. In-flight calibration runs were scheduled over various parts of the CRRES orbit as well as while the instrument was in the different command states, i.e. proton mode and normal mode. These data were analyzed on a micro-computer system at CSTC before pronouncing the experiment "healthy" and implementing the routine operations plan.

Figure 20 shows the results of an In-Flight Calibration (IFC) run analyzed at CSTC. The instrument was in normal mode and the run was taken during a pass through the outer belt region. Plotted are the deviations of the IFC points from a best fit straight line. Of significance is the spread of the points which appears "bad" for P1, E1, P2 and E2, the amplifiers on the top two detectors in the telescope. For the other amplifier chains the deviations appear normal. When analyzed completely, the gains deduced from this run were all $<0.15\%$ different compared to IFC run taken on the ground well before launch. Thus, it appears that the instrument maintained its absolute calibration through launch operations. Further, data taken in high background environments such as the outer belt may be subject to variations, at least in the top two PDS's.

Figure 21 shows the P3 counting rate as a function of time for a full orbit of data analyzed at CSTC. The instrument was in proton mode at the time. Note that P3 responds strongly to both the inner and outer belts but is relatively quiet under the

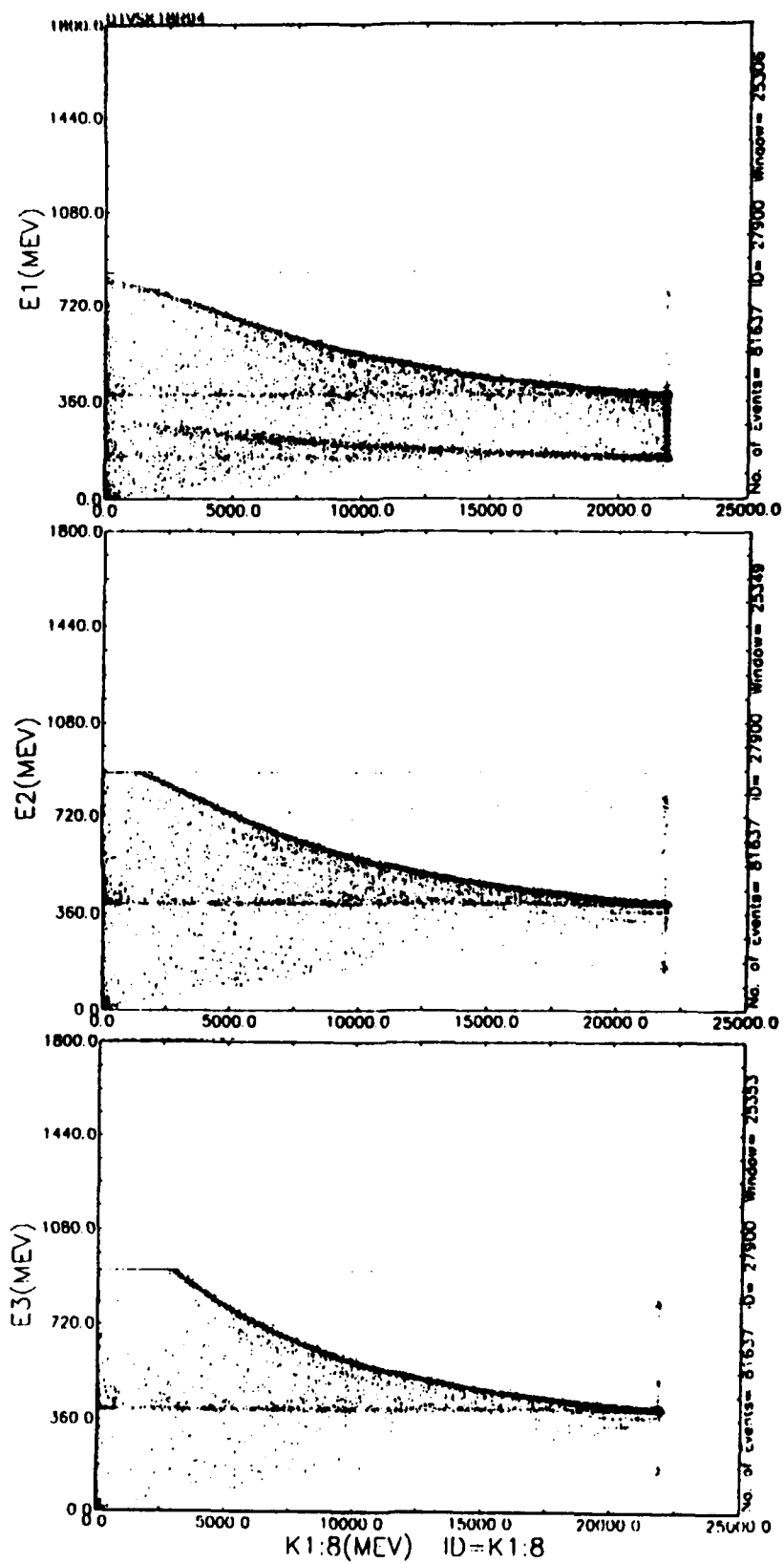


Figure 19. Energy deposits in D1 (top), D2 (middle) and D3 (bottom) versus K1-K8 for iron events taken WITH the radioactive source.

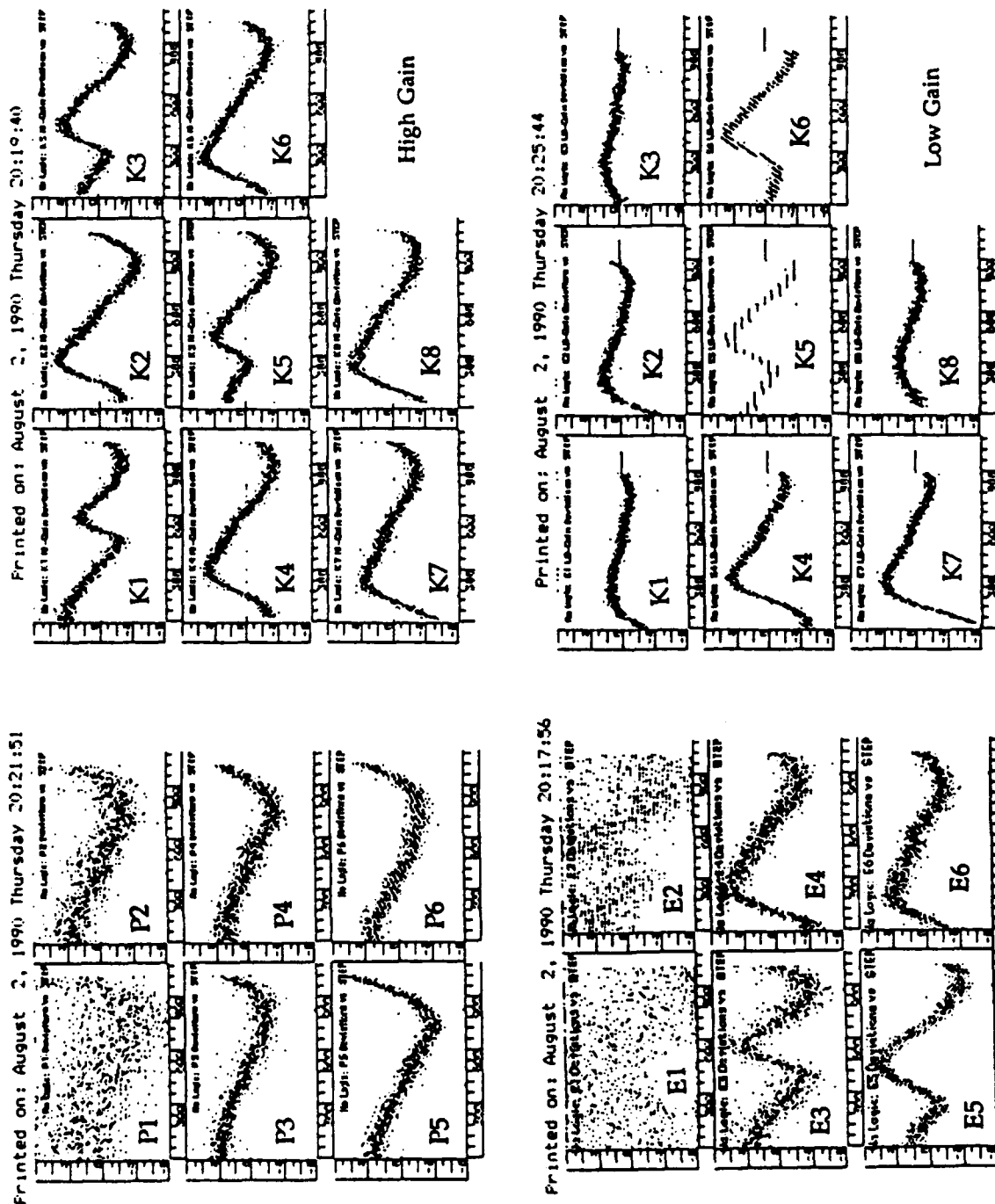


Figure 20. GSE Run 530, IFC Run at CSTC. Deviations of the points for each amplifier from a straight line.

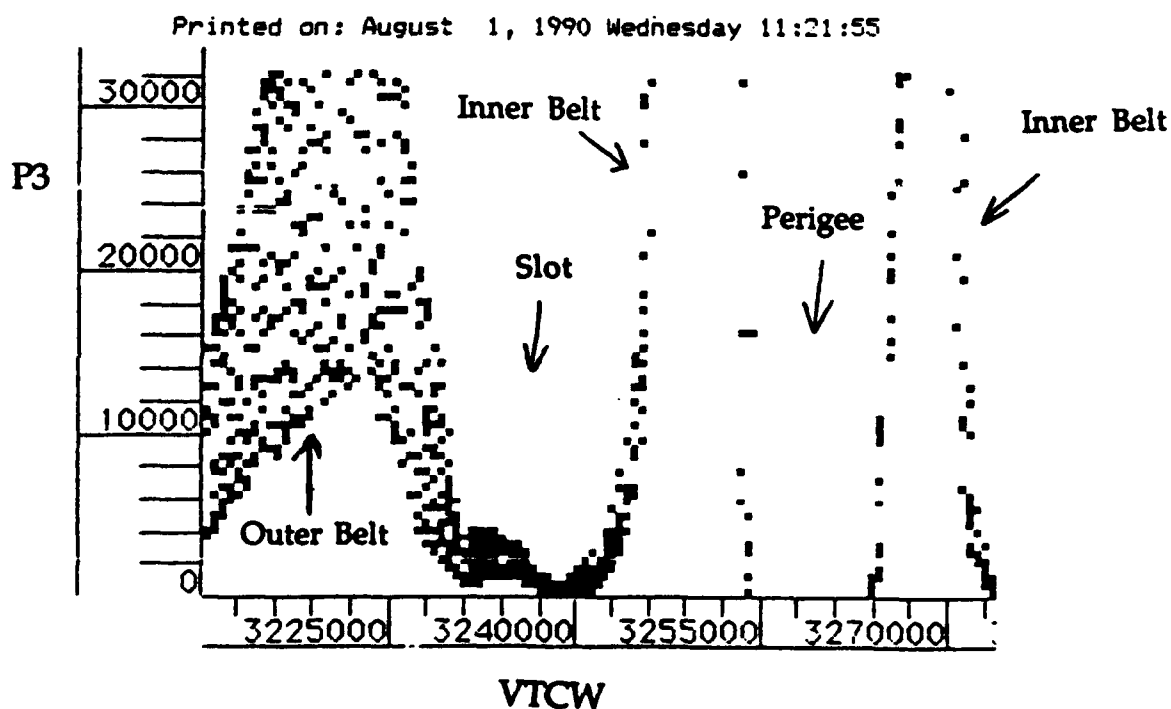
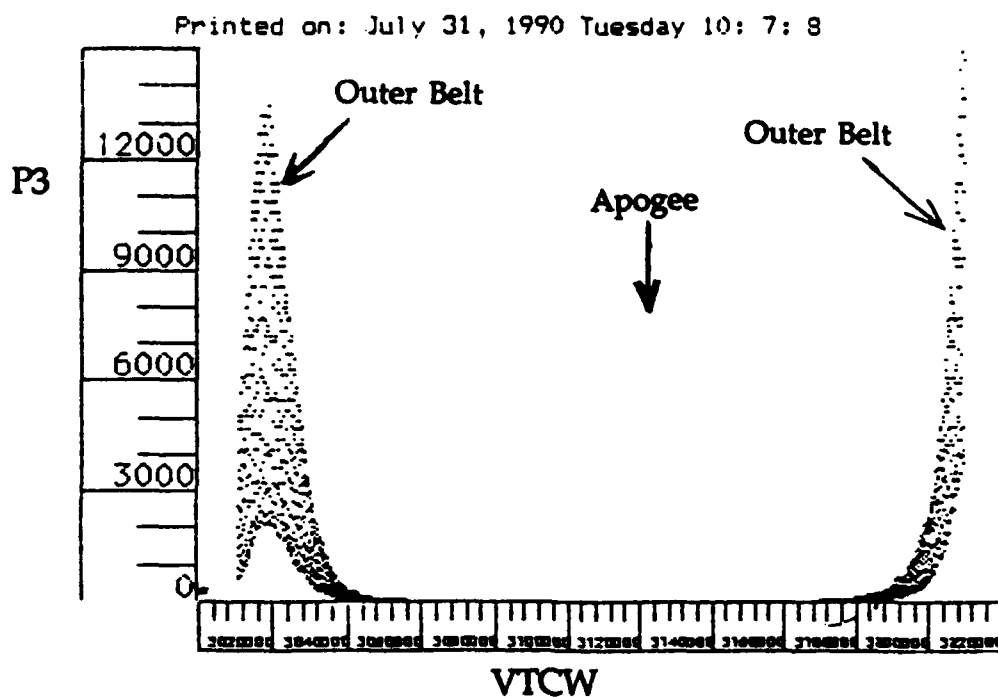


Figure 21. One of the first full orbits of data from ONR-604. Plotted is the P3 counting rate versus the Vehicle Time Code Word (VTCW) for the Apogee and Perigee portions of the orbit (GSE Run 515).

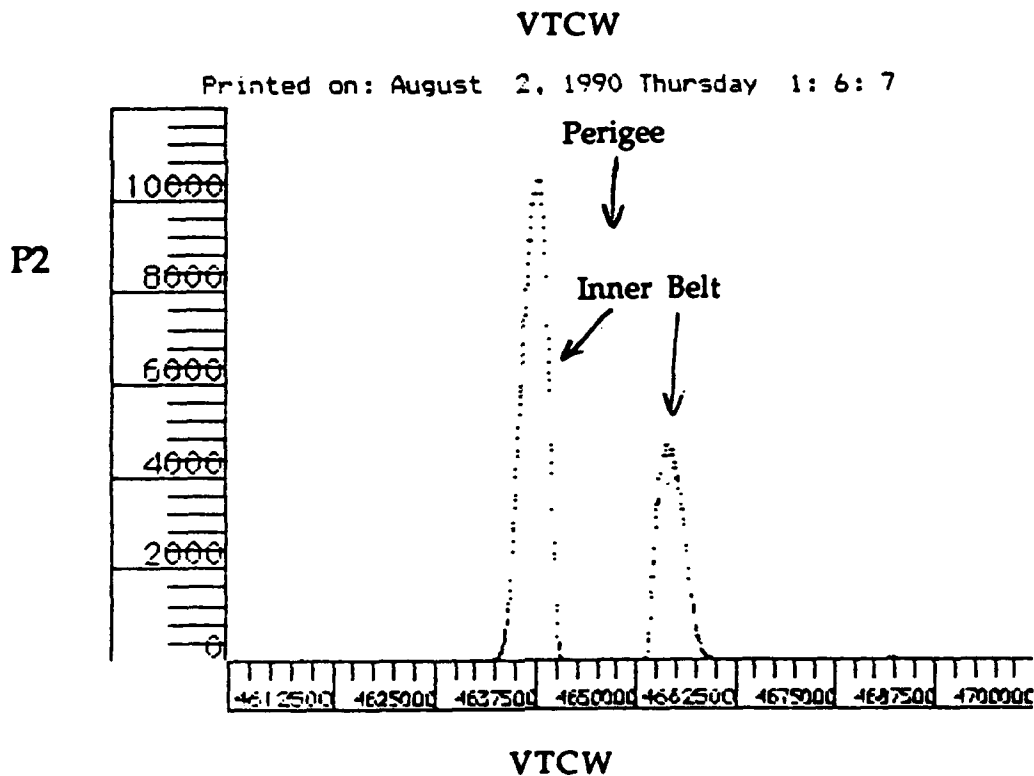
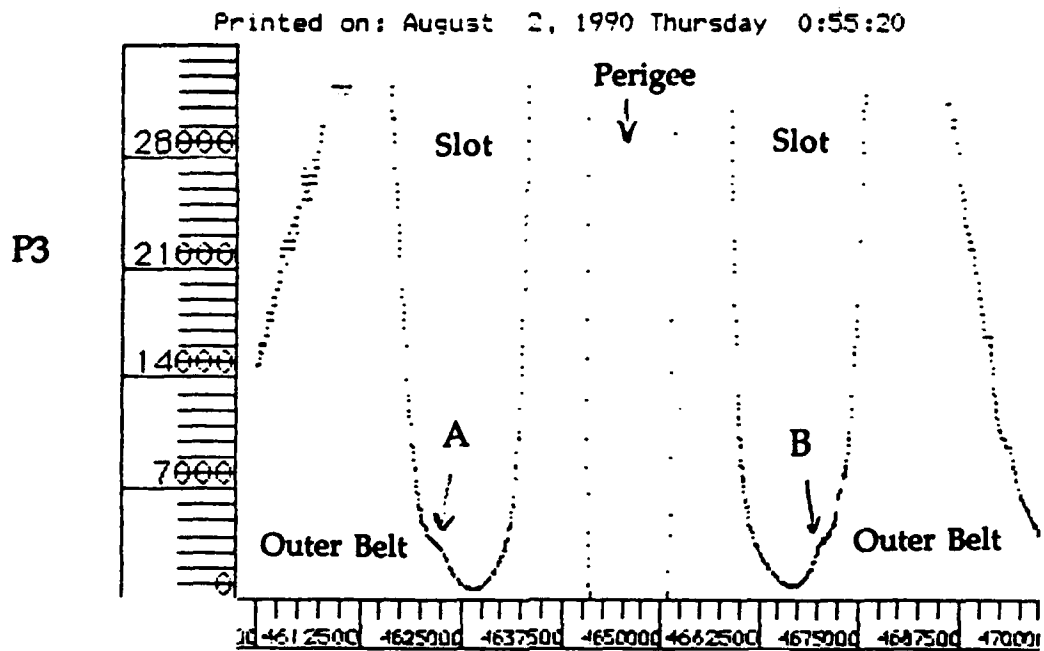


Figure 22. P3 and P2 rates versus VTCW for a full orbit of ONR-604 data in proton mode (GSE Run 521).

belts at perigee and during this apogee pass. Figure 22 shows a comparison of the P3 and P2 rates for a later pass with the instrument still in proton mode. Two features (marked A and B) appear in the slot region and appear to have longitudinal symmetry. The surprise here is the lower plot in which P2 (nominally $Z \geq 2$) shows a strong response in the inner belts but is insensitive to the outer belt particle population. The inner belt response may be to proton interactions or to event pile-up (such as observed during the accelerator calibration runs), but the exact nature of the response must be investigated further.

The data shown on Figure 21 and 22 indicate that (1) the P3 counting rate (and the D1, D2, D3 amplifiers) reach exceptionally high values in the inner magnetosphere, and (2) the P2 pulse height analysis will work only outside of the inner zone. Thus, it was prudent to protect the top detector systems by commanding the instrument into normal (=heavy) mode. However, this eliminates the measurements of protons at apogee. Therefore, an operational plan was developed and implemented at CSTC whereby on every orbit the instrument is commanded into proton mode at an altitude of ~26,600 km outbounds and is returned to normal mode at the same altitude on the inbound leg of the orbit. This is the operational sequence shown in Figure 10a and has been followed for essentially all of the mission thus far.

Figure 23 shows an expanded view of the outer belt region as seen in the D2 and the P3 counting rates. Note the strong spin modulation in the rates (spin rate ~2.6 rpm at this time). Demodulating the rates, in order to look at data on short time scales (~4 seconds), will be necessary to understand the instrument response within the radiation belts.

d. Post-launch Performance

The ONR-604 experiment is monitored continuously through periodic IFC runs, through the singles and coincidence counting rates and through the pulse height analyzed events. With one exception (discussed below) the instrument continues to function nominally. The engineering parameters are also watched to ensure a constant temperature, and there has been little or no short term variation and an acceptable long term drift.

ONR-604 has suffered one minor degradation. It was noticed that in late October the P1 amplifier failed to produce a full signal. The maximum output was a factor of 10 smaller than expected. The other amplifier on that detector (E1) continues to respond normally to both IFC runs and to particle events. Thus, we conclude that the problem is not in the detector itself, but is probably a component failure in the pre-amplifier circuit. In any case, the position information from D1 is degraded. Position is given by the ratio P1/E1 so that a P1 signal down by a factor of 10 will give a position always on one side of the detector. In fitting a trajectory to the

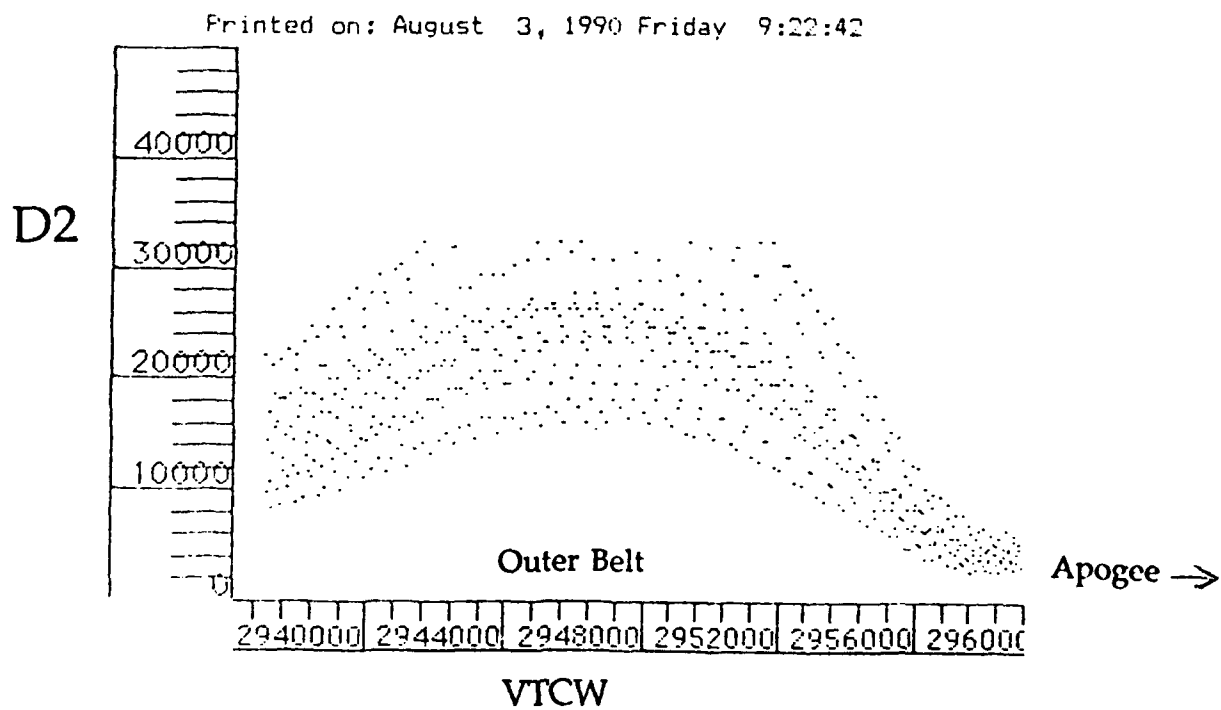
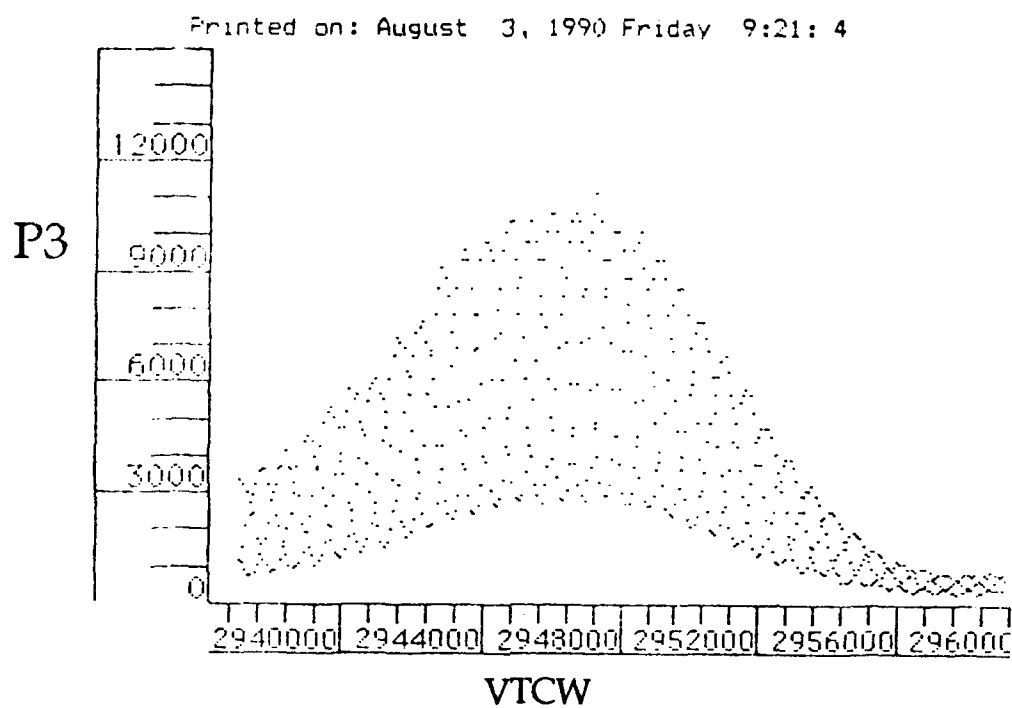


Figure 23. Expanded plot of the P3 and D2 counting rates for an outer belt pass approaching Apogee (GSE Run 508) showing the spin modulation in the rates

PSD positions, this aberrant point will affect the fit and will show up as a large "int residual," a parameter that is calculated for each trajectory. However, there are three PSD's (D1, D2, D3), for redundancy, in the top layer, so that the loss of position information from one of the three is not a significant degradation to the instrument's capability for reconstructing the particle trajectory.

The difficulty here is that the processing software had been constructed for six PSD signals. A new algorithm had to be implemented that used only five signals. This then had to be de-bugged and tested and incorporated into the processing software. This halted all processing until the algorithm was available, and required reprocessing of some of the affected orbits. However, when compared to the trajectories derived from six PSD's, the five PSD results are essentially identical. It is difficult to see any loss of precision in the trajectories. P1 is still being monitored but, so far, has not returned to good health.

Figure 24 shows a comparison of the P1 events that have been analyzed for the first ~9 months of the mission with the accelerator calibration data. Note that the segmented Neon track appears in both plots, Mg and Si are reasonably distinct and the iron track appears in the proper location. The flight statistics are still too meager to unambiguously identify many of the other elements, but preliminary charges can be assigned based upon calculated positions of the tracks. From this comparison, we conclude that the amplifiers have remained in calibration and that the detectors continue to function properly.

4. DATA SYSTEM DEVELOPMENT

In order to accomplish the tasks previously discussed, the ONR-604 raw data must be processed to (i) convert the data to "physics" units (e.g. particle trajectory angles in degrees, energy deposits in MeV), (ii) obtain auxiliary information necessary for maintaining the health and calibration of the instrument, and (iii) prepare the data for subsequent analysis. This processed data must then be further reduced to selected rates and elemental fluxes for particular geomagnetic environments and times before information on, for example, the level of solar modulation, active/quiet times and GCR/SEP composition and spectra can be obtained. Much of this years effort at LSU has been associated with developing such a data system, including the correct procedures and software for data processing and reduction. To date, most of the fundamental processing activities have been established, but additional effort is still required to implement the higher level data reduction. In addition, the system must include ancillary data that will be employed for model analysis.

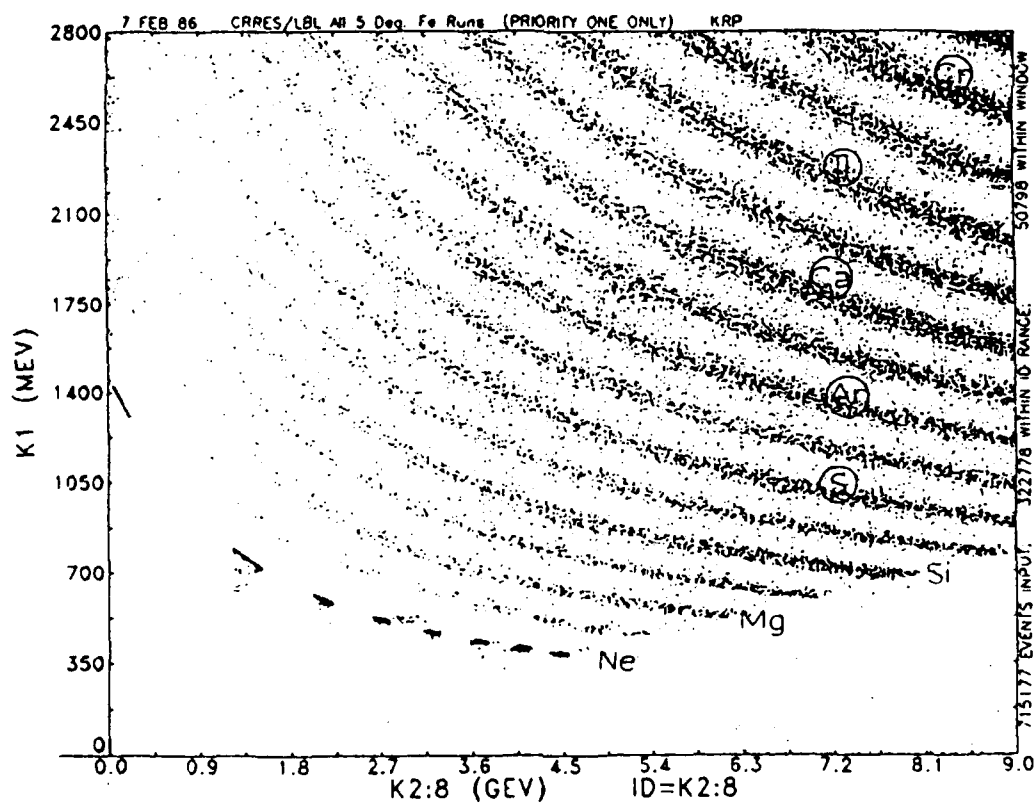
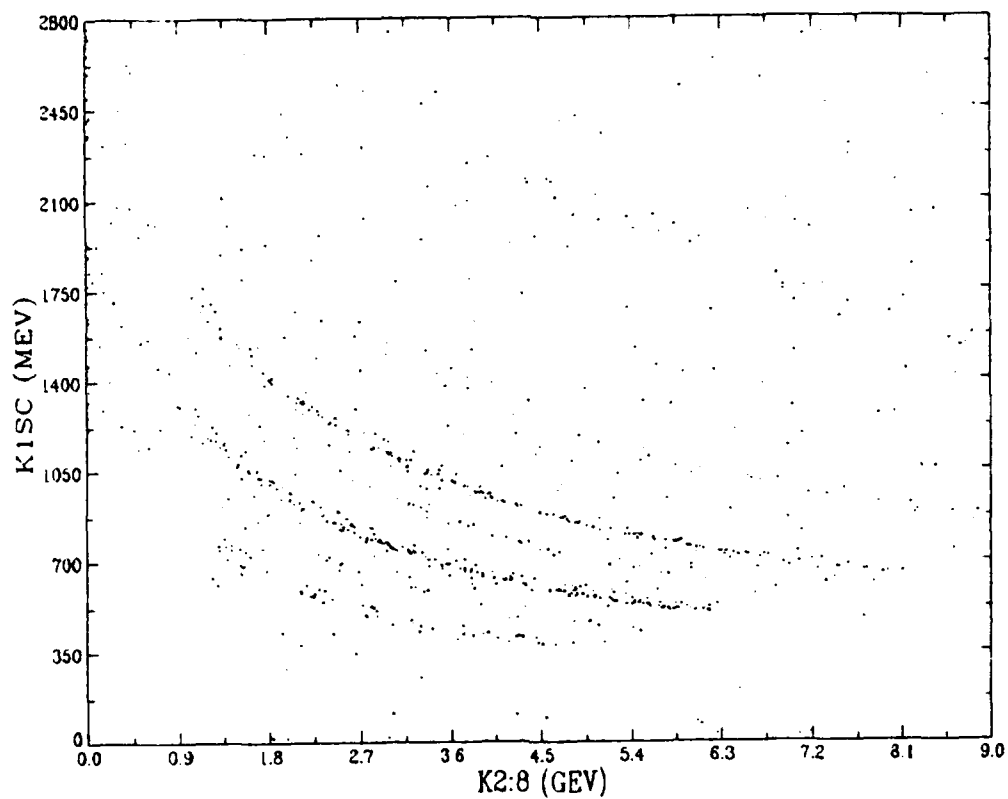


Figure 24. Comparison of the K1 versus K2-K8 matrix for P1 events from flight data (top) and accelerator calibration data (bottom).

a. Reduction and Processing

The data flow through the current LSU processing and reduction software is shown in Figure 25. Data from ONR-604 is received by LSU from the University of Chicago (UC) in the form of a processed C2ET data tape. These tapes contain the raw and processed PHA events, rate records, engineering/housekeeping data and associated magnetometer and ephemeris information for 5 consecutive orbits with a file for each orbit. Startup delays in generating Agency Tapes for UC and final debugging of the UC processing software delayed the beginning of routine production of C2ET tapes until the beginning of 1991. Currently, however, LSU is now receiving 10-15 tapes from UC every 3 to 4 weeks. As of 7 October 1991 LSU has received 168 C2ET tapes from UC containing data up to orbit 840 (\approx 15 July 1991) and has completed initial processing up to orbit 725 (\approx 22 May 1991). Initial on-orbit spacecraft and instrument checkout occurred during the first 60-70 orbits of these data and correct attitude information is not available. Thus, the first GCR Model Report will include 6 months of data beginning \sim 1 September 1990.

The initial step in the LSU processing is to use the COPY_FILES program to generate a duplicate of the C2ET tape in a format compatible with the LSU VAX/VMS processing equipment. The program LIST_FILES is then run on the LSU C2ET to validate the duplicate and generate an "overview" listing of the tape contents. Once the LSU C2ET tapes are verified the original tapes are returned to UC for reuse. Backup versions of the C2ET are archived at UC and only one copy of these tapes are kept at LSU.

The next major operation is to use the program RATE_GEN to generate a Rate Parameter Tape. This tape is formatted specifically as input to the PIMPLOT production plotting program and contains data on the singles, coincidence and PHA priority rates as well as some ephemeris and housekeeping data. Time history plots (see Figure 10a-e), of these data are generated for each orbit on a pen plotter, are archived and are used to monitor instrument health and calibration, to monitor geomagnetic particle activity, and for the initial analysis of Solar Energetic Particle events.

The detailed analysis of the ONR-604 data usually requires only specific portions of the full dataset contained on the C2ET tape. Thus, as indicated in Figure 25, the program SPLIT_FILES is used to generate several data subsets which are then archived for later use. Processing and reduction software for the subsets is still under development and we have initially concentrated on interpreting the instrument rates as these are the key to reliably selecting particle active/quiet times and to determining the absolute particle flux. As a result several programs now exist which process the Rates dataset into higher order information. The program SC_Z provides information on the precise position and orientation of the instrument with respect to the geomagnetic field. This is needed for determining geomagnetic cutoffs and for tracing particle trajectories through the field in order to determine if the event is a trapped particle or has penetrated from interplanetary

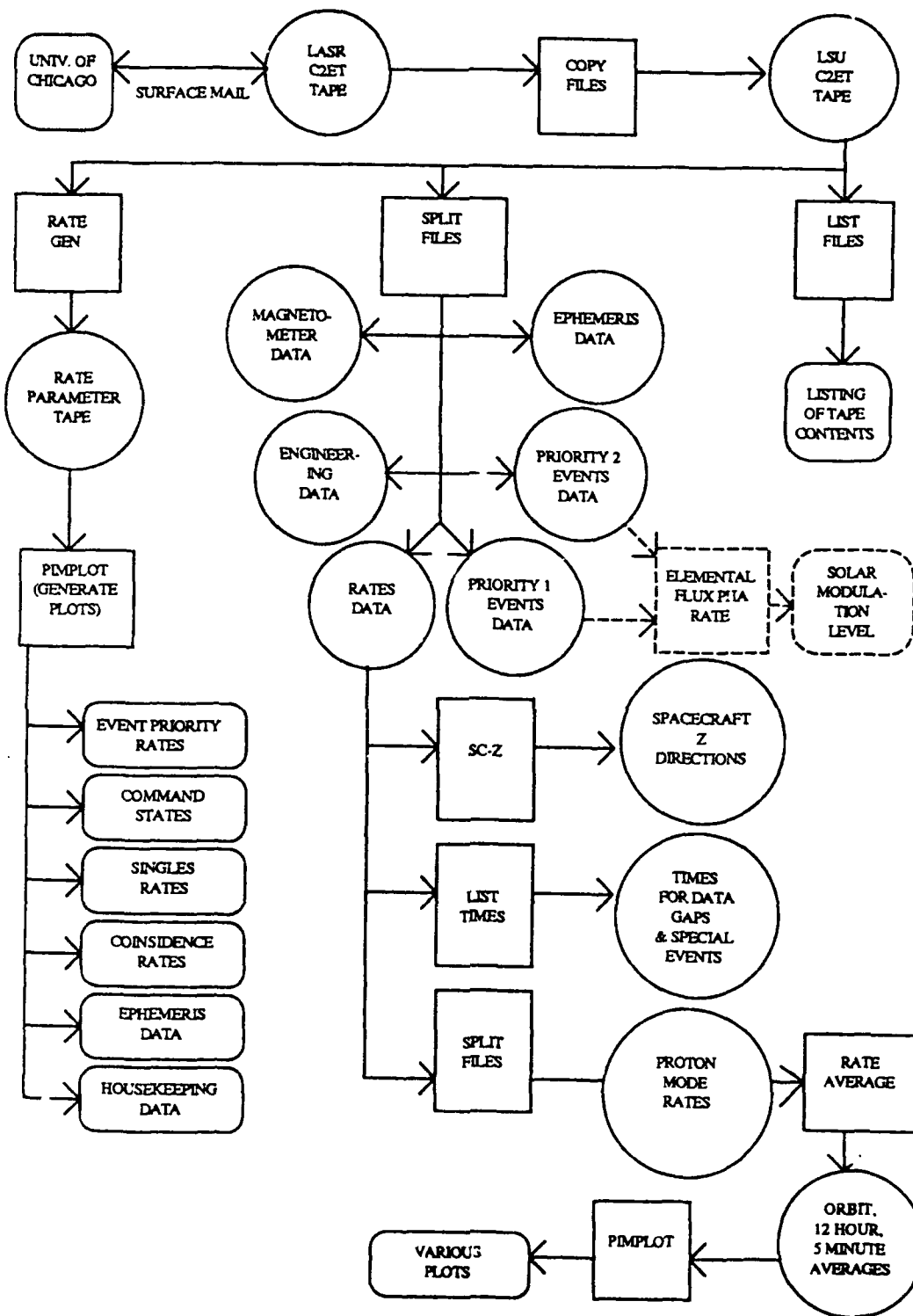


Figure 25. Data Flow through the current LSU Processing System.

space. The program LIST_TIMES identifies start and stop times for data gaps, orbits, JFC runs, gain changes and other special events. This information is needed for correctly determining and evaluating rate averages. Using SPLIT_FILES the Rates data is further selected for that portion of the spacecraft orbit which is nearest apogee, at the highest L shell values (generally greater than 4) and also when the instrument gain changes to "Proton Mode". Proton Mode allows ONR-604 to collect proton events which are normally excluded during passes through the intense radiation belts. Averages of these rates for 5 minute, 1/2 hour and orbit time periods are generated by the RATE_AVERAGE program and time history plots are generated once again by PIMPLOT. These "Proton Mode Rates" are then used to examine the particle environment which is least affected by geomagnetic effects and which should be dominated by interplanetary GCR and SEP particles.

Currently, software to process the Event data subsets is under development. Two such subsets are split from the C2ET tapes according to their assigned PHA analysis priority; Priority 1 is assigned to events which appears to be of charge ~ 10 or above and Priority 2 is assigned for charge ~ 2 and above. PHA events assigned the remaining, lowest priority (3) will also be split from the C2ET tapes once methods for handling the electron and proton pile-up background evident in these low charge data are developed. Current effort, however, is focused upon obtaining a measure of the Solar Modulation Level as a function of time from the Priority 1 and Priority 2 events. This involves converting the PHA counts into a "rate" for use in determining instrument live time and event collection efficiency; further subdividing the data into quiet and active times to separate the data associated with the GCR from that associated with SEP; determining the event charge, energy and trajectory just outside of the spacecraft; isolating geomagnetically trapped and penetrating particles using trajectory tracing or cutoff calculation; and applying appropriate instrument geometry factors, collection efficiencies and live times to determine absolute elemental fluxes. The Solar Modulation Level is then obtained by adjusting this parameter in the GCR Model until a best fit is obtained with the elemental fluxes. After this effort is completed we will then move on to establishing the processing methods for modeling SEP events. At this point SEP active times should already be isolated in separate datasets and the raw data should be converted in flux measurements. Thus, the remaining effort here will be to model the time profile and to determine the relative enhancement of heavy ions for each SEP event.

Analysis of the ONR-604 particle environment data is neither straight forward nor simple due to the complexity of both the instrument and the environment. It is likely that with improved understanding of both, the data processing and reduction requirements for ONR-604 will be altered. This can lead to unanticipated developments or simplifications to the processing scheme outlined in Figure 25.

b. Ancillary Databases

While the ONR-604 data is the major component in the LSU analysis effort, it can not provide all of the information required for a complete model of the particle environment. Thus, LSU has begun to establish a database of auxiliary information which will be used to complement the ONR-604 analysis. Components of this database which are now established and maintained at LSU, are shown in Figure 26.

The auxiliary data include IMP-8 proton and helium fluxes and quiet time selections in various energy bins and the Climax station neutron monitor data from the University of Chicago. These data are regularly downloaded to LSU over the NSI/DECnet network, and plotted for use in the selection of quiet and active time periods and, eventually, to aid in determining the solar modulation level.

Daily reports of solar activity are obtained from the NOAA Space Environment Laboratory again using the NSI/DECnet network. These reports which include X-ray fluence plots, geomagnetic storm and solar activity summaries and forecasts, and listings of recent solar events are printed and archived. In addition, the event reports are stored online for later "real-time" access. Geomagnetic and Solar Indices such as K_p and D_{st} are obtained from the National Geophysical Data Center on floppy disks. These are read on a IBM-PC and transferred to the online VAX database using the local DECnet network. These indices are used to correlate the active particle fluxes measured with ONR-604 to geomagnetic and solar disturbances.

Proton and electron particle data is also obtained from the geosynchronous GOES satellite from the National Geophysical Data Center. This data is received in the form of 5 minute averages on floppy disk and for the full time resolution (3 seconds) on magnetic tape. In addition, the 5 minute averages are received every month and are usually only a month or so off real time, while the full time resolution dataset can be delayed up to 8 months. Finally, the OMNI interplanetary conditions (e.g. solar wind velocity, interplanetary field) are obtained from the NSSDC over the NSI/DECnet network.

It is expected that this database will be expanded in the future to include data from other CRRES instruments as these become available in the Science Summary Database maintained online at AFGL. In particular, proton and electron data may be used for direct comparison with the IMP-8 and GOES data and for completing the low charge, low energy portion of the GCR Model.

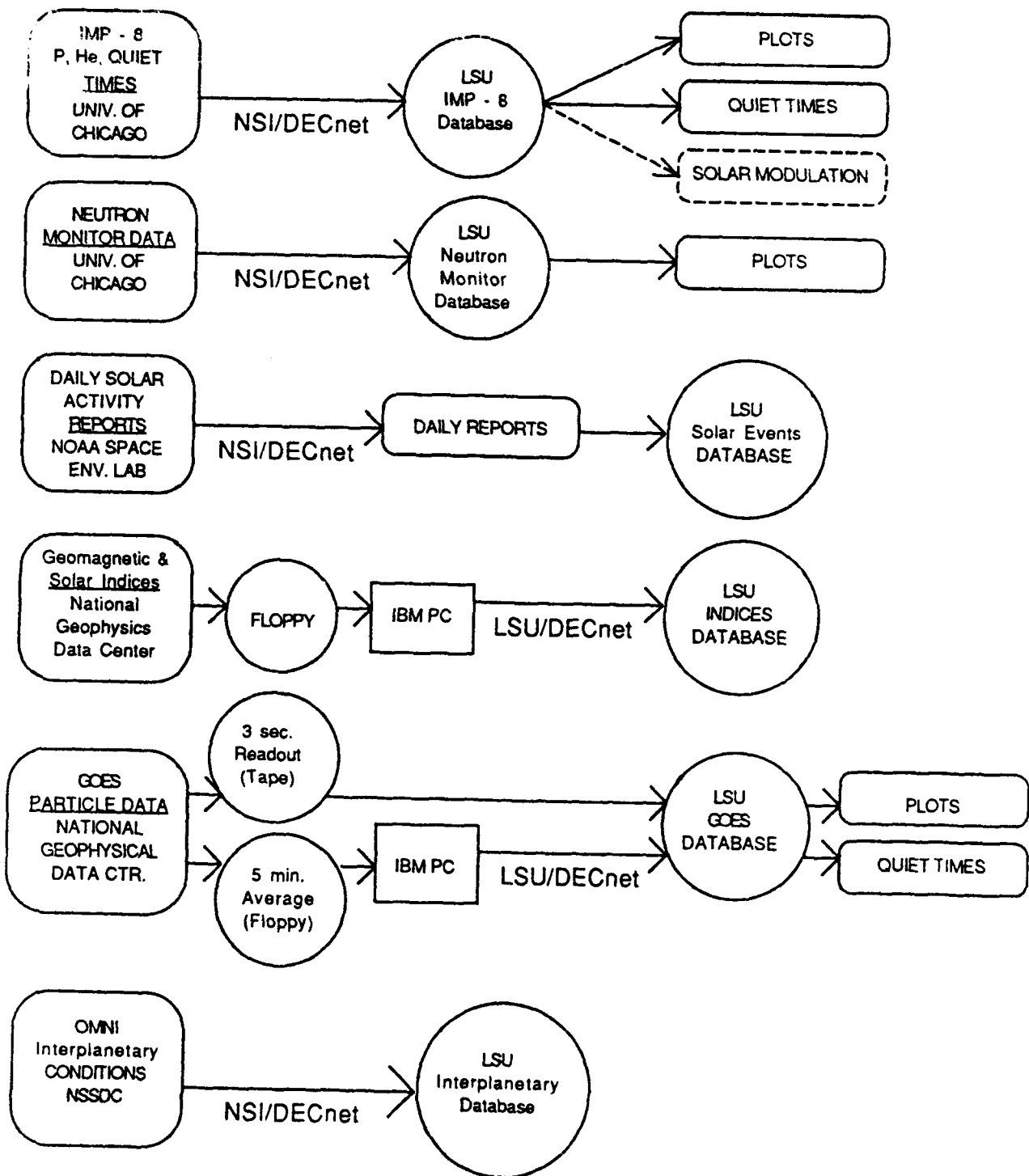


Figure 26. Auxillary databases established as part of the modeling effort.

5. THE HEAVY ION ENVIRONMENT IN LATE 1990-EARLY 1991

a. Overview

The CRRES spacecraft was launched during a period near the maximum of the solar activity cycle, as illustrated in Figure 27 (top), which shows the last four solar cycles as seen by ground based neutron monitors. Data from both Climax and McMurdo are shown, and these two stations "track" well. McMurdo, located near the south pole, has a lower geomagnetic cutoff than Climax, Colorado but the mean energy of the incident particles producing the counting rate is almost the same. Note that 90-91 was a period in which the neutron monitors reached their lowest level, compared to previous solar cycles. This low level indicates very strong solar modulation for the cosmic rays.

The bottom portion of Figure 27 shows an expansion of the late 1990-early 1991 period. CRRES was launched just after the minimum in the neutron monitor rate, and was on an increasing intensity curve (recovering towards solar minimum conditions) until late March 1991 when the flare activity halted the recovery. However, the time period between ~1 Sept. 90 and 1 March 91 appears to be a relatively quiet period and was selected as the first six month period for model analysis.

Figure 28 shows the selected period in more detail. Compared are the P2 and P3 rates for Apogee ($L > 6.5$) and for all proton mode data (PM, at bottom) and the GOES proton counting rates P5 (39-82 MeV) and P3 (8.7-14.5 MeV). Note the ONR-604 P2 ($\geq \text{He}$) rate which appears relatively constant. No major heavy ion flares occurred during this period. The ONR-604 P3 ($L > 6.5$) rate, however, does show some proton or electron events. These are correlated, for the most part, with the low energy proton increases seen in the GOES P3 channel. The larger events are discernable in the GOES P5 rate as well. Now, when the ONR-604 rates are plotted for all proton mode data (bottom two plots), the P3 rate shows considerable activity while P2 remains relatively constant. The extra spikes in P3 are, presumably, of magnetospheric origin. Only near apogee can the ONR-604 counting rate for P3 be used to trace the interplanetary proton component.

The top panel of Figure 28 shows the interplanetary quiet times (unshaded) as determined from IMP-8 proton data. The correlation of the shaded areas with the increases seen in the GOES P3 rate is reasonably good. A full picture of the IMP-8 quiet time selections for 1990 and the first part of 1991 is shown in Figure 29, where the energies corresponding to the three proton and three helium channels are indicated at the right. Plotted are the raw counting rates, overlaid with the quiet time selections. As expected, the lower the energy interval, the more "active" appears the interplanetary medium and the smaller are the intervals selected as "Quiet Times." For heavy ion analysis, however, the 25-93 MeV/nucleon Helium interval is most applicable. For this rate there are only a few "non-quiet" periods, which agrees with the CRRES P2 rate in Figure 28. Thus, for the selected period

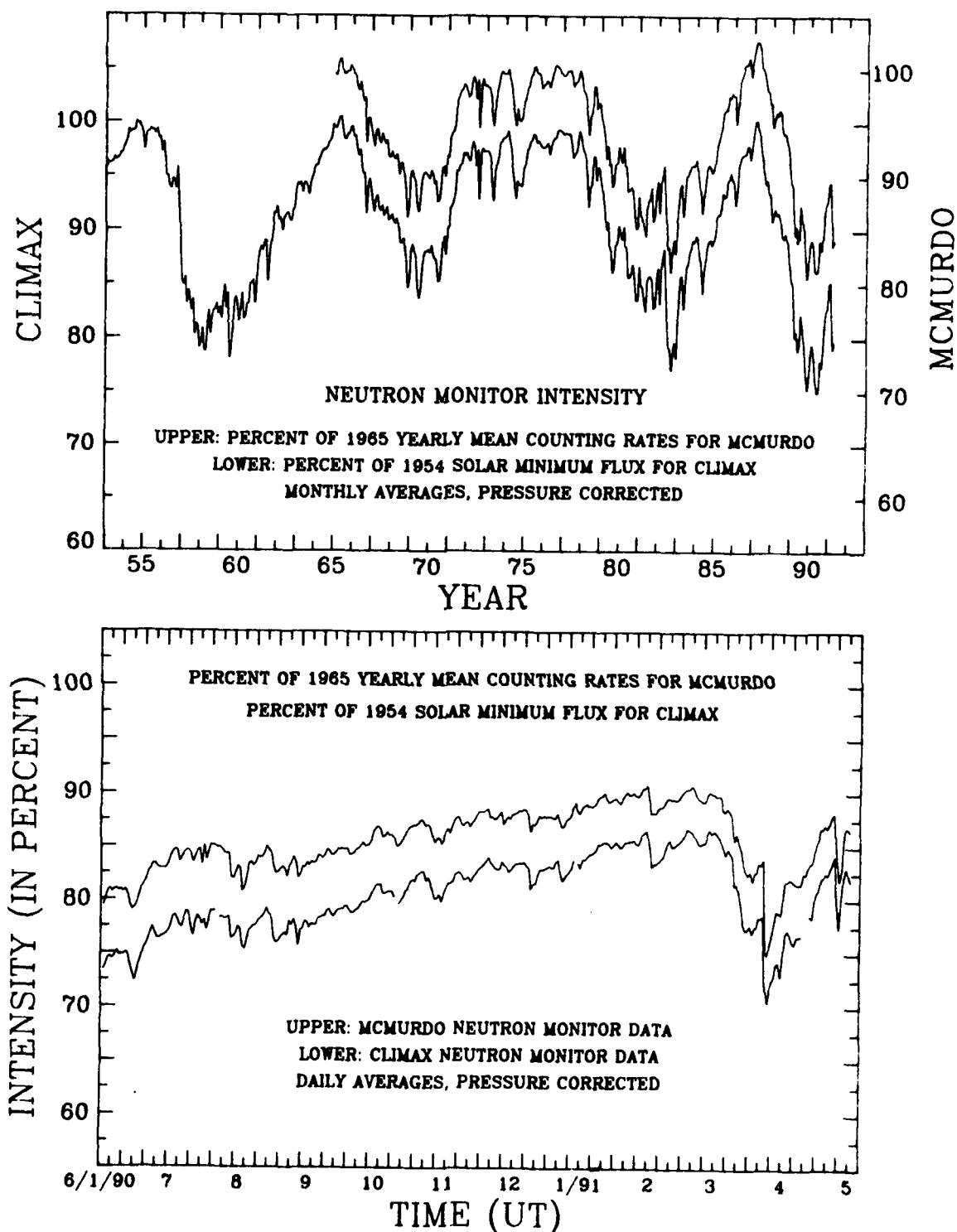


Figure 27. (Top) Four solar cycles of neutron monitor data from Climax (courtesy University of Chicago) and McMurdo (courtesy Bartol Research Institute). (Bottom) Expansion of the latter half of 1990 and the first part of 1991.

essentially all of the ONR-604 P2 and P3 data from proton mode periods can be employed for environment analysis.

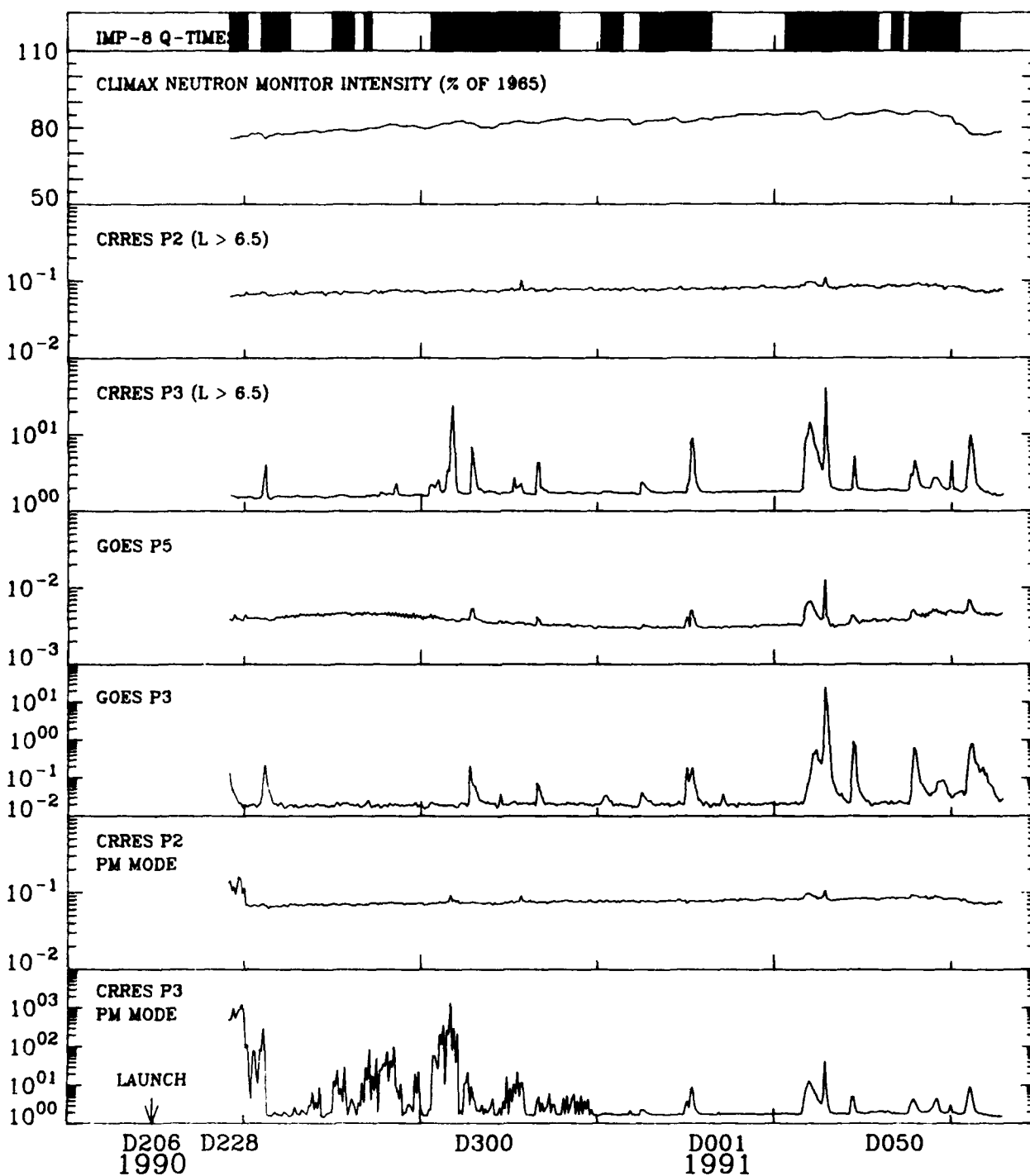


Figure 28. Comparison of ONR-604 CRRES rates with GOES and neutron monitor data.

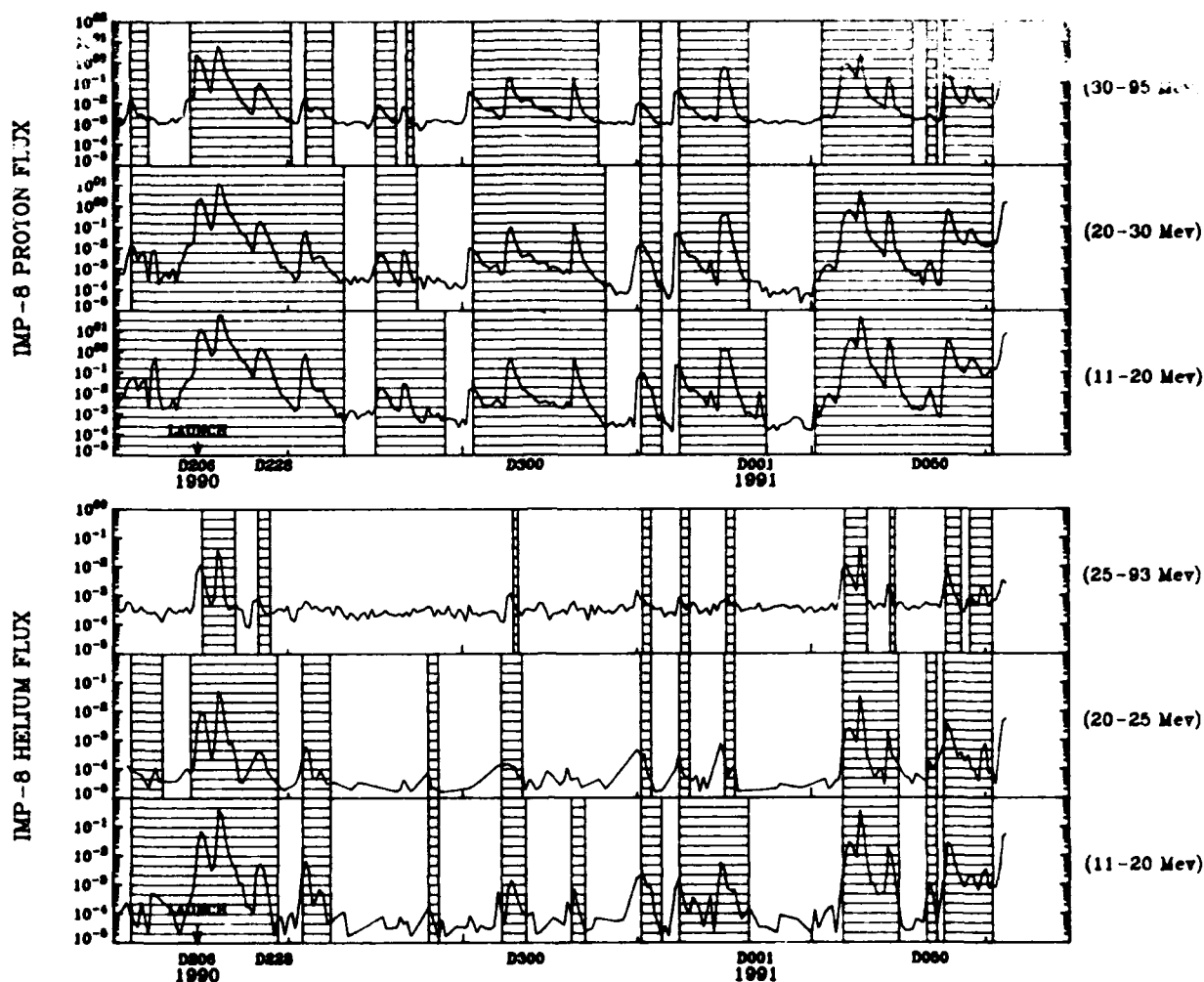


Figure 29. IMP-8 quiet time (clear areas) determined from six different channels.

Figure 30 (top) shows the number of P1 events recorded as a function of orbit and the L distribution of P1 events (bottom). The 22-24 March flare period starts at orbit 584, for which no noticeable increase is observed. There is a gradual increase in the overall rate which is consistent with the decreasing modulation shown by the neutron monitors (Figure 27). In L Space, most of the events occur at $L > 5$ with a band at $L = 6.5$ which is the location of the geomagnetic equator. The CRRES orbital plane and the geomagnetic equatorial plane are effectively aligned at ~orbit 500. What is interesting is that there are a handful of events observed at low L values. These are most likely high energy GCR events but could also be pseudo-trapped particles or sub-threshold events, as have been reported by others (Oschlies et al., 1989; Durgaprasad et al., 1990; Adams et al., 1991).

During initial processing of the ONR-604 data, each event is assigned a preliminary charge and a preliminary energy. The preliminary charge and energy distributions are shown in Figure 31. The Mg shows the largest abundance as expected since part of the Ne is in priority 2. The iron peak is also evident as are a few events of Co + Ni. Note, however, that there are events above Ni and events

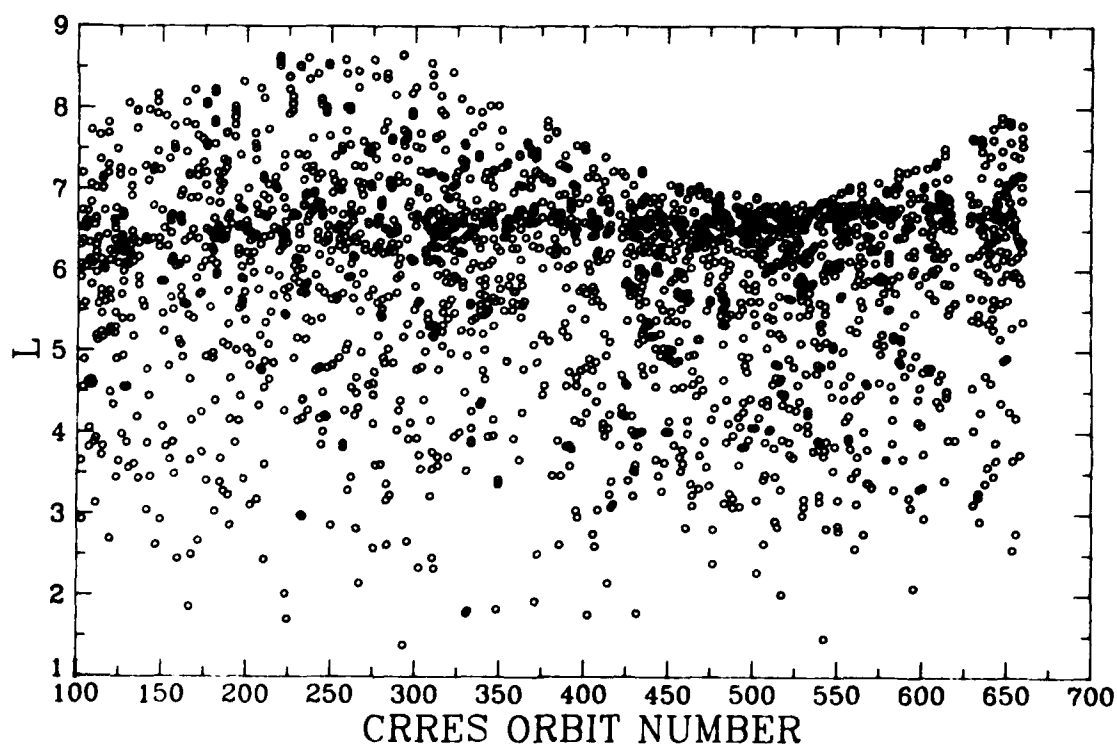
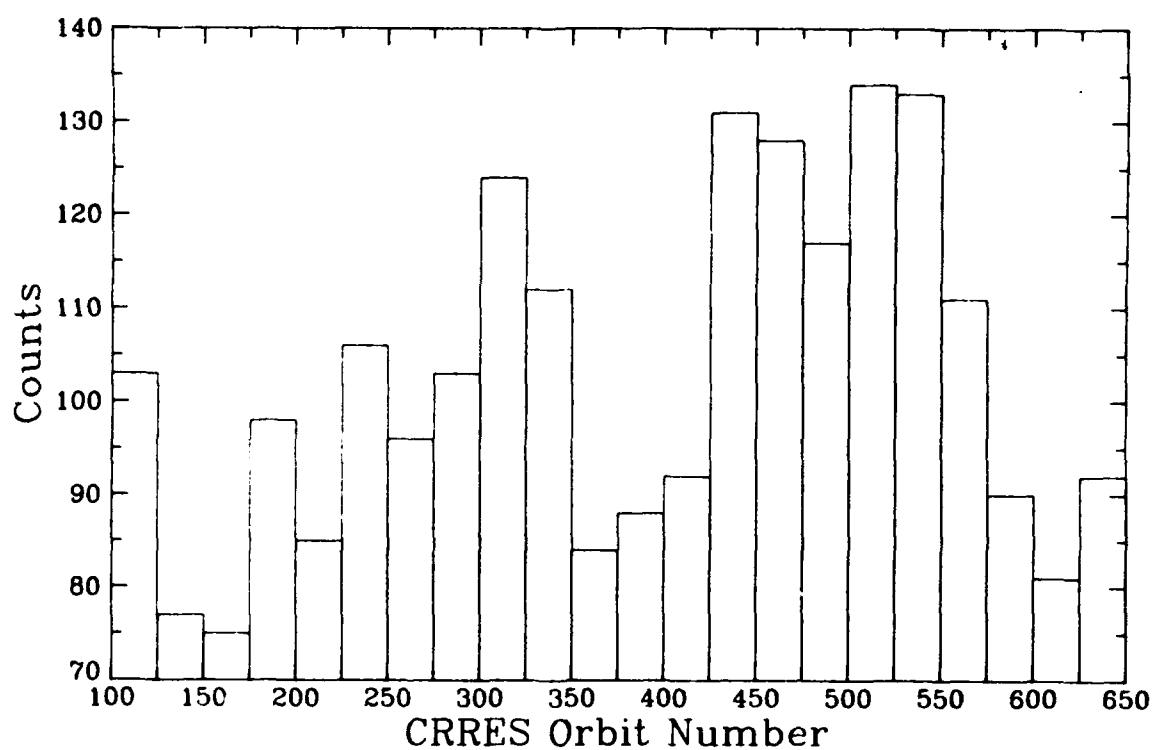


Figure 30. The number of P1 events as a function of orbit number (top) and the L distribution of P1 events (bottom).

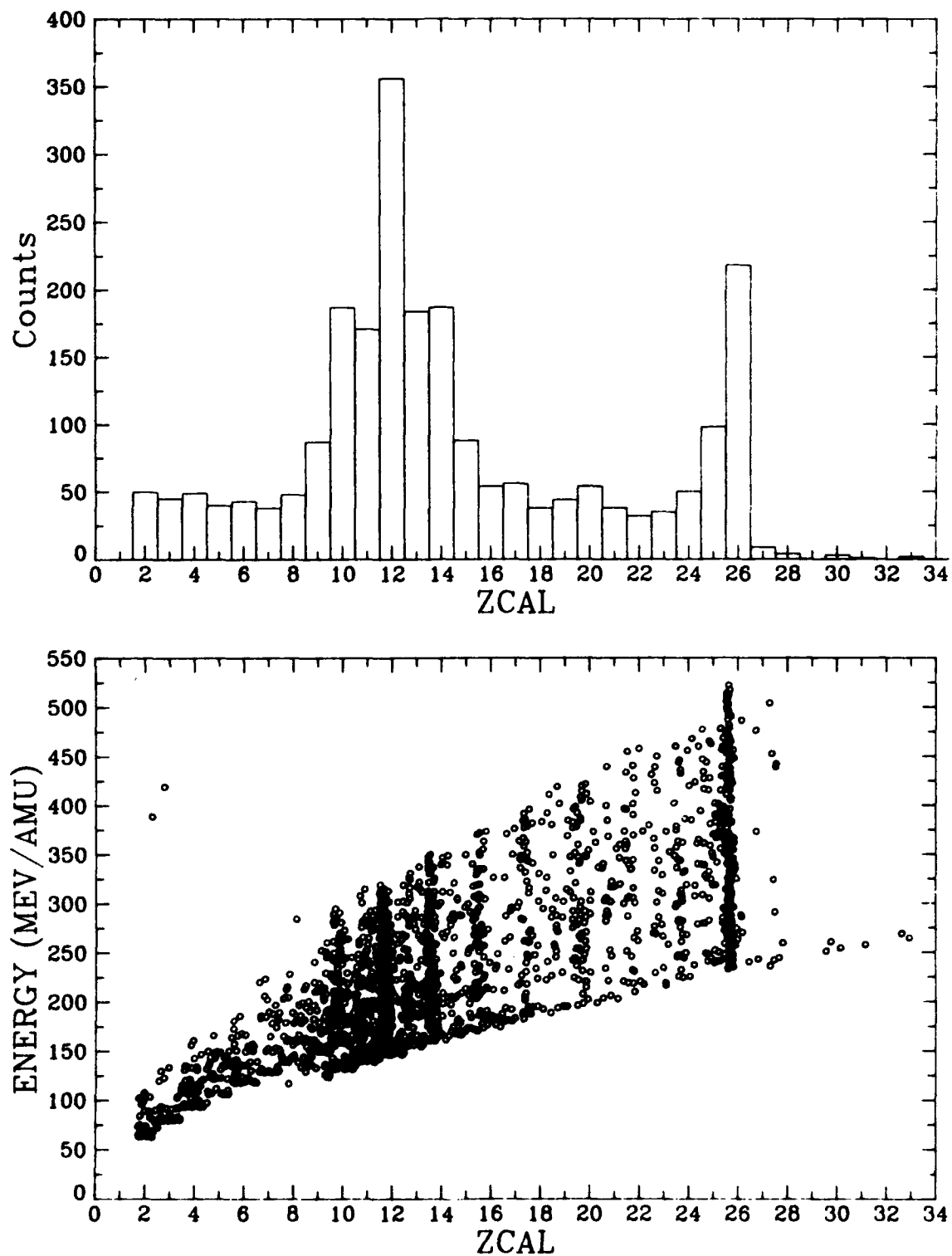


Figure 31. Charge distribution (top) and energy vs charge plot (bottom) for P1 events.

below Oxygen. Also, the odd-Z elements are more abundant than expected. This suggests that (1) the preliminary ZCAL charge assignment is not completely accurate, and (2) there is potential "background", at the <15% level, among the P1 events. The energy distribution shows the expected energy ranges (c.f. Figure 9) for each element, with the exception of the low-Z events which should not appear in P1. There are only a few events outside the nominal energy limits.

The preliminary Z values are calculated from only the information in the last two detectors triggered. Thus, if a particle interacts in the stack sending a low-Z fragment forward, it is the fragment's Z that will be assigned. This can account for some of the low-Z events, but probably not all. Multiple particles are also a possibility as are bit errors that assign a P2 event to the P1 category. Considerably more investigation is required both to develop a better charge calibration and to understand the background contributions among the P1 events.

b. Solar Modulation

It is well known (see reviews by Jokipii 1971, Fisk 1979, McKibben, 1986) that at energies below a few GeV per nucleon the intensity and the spectral shape of the cosmic rays arriving at the orbit of Earth are significantly modified by solar modulation. The cosmic rays diffuse into the heliosphere against the outward-flowing solar wind, carrying frozen-in interplanetary magnetic field, which convects the cosmic rays out of the heliosphere. In this process, the cosmic rays lose energy to the expanding field (adiabatic deceleration), and their energy spectrum is modified.

A spherically symmetric model of solar modulation has been developed (Parker 1965; Jokipii 1971; Urch and Gleeson 1972; Fisk 1979) which explains most of the gross features of the modulation process. This model includes the effects of diffusion, convection, and adiabatic deceleration (but not drifts due to the gradient and curvature of the magnetic field) and assumes that these three physical processes are in equilibrium in the heliosphere. Quantitatively these effects are represented by a Fokker-Planck equation in which the parameters are the solar wind velocity, the diffusion coefficient and the radius of the heliosphere, with the cosmic-ray differential energy spectrum in local interstellar space as a boundary condition.

Evenson et al. (1983) (see also, Garcia-Munoz et al. 1986), solving this equation numerically, have analyzed the simultaneous modulation of electrons, protons, and helium nuclei over the 1965-1979 period involving more than one solar cycle. They find that in general the model fits the data quite well. In this model the degree of modulation at a heliospheric radius r is given by the modulation parameter

$$\phi(r) = \frac{1}{3} \int_0^r \frac{V(r')}{K(r')} dr' , \quad (1)$$

where $V(r')$ is the solar wind velocity, $K(r')$ is the radial part of the diffusion coefficient, and R is the radius of the heliosphere. An insight into the physical meaning of ϕ is obtained from the "force-field" approximation (Gleeson and Axford 1968) in which Φ corresponds to a "potential energy," that in the particular case in which the diffusion coefficient is proportional to particle rigidity takes the simple form

$$\Phi = |Ze| \phi(r), \quad (2)$$

where Ze is the particle charge. This potential energy has been identified as the mean energy loss that the particles experience in penetrating the heliosphere to a radius r . The parameter may be expressed in rigidity or energy units, connected through,

$$\Phi \text{ (MV)} = \frac{A}{Z} \phi \text{ (MeV/nucleon)}$$

The modulated nucleonic differential energy spectra obtained by the numerical solution of the Fokker-Planck equation are almost completely determined by the value of the modulation parameter ϕ . Combinations of the parameters R , r , $V(r)$, and $K(r)$ giving the same value of ϕ will lead to modulated nucleonic spectra which are very nearly equal to each other (Urch and Gleeson 1972). Therefore, values of the modulation parameter ϕ are used to specify different levels of modulation, as was shown in Figure 4 for calculated Hydrogen and Helium spectra for different values of the parameter Φ .

Figure 32 (from Garcia-Munoz et al., 1987) shows the time dependence of the modulation parameter used by Evenson et al. (1983) for 1973-1980, compared with the time dependence of the Climax Neutron Monitor count rate (given as the percent decrease below the 1954 solar minimum level). The period 1974-1978, corresponding to solar minimum conditions, was characterized by a nearly constant level of solar modulation for which the average value of the modulation parameter was about $\phi = 490$ MV, or $\Phi = 245$ MeV per nucleon for $A/Z = 2$ particles. This time period, during which much cosmic ray data was recorded, becomes a baseline to which more recent data, in particular the CRRES results, are compared.

There are several approaches to determining the solar modulation level for a specific time period during the CRRES mission:

- (a) Demodulation of CRRES elemental spectra
- (b) Demodulation of IMP-8 elemental spectra
- (c) CRRES Heavy Ion Rate Modeling
- (d) Neutron Monitor Correlation

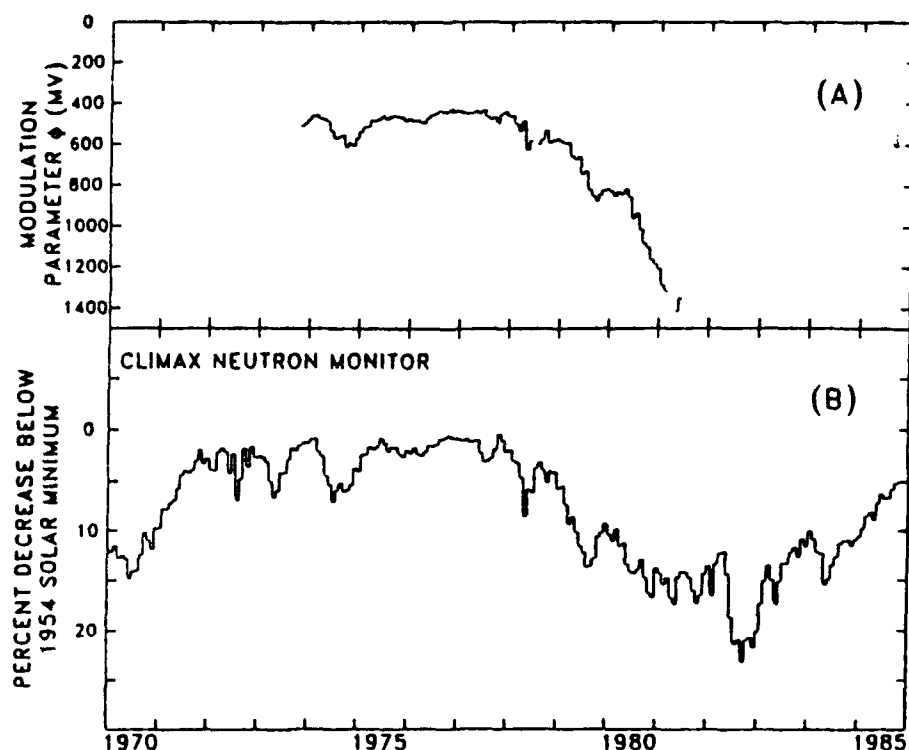


Figure 32. The modulation parameter Φ (MV) for 1974-1980 determined by Evenson et al. (1983) from the flux of 70-95 MeV/nucleon Helium compared to (B) the Climax Neutron Monitor rate.

The normalization procedures and background subtraction methods for ONR-604 have not yet been completed, so that actual flux values, which could be fit by the solar modulation model described above, are not available. However, IMP-8 can be used in the same way, and some preliminary IMP-8 data has been provided by Chicago. Technique (d) exploits the correlation shown in Figure 32, developed for the previous solar cycle. It is not known whether the same correlation holds for the present cycle, and this approach remains to be investigated. What we have concentrated upon during the past year is method (c), which will be described below, and using (b) for validating or comparing the results obtained.

The ONR-604 P1 and P2 rates are dominated by heavy ions -- Mg - Fe for P1 and He - O for P2. Both rates respond mainly to GCR and are relatively insensitive to magnetospheric populations, at least during the apogee portion of the orbit as was indicated by Figure 28. Thus, using the instrument description and operating modes described in section 2, it should be possible to calculate the expected priority rates for any given particle spectrum outside the spacecraft.

What has been done is the following. For each element, the energy range appropriate to a given logic condition is determined (c.f. Figure 9). Then the geometry factor is calculated as a function of energy (range) as illustrated in the left part of Figure 33. Any incident spectrum can then be integrated over the

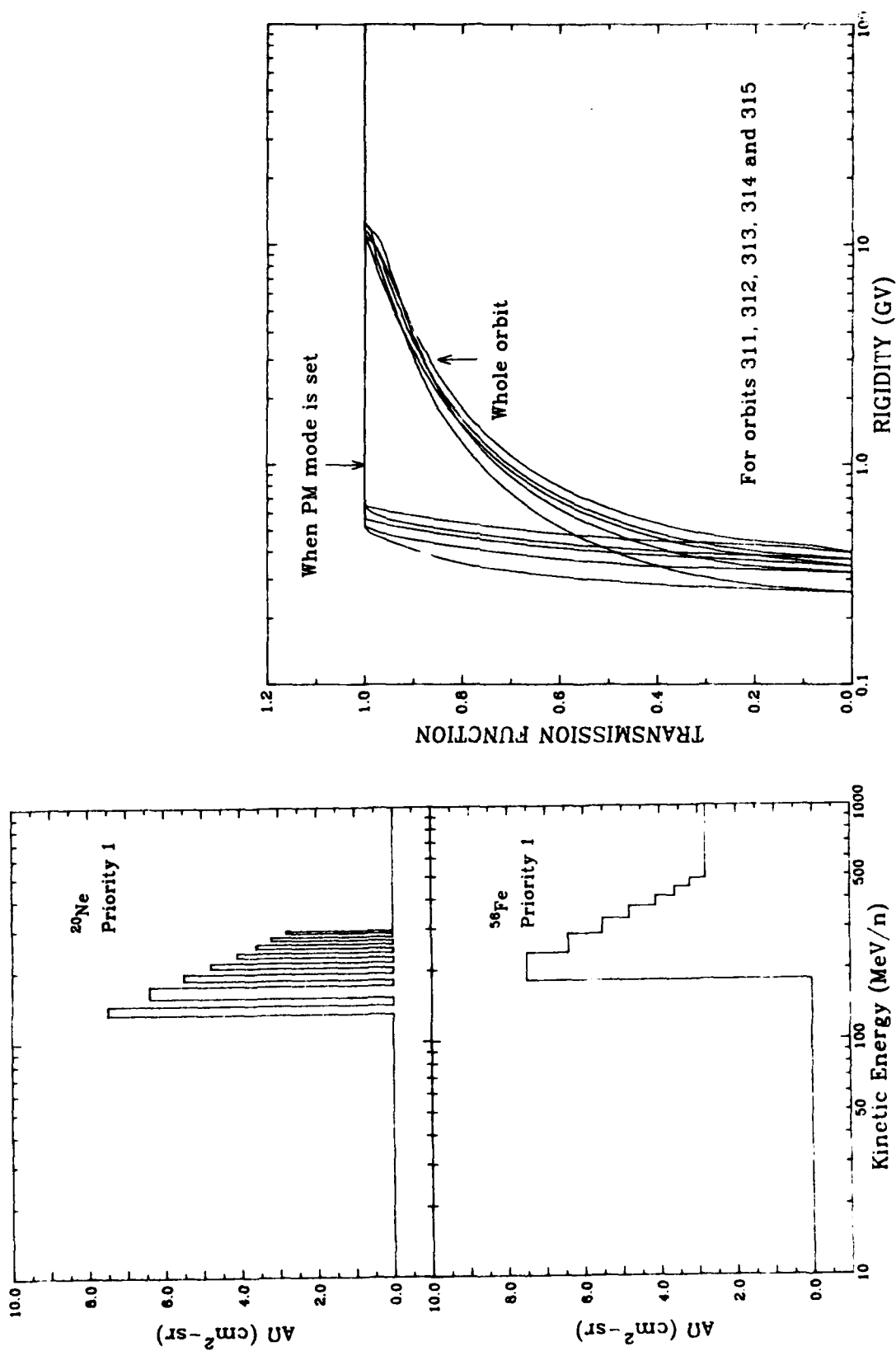


Figure 33. Energy dependent geometry factors for Ne and Fe events (left) and the geomagnetic transmission function (right).

appropriate energy range, folding in the geometry factor, to predict the number of events per second. Repeating the process for all of the elements in a particular logic condition (such as P1), and summing the results, gives a calculated rate (counts/second) to compare to the flight data.

The input spectra for such a calculation are the differential energy spectra outside the instrument, i.e. at the CRRES orbit. This is obtained by folding the interplanetary spectra with the geomagnetic transmission function (see the right portion of Figure 33). For data limited to the apogee portion of the orbit (proton mode for ONR-604) there is little geomagnetic inhibition except at the lowest particle energies. The interplanetary spectra are calculated by modulating the spectra in local interstellar space (LIS) to the orbit of Earth. In this process Φ is the parameter, so that the calculations can be performed repeatedly for a variety of values of Φ . The value of Φ that gives calculated rates in accord with the data is then the appropriate level of modulation for the time interval being studied.

Figure 34 shows an example of such a study for P1 and P2 rates. Plotted are calculated counting rates for: $P1 = P1\bar{S}$, $P1^* = P1\bar{S}\bar{A}$, $P2 = P2\bar{A}\bar{S}$, $P2^* = P2\bar{A}\bar{S}$ ($Z > 2$), which correspond to particles not entering or leaving the sides of the experiment and, except for P1, stopping in the detector stack. The curves are the result of many calculations, each for a different level of modulation, shown on the horizontal axis in units of MeV/nucleon. Solar minimum conditions exhibit a residual modulation level of ~ 250 MeV/nucleon, so the lower values of Φ will not be applicable, while previous solar maximum conditions have given Φ values of 600-800 MeV/nucleon. The P1* and P2* rates respond principally to low energy (stopping) Mg-Fe and C-O nuclei, respectively, and are slightly more sensitive to changes in Φ than is P1 which includes penetrating particles as well. The P2 rate is shown for comparison but is not used since the helium region of P2 events shows some background contamination.

The equivalent counting rates must be obtained from the pulse height analyzed events, since the hardware logic circuitry does not conform to any of the conditions specified above. Each event is read from tape and its discriminator bit pattern is compared to the conditions described previously. In the case of P2*, a preliminary charge assignment of $ZCAL > 2.8$ is required as well. Each event meeting the criteria is counted over a specified active time interval to obtain the "measured" counting rate. These are shown, for P1, P1* and P2*, at the right side of Figure 34. Note that the three rates, when extended to the appropriate curve, all give a relatively consistent value for the solar modulation parameter, $\Phi = 550 \pm 50$ MeV/nucleon.

While Figure 34 shows a consistent result for Φ , it remains to be demonstrated that this value is correct. Such a validation can be provided by IMP-8 data (in the absence of normalized CRRES spectra) since the IMP-8 instrument is well

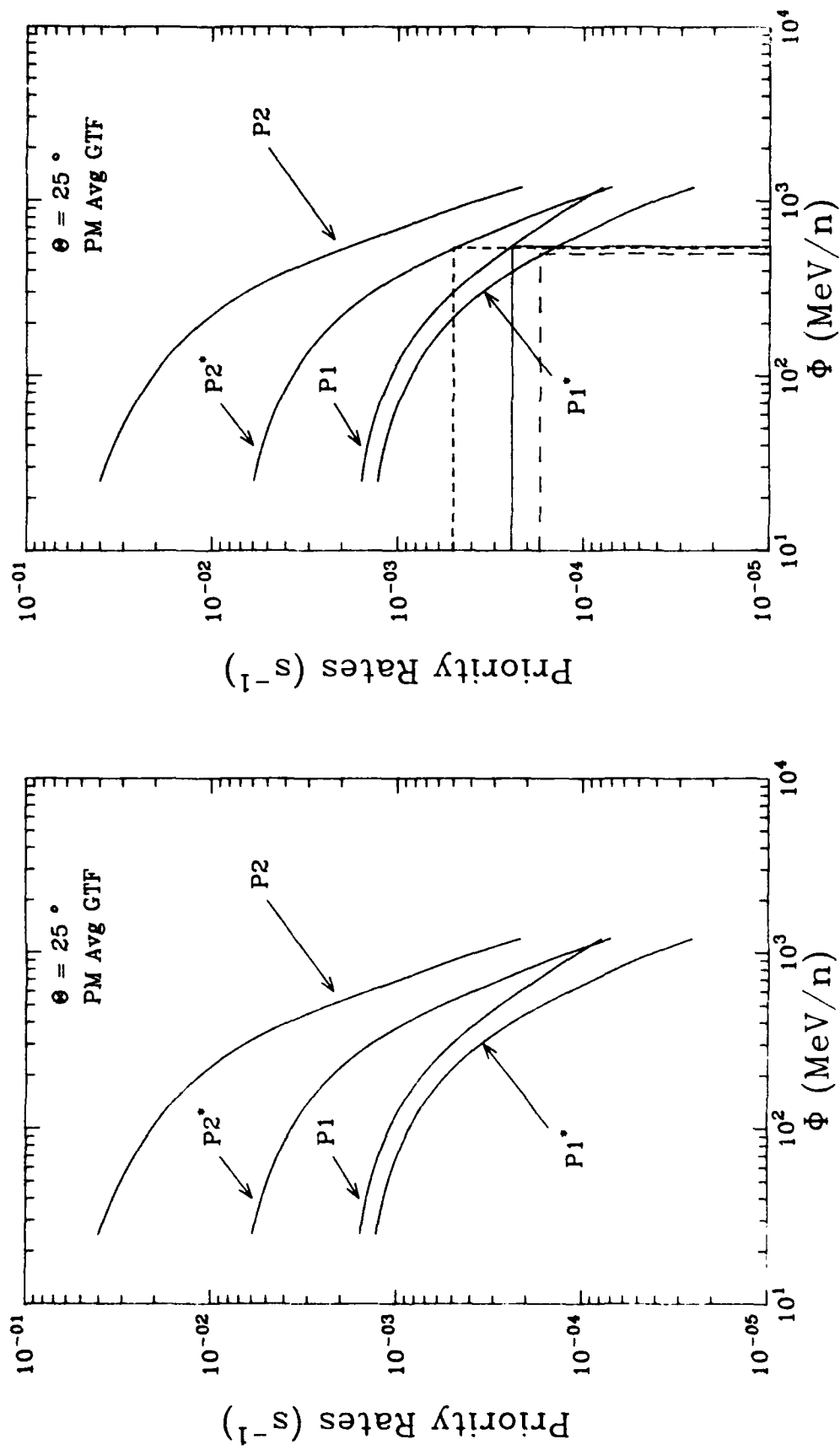


Figure 34: Calculated priority counting rates for ONR-604 (left) and comparison of the calculations to the data (right).

understood and has been utilized for many years in such studies. Figure 35 (top) shows IMP-8 oxygen spectra provided by M. G. Munoz for the late 1990-early 1991 period, as well as for previous periods, to be used in comparative studies. Beginning with the PLEXP model for local interstellar spectra, the lower set of curves in Figure 35 (bottom) shows the solar modulation prediction compared to the IMP-8 data. A best fit value of 650 ± 30 MeV/nucleon (1300 ± 60 MV) is obtained, somewhat above the values for Φ inferred from the priority rate analysis. Assuming that the IMP-8 level is correct, then there must be a problem with the rate model or with the ONR-604 data itself. Alternatively, the PLEXP local interstellar spectra may not be the most applicable, and this would affect the curves shown in both Figures 34 and 35 (bottom).

There are other calculations of the local interstellar spectra, each corresponding to a different pathlength distribution for galactic propagation (see the discussion in the next section). Of course, each model must reproduce the solar minimum spectra that were shown in Figure 3, so the differences in LIS are small. The effect of these different local interstellar spectra on the calculated P1, P1* and P2* counting rates is shown in Figure 36 where each of the curves corresponds to a different model. Note that the effect on the calculated rates in the Φ region of interest is very small, corresponding to introducing an uncertainty of ± 50 MeV/nucleon into the inferred value of Φ .

The geomagnetic transmission function has been checked, as has the energy dependent acceptance, and no major uncertainties have been found. Since the rate analysis shows a lower value of Φ , the measured counting rate should be lower to bring the inferred Φ values into agreement. This might indicate a residual background among the P1 and P2 events which has not been removed by the strict logic cuts employed. Further investigation will be required to try to resolve the apparent discrepancy. However, for the purposes of this report a preliminary value of $\Phi = 625 \pm 75$ MeV/nucleon is adopted.

c. Galactic Cosmic Rays

The Galactic Cosmic Rays (GCR) are a continuous source of ionizing radiation of extra-solar origin. For the past several decades the composition and energy spectrum of these high energy nuclei have been measured by a number of satellite experiments and ONR-604 represents the latest, current technology instrument in this series. Thus, the GCR Model to be developed under this effort has a wealth of previous measurements which can be used as a baseline. In fact, ONR-604 will not provide measurements over the full charge and energy range required by the Model, so the baseline dataset will be needed to set and/or constrain a majority of the Model parameters.

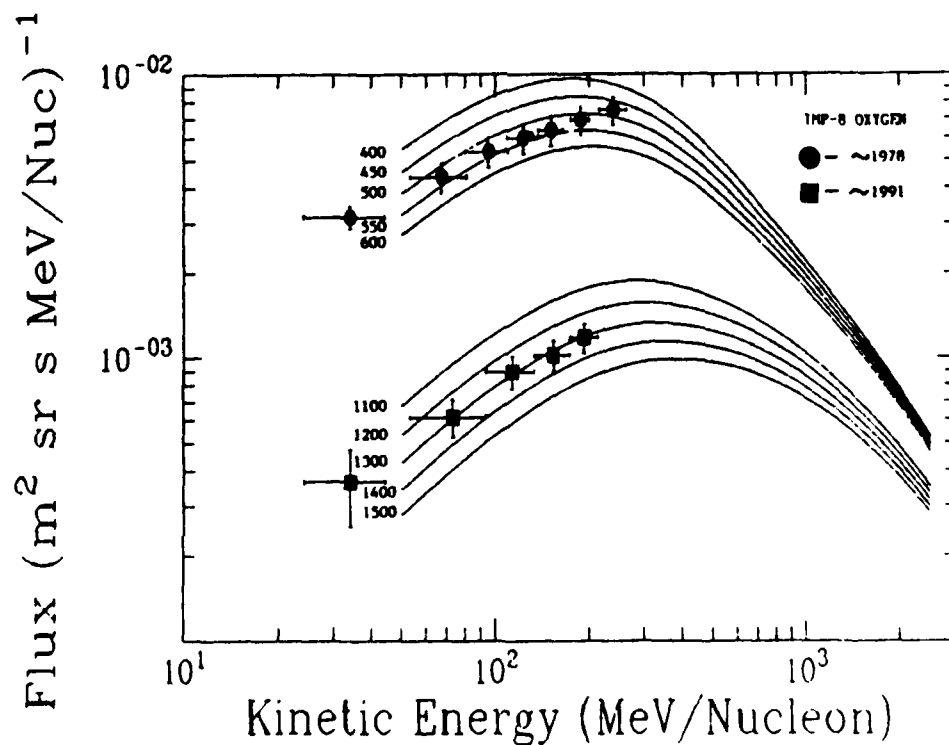
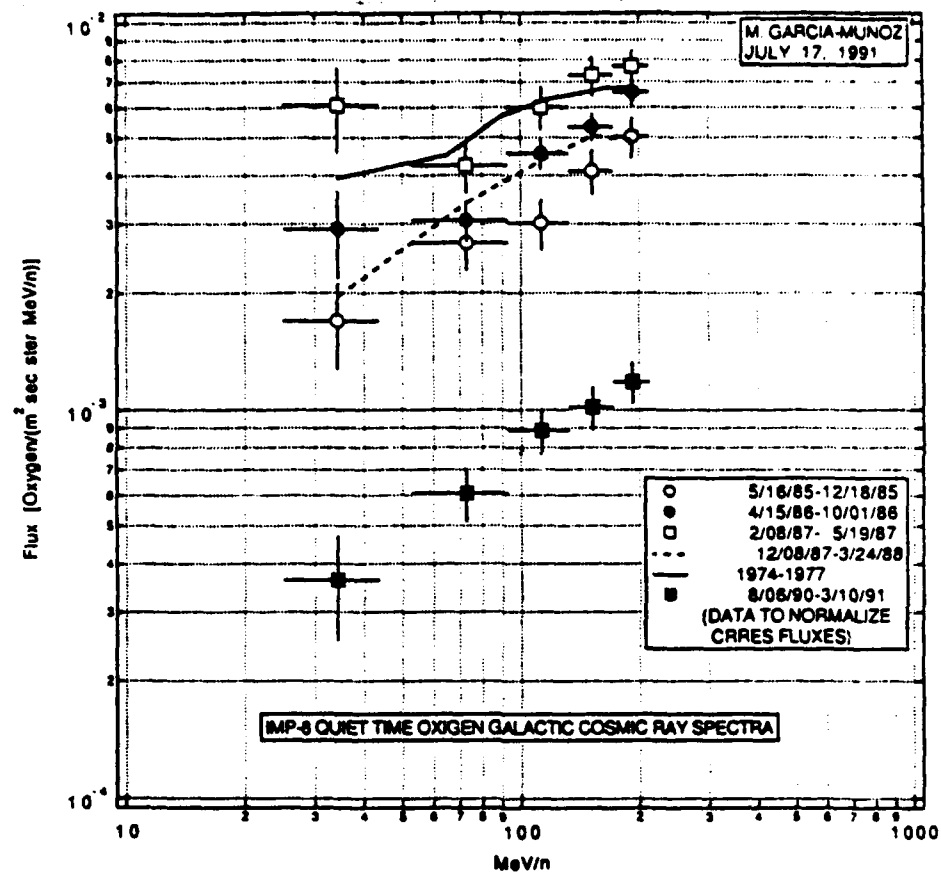


Figure 35. Oxygen energy spectra from IMP-8 for different time periods (top) and modulation fits to the IMP-8 data for 1978 and 1990-91 (bottom).

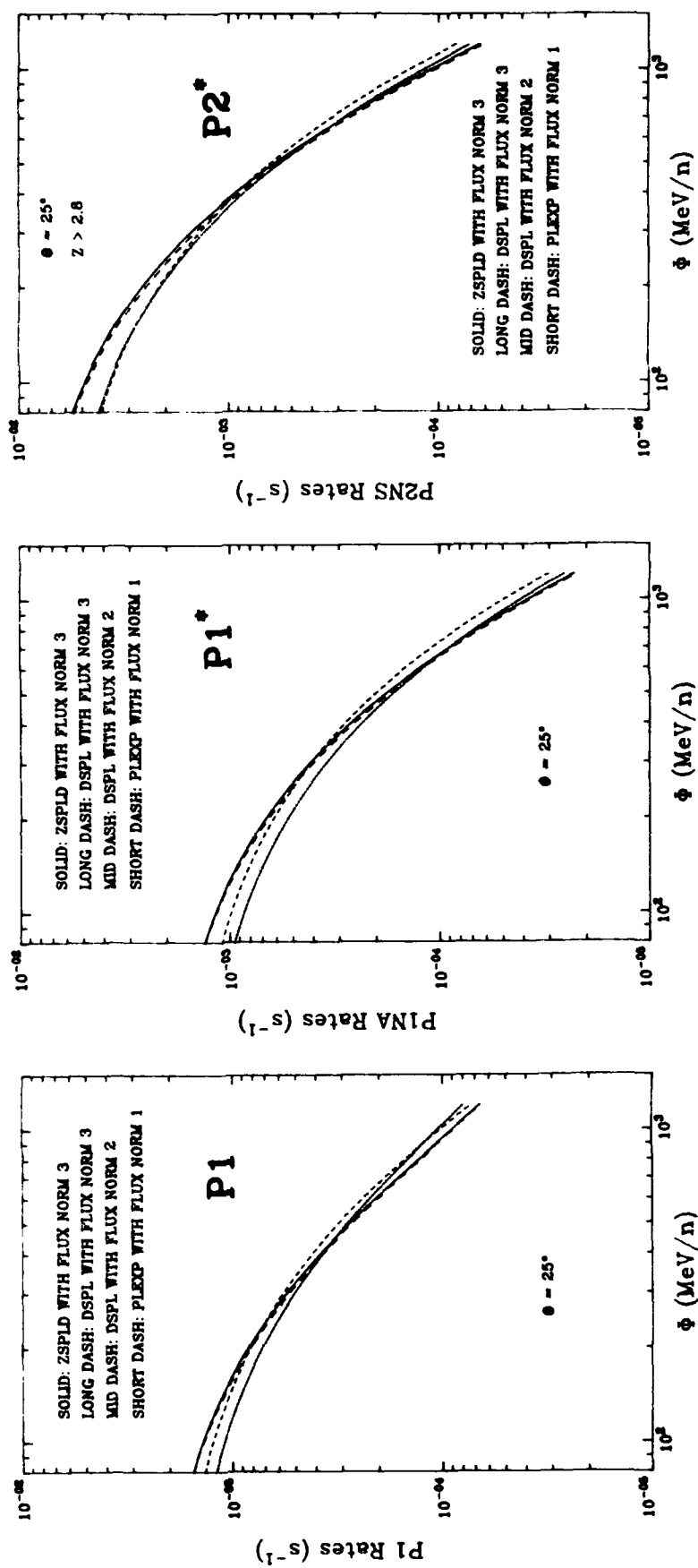


Figure 36. Comparison of calculated P1, P1* and P2* rates for different local interstellar spectra.

The current GCR baseline database contains close to 1000 data points from more than 50 literature references and covers the most important elemental ratios and spectra. The database was initially developed in the early 1980's and a majority of the measurements available then were made during the extended solar minimum period of 1972 - 1978. Since then relatively few, new missions have been flown and the statistics collected during the current solar cycle have been hampered by the two relatively deep solar maximums bracketing a rather narrow solar minimum period (c.f. Figure 27).

Recently, some new data has become available (e.g. Seo et al., 1991; Engelmann et al., 1990; Ferrando et al., 1991), and these need to be incorporated into the database. However, these measurements were made under solar modulation conditions, very different, in some cases, from the measurements in the baseline database. For example, Ferrando et al. (1991) reports on low energy (~ 100 MeV/nucleon) GCR composition measurements made during 1986-1987 with the High Energy Telescope onboard the Voyager 2 spacecraft while the spacecraft was at 22 AU. While the time period involved corresponds to the last solar minimum, these outer heliospheric measurements can not be directly compared with those made at the orbit of Earth. Thus, we will need to devote some effort to evaluating new measurements before including them in the database.

A portion of the energy spectra measurements from Figure 3 are shown in Figure 37, for He, C and Fe data with curves from initial GCR Model calculations. These results used a calculated local interstellar spectrum (LIS) modulated by the technique described earlier with solar minimum conditions corresponding to the 1972 - 1978 period ($\Phi = 490$ MV). The LIS was calculated using a computer program that is based upon the weighted-slab GCR interstellar propagation technique (Fichtel and Reames, 1968) and which is fully described in Garcia-Munoz et al. (1987). In essence, this technique starts with a set of relative abundances of elements and isotopes at the GCR source, assumes a common source energy spectrum, as well as a particular interstellar medium (ISM) composition and density, and then calculates new abundances and spectra for a series of discrete ISM slabs. This calculation includes the effects of production and loss of species via nuclear interaction, radioactive decay (β^+ , β^- , and e^- capture), electron capture and loss, and ionization energy loss. These "slab results" are then integrated over an assumed pathlength distribution (PLD) to obtain the LIS.

One might note at this point that the "Slab Calculations" involve only atomic and nuclear effects which can, in principal, be measured in the laboratory, while the PLD involves the astrophysical details of GCR interstellar propagation and must be either theoretically derived or obtained from the GCR data. Thus, obtaining a good representation of the Galactic Cosmic Rays is actually a multi-parameter problem and it is important to use laboratory measurements, GCR data and other astrophysical information to constrain as many of these parameters as possible. For example, of particular importance are the nuclear interaction cross sections, but only

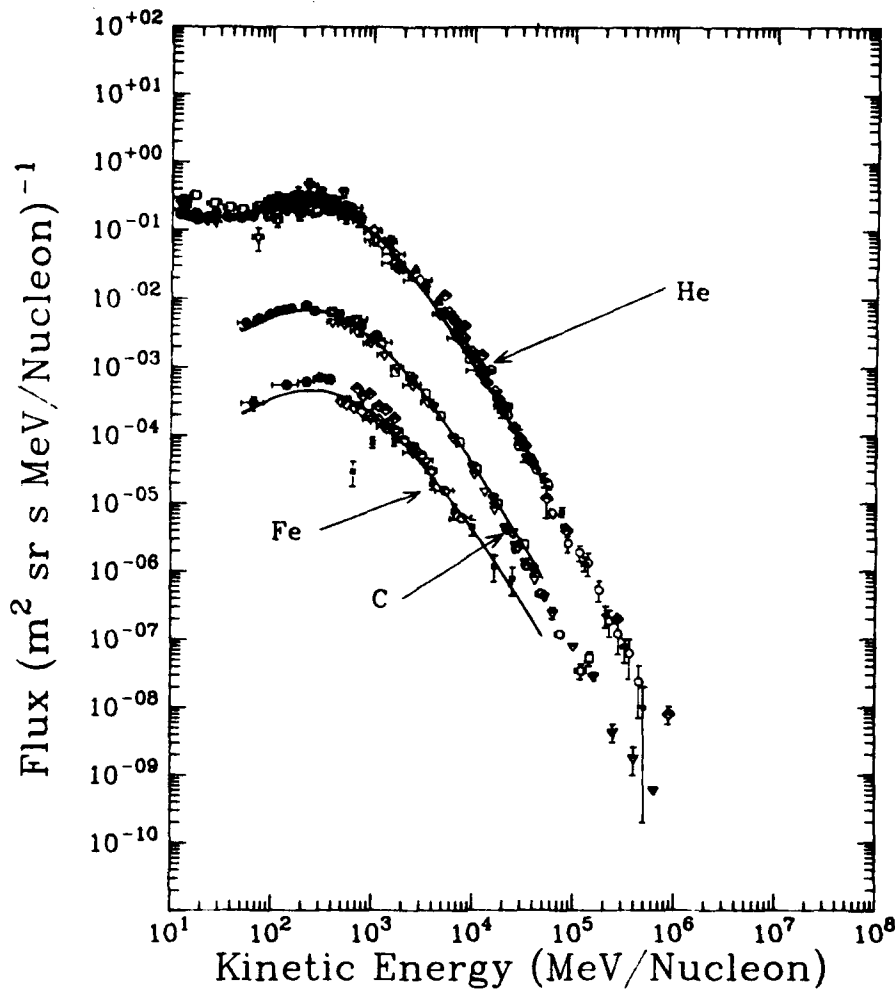


Figure 37. Measurements of GCR He, C and Fe flux from the baseline database along with predictions (solid curve) of the initial GCR Model.

a few interaction channels have been measured over the energy range required by the cosmic ray problem (Guzik, 1990). Therefore, there is a heavy reliance on calculated cross sections (e.g. Silberberg and Tsao, 1990) but these can differ from measured values by up to 60% (Webber, Kish and Schrier, 1990). Constraining the Model parameters is, thus, a complex process involving direct laboratory measurements, semi-empirical calculations and good judgement. Considerable effort was required to establish the parameter database for the initial GCR Model calculations and additional effort will be required to maintain this database as new laboratory measurements or other constraints become available.

The PLD used for the results shown in Figure 37 is an exponential distribution of pathlengths with a mean that is a decreasing power law in total energy. This distribution, referred to as the Power-Law Exponential (PLEXP), is consistent with a homogeneous model of cosmic ray propagation which allows a small, but increasing "leakage" from the "galactic" confinement volume with increasing energy. These results appear to fit the data of Figure 37 quite well. Helium, Carbon and Iron,

however, are "primary" species. That is, their relative abundance in the measured GCR is dominated by their abundance at the source and is not significantly affected by the "secondary" component generated by the nuclear fragmentation of heavier species. Therefore, primary species reflect conditions at the cosmic ray source rather than conditions during GCR propagation. Pure secondary species, which have a negligible source component, are very sensitive to the exact form of the PLD. In fact, by examining ratios of secondary to primary elements the PLD parameter in the GCR Model can be constrained.

Figure 38 shows measurements from the GCR database for the B/C secondary to primary ratio, along with the GCR Model results using the PLEXP PLD (long dashed curve). For energies greater than 1 GeV/nucleon the prediction represents the data, but overestimates the measurements for lower energies. Thus, while the Model may correctly predict the primary spectra it will overpredict the flux of secondary GCR at 100 MeV/nucleon by ~60%. An alternative PLD referred to as the Double-Sided Power Law (DSPL) pathlength distribution is shown as the solid curve in Figure 38 and provides a much better fit to the ratio. The DSPL has, in essence, the same form as the PLEXP for high energy (> 1 GeV/nucleon), but for low energy the exponential mean is a decreasing function of decreasing energy. Such a PLD may be consistent with propagation models which involve a "galactic wind" that flows outward from the galactic plane in a fashion similar to the solar wind which flows outward from the Sun (Garcia-Munoz et al., 1987).

Further details of the PLD can be constrained by requiring multiple secondary to primary ratios widely separated in charge to be simultaneously fit. Figure 39 shows the collection of data for the ratio Sub-Fe/Fe where the "Sub-Fe" group includes the elements Sc, Ti, V, Cr and Mn. The DSPL results which fit the B/C ratio is shown as the solid curve and is quite likely low of the data for energies less than ~1.0 GeV/nucleon. This discrepancy has been used to argue that the PLD must be depleted of short pathlengths (Garcia-Munoz et al., 1987). Since the Iron group species have a larger total nuclear interaction cross section, and hence a shorter mean interaction length, than the Carbon group nuclei, the iron secondaries will be more sensitive to the short pathlength characteristics of the PLD. By removing or "truncating" the short pathlengths from the PLD the calculation will cause more Iron nuclei to interact and raise the Sub-Fe/Fe ratio (dashed curves in Figure 39) while not affecting the prediction for B/C (short dashed curve in Figure 38).

The spectra calculated using these various PLDs are shown in Figure 40. The solid curves are the same as in Figure 37, that is using the PLEXP, the short dashed curves are results using the DSPL and the long dashed curves result from a "truncated" PLD. For Helium and Carbon the three PLDs yield almost identical results, but the differences are apparent in the low energy (< 700 MeV/nucleon) Iron spectrum. As energy deposit is proportional to Z^2/E an error made in calculating the low energy Iron spectrum may translate into a relatively large uncertainty in the Linear Energy Transfer (LET) spectrum.

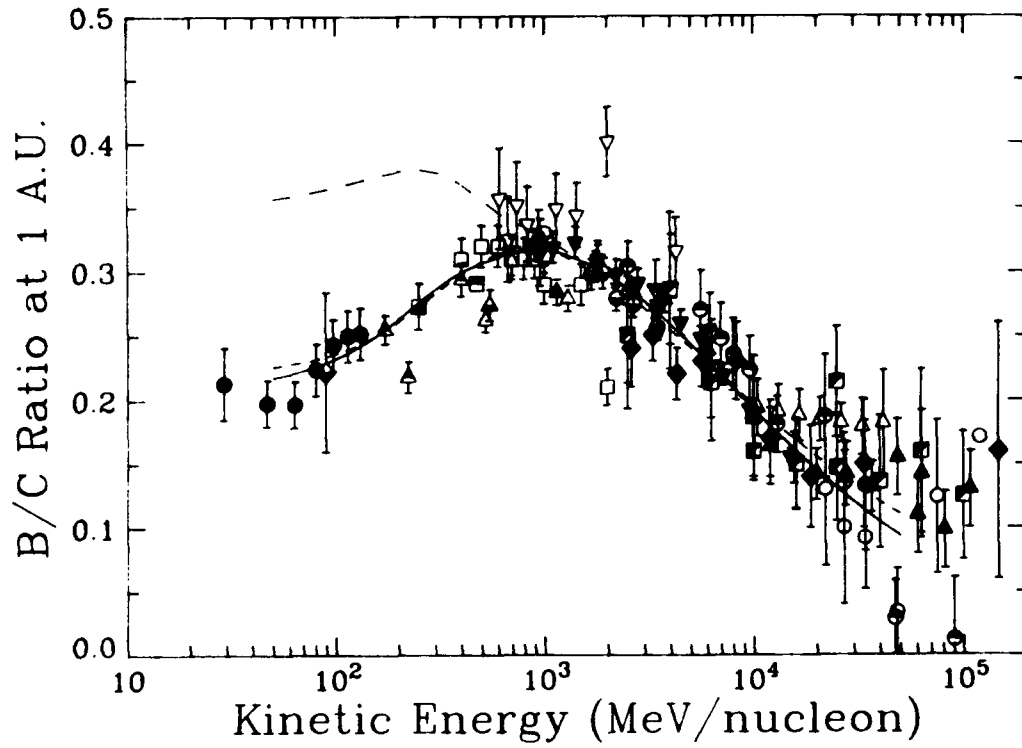


Figure 38. Measurements of B/C with Model predictions using different PLDs.

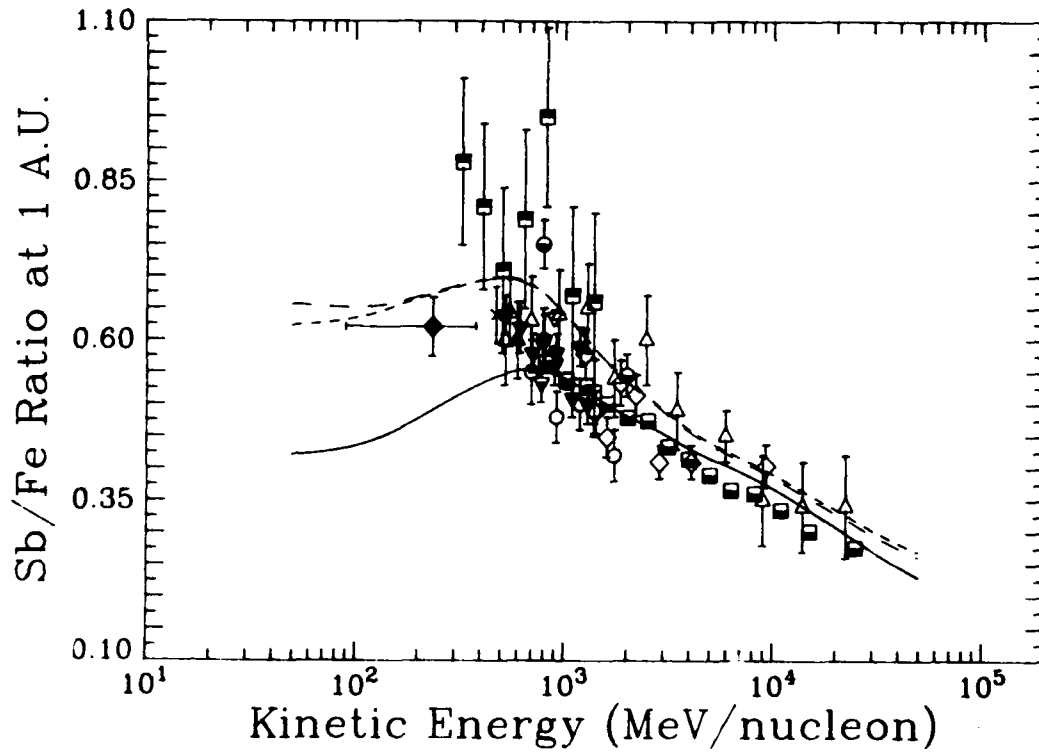


Figure 39. Measurements of Sub-Fe/Fe with Model predictions using different PLDs (see text).

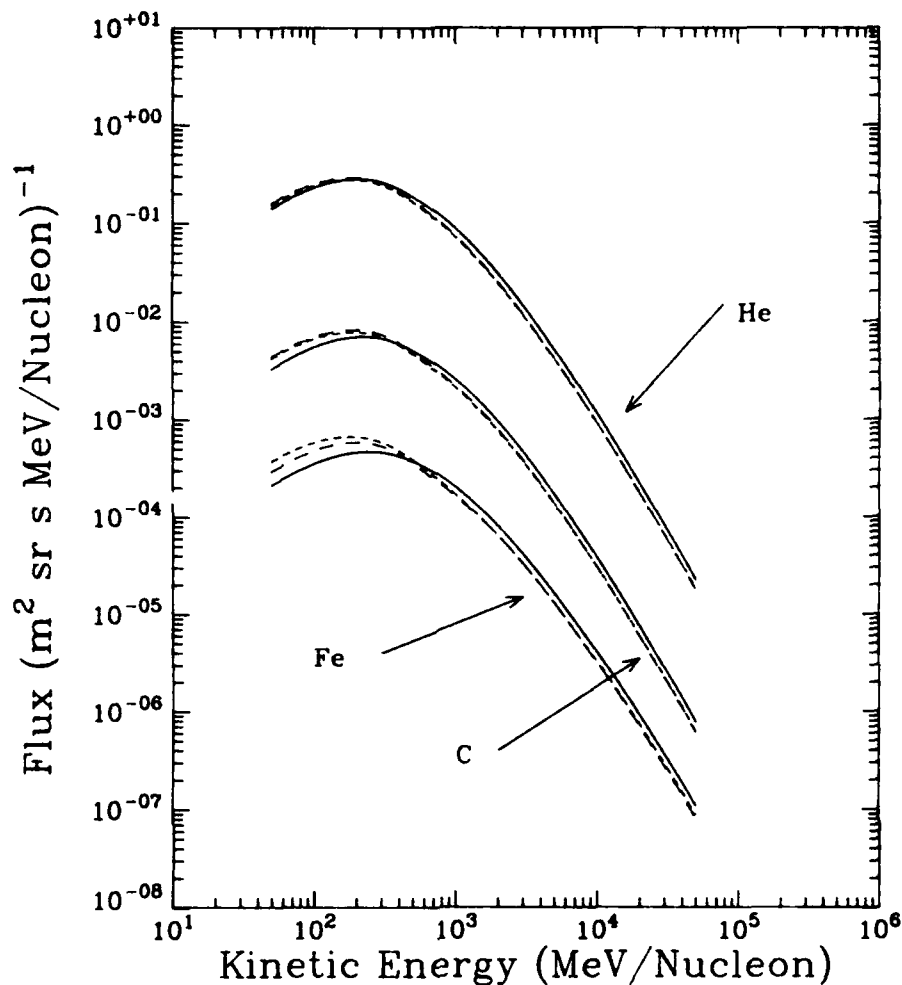


Figure 40. Spectra predicted by the GCR Model for different PLDs (see text).

In fact, the accuracy to which the PLD can be determined and, consequently, the spectra can be calculated, depends upon the accuracy of the other Model parameters. For example, while the solid curve in Figure 39 (no truncation) appears to underpredict the low energy data, it can be argued that the dashed curves (with truncation) are high for all energies. This could be due to having an incorrect source abundance for the Sub-Fe species in the Model, and reducing these abundances would lower the dashed curves. In addition, PLD truncation is still controversial and the case for truncation is based largely on the low energy IMP-8 measurement (filled diamond in Figure 39). The recent measurement by Ferrando et al. (1991) provides the only other data in the IMP-8 charge and energy range. Their value for Sub-Fe/Fe is about 30% less than the IMP-8 measurement and is in good agreement with the solid curve (no truncation) of Figure 39. As discussed above, however, it is not immediately clear whether the Ferrando et al. measurement made with an instrument onboard the Voyager 2 spacecraft at 22 AU can be so directly compared with the IMP-8 data made in the vicinity of Earth.

Finally, the nuclear interaction cross sections for the production of Sub-Fe species from Iron are also largely unmeasured and, thus, the Model uses mostly calculated cross sections. If these calculated cross sections are increased in value then the solid curve in Figure 39 would move up and it may be possible to fit the Sub-Fe/Fe and B/C data simultaneously without requiring a truncated pathlength distribution.

Refining the GCR Model and evaluating the consequences of these uncertainties is a time consuming process involving multiple calculations. First an alternate set of input parameters, such as the source abundances, source spectra or nuclear cross sections, must be determined from the literature, derived or calculated. Next the "Slab Calculation" program, which takes roughly 10 to 12 CPU hours on an IBM 3090, must be run with the new inputs. Using these new slab results the PLD parameters must be adjusted so that the B/C and Sub-Fe/Fe data are simultaneously fit. The final results of this process are then compared with the spectra and ratio measurements from the baseline database. If further adjustments are still called for then the process begins again. Usually 3 to 4 iterations through this loop and several months of man-effort are needed to achieve an additional level of refinement in the GCR Model.

d. Preliminary Predictions

The preceding sections have discussed the needed inputs to the Interplanetary Heavy Ion model and the current state of the analysis. While it is still premature to issue a definitive environment model, a preliminary "working" prediction can be made. Since the time period of interest (1 Sept. 90 - 28 Feb. 91) contains no large solar flares, a flare component need not be considered. Thus, the first period environment is dominated by the Galactic Cosmic Rays.

Using the PLEXP spectra in Local Interstellar Space and a modulation level of $\Phi = 625$ MeV/nucleon, the LPARL group (D. L. Chenette, lead investigatory) has calculated the flux of cosmic rays at the orbit of Earth given in Table 2 and illustrated in Figure 41 for the elements H, He, O and Fe.

To investigate the effect of these particles on components, it is necessary to calculate the Linear Energy Transfer (LET) distribution for different LET thresholds and behind different levels of shielding. This has been done for shielding thicknesses of 50, 100, 200, 400, 800 and 1600 mils of Aluminum for a grid of different thresholds. The numerical results are given in Table 3 and are shown graphically in Figure 42. These preliminary results can be utilized by the Product Associated Working Groups.

What has not been completed is a study of the variation in spectra or LET distributions introduced by the uncertainty in the level of solar modulation or the different LIS spectra that were described above. Such a study will indicate the range of possible variation about the "working" values in Tables 2 and 3, and will allow

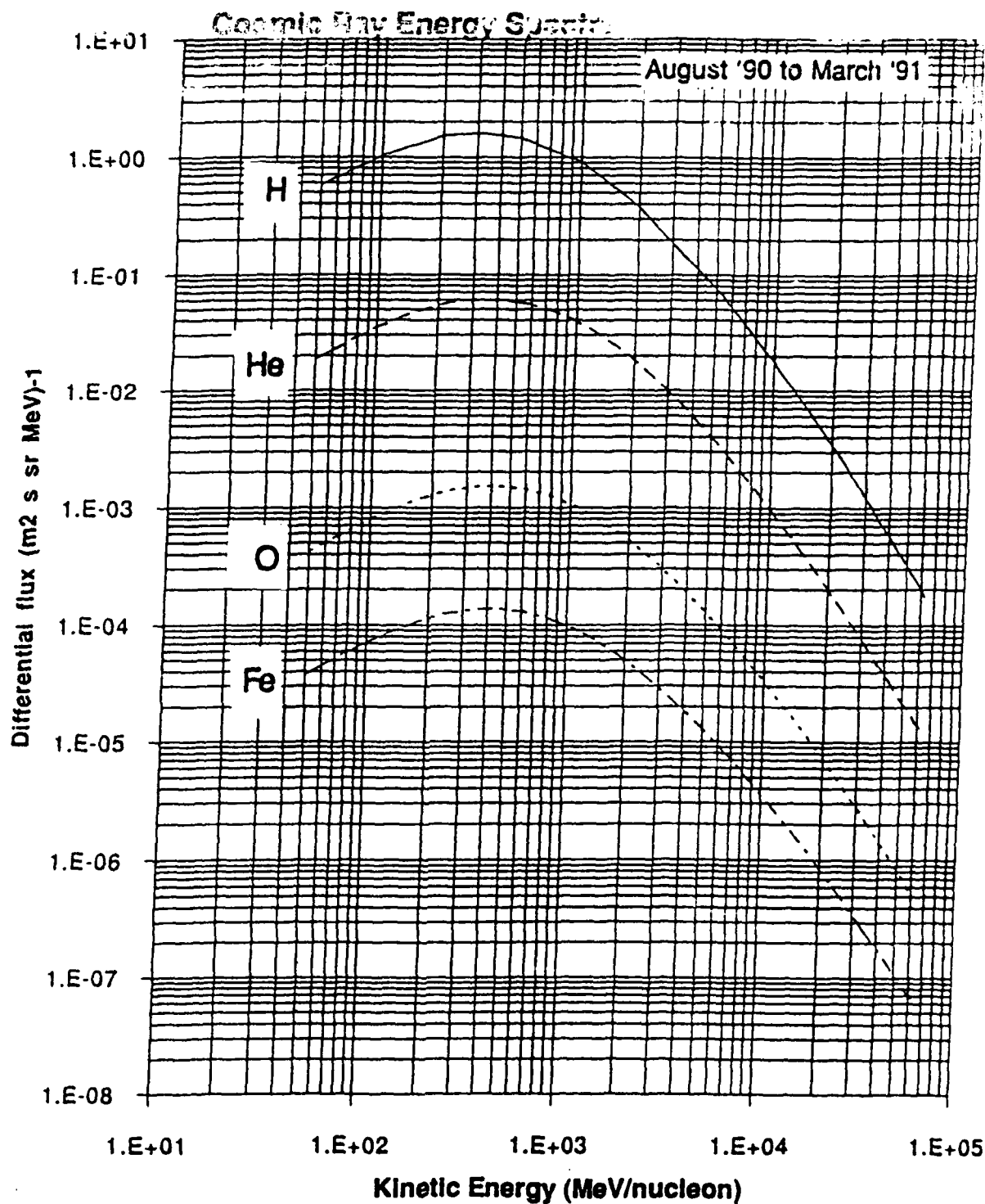


Figure 41. Predicted energy spectra for GCR nuclei H, He, O and Fe for the late '90-early '91 time period.

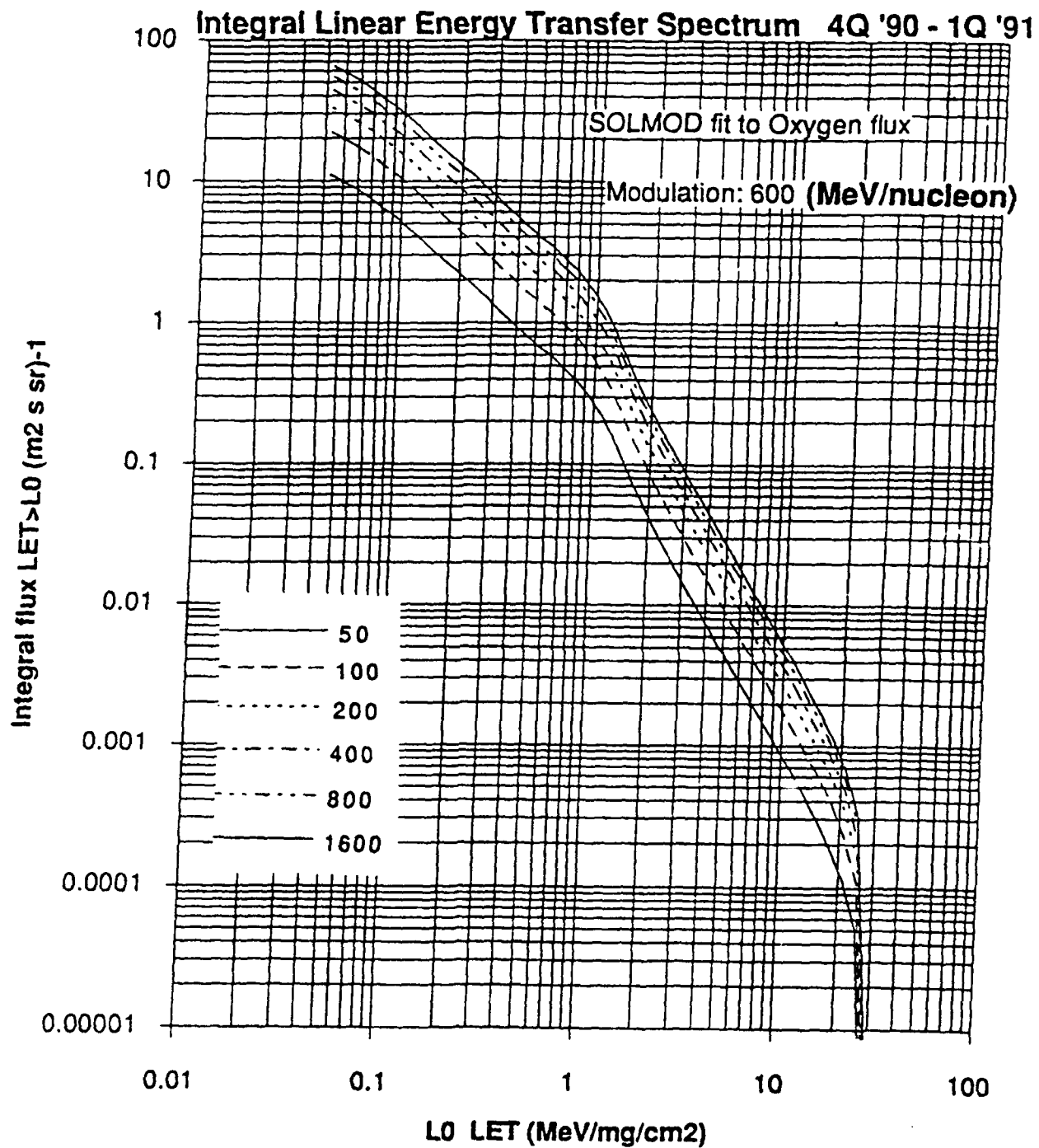


Figure 42. Integral number of particles with LET greater than threshold, LO, as a function of LO. The curves are labeled with the thickness of Aluminum shielding (in mils) assumed in the calculation.

the "user" of these results to estimate the uncertainties in his analysis. The study of these variations will be one of the next tasks undertaken by the modeling group.

6. SUMMARY

The CRRES mission provides an opportunity for new, detailed in situ observations of the Geospace radiation environment and its effects on microelectronic components. The ONR-604 experiment provides the monitoring of high energy heavy ions and, together with previous and contemporary data, provides a means for describing the radiation environment experienced by the CRRES spacecraft. This environment is being codified and described by an Interplanetary Heavy Ion model that has been subject of this interim technical report.

The overall modeling effort as well as the operation and performance of the ONR-604 instrument through pre-launch calibrations and initial on-orbit operations has been described in detail as necessary background information for the data analysis and modeling effort. The data reduction and processing system development has encompassed the reading, checking, formatting and splitting of the data into databases as well as the capability to plot and correlate the data in a number of ways. Auxiliary databases have been established and are used in the modeling effort. What remains is to develop the background subtraction and normalization portion of the system, in order to convert the ONR-604 results into meaningful flux values as a function of charge and energy. In addition, solar flare analysis and modeling routines have not yet been finished.

The analysis of the environment data, both CRRES and other data, has proceeded to the point of establishing a preliminary, "working" environment model for the period ~1 Sept. 90 - 1 March 91, characterized by relatively quiet interplanetary conditions. This environment is characterized by a high level of solar modulation ($\Phi = 625 \pm 75$ MeV/nucleon) and correspondingly depressed levels of Galactic Cosmic Rays.

The Solar Modulation process and the techniques developed to determine the level of modulation are reviewed in detail, revealing that the two techniques studied give similar results, qualitatively, but disagree quantitatively indicating that further, refined analysis is required.

Galactic Cosmic Ray spectral data from previous epochs are summarized and used to normalize the model calculations. New data is described as well as the techniques to obtain a fully self-consistent set of spectra in Local Interstellar Space. Current models do a reasonably good job in reproducing the measured data but are not optimum descriptions of the environment. Further refinements are needed in the GCR model to bring it to its optimum state for use in the Interplanetary Heavy Ion Model analysis.

The "working" environment presented here in terms of particle flux and LET spectra can be used by the community as a preliminary result for analyzing microelectronic data. It is hoped that the product associated working groups will provide both analyses and suggestions that can be folded into the process described in this report to help produce a better product for the user community.

Table 2: Calculated Galactic Cosmic Ray Spectra for $Z = 1$ to 28 and $E = 50$ to over 60,000 MeV/nucleon

Phi = 625

Kinetic Energy (MeV/nuc)	H 1	He 2	Li 3	Be 4	B 5	C 6	N 7	O 8	F 9
	1	4	6.46	8.09	10.7	12.04	14.33	16.03	19
50.00	5.80E-01	1.86E-02	1.38E-04	5.46E-05	1.99E-04	4.90E-04	1.40E-04	4.20E-04	1.20E-05
62.95	7.01E-01	2.31E-02	1.72E-04	6.82E-05	2.47E-04	6.11E-04	1.75E-04	5.25E-04	1.50E-05
79.24	8.47E-01	2.85E-02	2.13E-04	8.44E-05	3.05E-04	7.55E-04	2.16E-04	6.49E-04	1.86E-05
99.76	1.02E+00	3.46E-02	2.58E-04	1.03E-04	3.70E-04	9.20E-04	2.63E-04	7.92E-04	2.27E-05
125.59	1.17E+00	4.11E-02	3.08E-04	1.24E-04	4.41E-04	1.10E-03	3.15E-04	9.50E-04	2.72E-05
158.11	1.33E+00	4.77E-02	3.58E-04	1.45E-04	5.11E-04	1.29E-03	3.68E-04	1.11E-03	3.19E-05
199.05	1.52E+00	5.36E-02	4.03E-04	1.65E-04	5.72E-04	1.46E-03	4.17E-04	1.27E-03	3.63E-05
250.59	1.57E+00	5.80E-02	4.37E-04	1.81E-04	6.17E-04	1.60E-03	4.55E-04	1.40E-03	3.99E-05
315.48	1.59E+00	6.02E-02	4.54E-04	1.92E-04	6.36E-04	1.68E-03	4.76E-04	1.48E-03	4.22E-05
397.16	1.52E+00	6.00E-02	4.53E-04	1.95E-04	6.26E-04	1.70E-03	4.78E-04	1.51E-03	4.29E-05
500.00	1.45E+00	5.75E-02	4.36E-04	1.91E-04	5.92E-04	1.65E-03	4.60E-04	1.48E-03	4.18E-05
629.46	1.24E+00	5.29E-02	4.04E-04	1.79E-04	5.38E-04	1.54E-03	4.25E-04	1.39E-03	3.90E-05
792.45	1.06E+00	4.66E-02	3.59E-04	1.61E-04	4.67E-04	1.37E-03	3.75E-04	1.25E-03	3.46E-05
997.63	9.07E-01	3.92E-02	3.01E-04	1.37E-04	3.87E-04	1.17E-03	3.16E-04	1.07E-03	2.94E-05
1255.94	6.81E-01	3.17E-02	2.40E-04	1.10E-04	3.07E-04	9.59E-04	2.56E-04	8.81E-04	2.39E-05
1581.14	5.11E-01	2.46E-02	1.82E-04	8.56E-05	2.34E-04	7.53E-04	1.98E-04	6.98E-04	1.87E-05
1990.54	3.83E-01	1.83E-02	1.32E-04	6.35E-05	1.71E-04	5.69E-04	1.48E-04	5.31E-04	1.40E-05
2505.94	2.56E-01	1.32E-02	9.22E-05	4.51E-05	1.19E-04	4.15E-04	1.06E-04	3.90E-04	1.01E-05
3154.79	1.71E-01	9.16E-03	6.14E-05	3.06E-05	7.97E-05	2.91E-04	7.30E-05	2.77E-04	6.96E-06
3971.64	1.14E-01	6.16E-03	3.92E-05	2.00E-05	5.12E-05	1.98E-04	4.84E-05	1.90E-04	4.63E-06
5000.00	7.62E-02	4.03E-03	2.41E-05	1.25E-05	3.17E-05	1.31E-04	3.10E-05	1.27E-04	2.98E-06
6294.63	4.69E-02	2.57E-03	1.44E-05	7.61E-06	1.90E-05	8.44E-05	1.93E-05	8.29E-05	1.86E-06
7924.47	2.89E-02	1.60E-03	8.32E-06	4.50E-06	1.11E-05	5.32E-05	1.17E-05	5.29E-05	1.13E-06
9976.31	1.78E-02	9.82E-04	4.69E-06	2.58E-06	6.33E-06	3.29E-05	6.96E-06	3.31E-05	6.69E-07
12559.43	1.03E-02	5.91E-04	2.58E-06	1.44E-06	3.51E-06	1.99E-05	4.03E-06	2.03E-05	3.88E-07
15811.39	6.00E-03	3.50E-04	1.39E-06	7.87E-07	1.90E-06	1.19E-05	2.29E-06	1.22E-05	2.20E-07
19905.36	3.49E-03	2.04E-04	7.29E-07	4.19E-07	1.01E-06	6.99E-06	1.28E-06	7.28E-06	1.22E-07
25059.36	1.92E-03	1.18E-04	3.79E-07	2.20E-07	5.30E-07	4.07E-06	7.05E-07	4.28E-06	6.73E-08
31547.87	1.06E-03	6.76E-05	1.94E-07	1.14E-07	2.74E-07	2.34E-06	3.84E-07	2.49E-06	3.66E-08
39716.41	5.82E-04	3.87E-05	9.88E-08	5.84E-08	1.41E-07	1.35E-06	2.09E-07	1.44E-06	1.98E-08
50000.00	3.20E-04	2.15E-05	4.88E-08	2.90E-08	7.00E-08	7.50E-07	1.10E-07	8.11E-07	1.04E-08
62946.27	1.74E-04	1.30E-05	2.75E-08	1.65E-08	3.95E-08	4.57E-07	6.49E-08	4.96E-07	6.11E-09

Table 2: Calculated Galactic Cosmic Ray Spectra for $Z = 1$ to 28 and $E = 50$ to over 60,000 MeV/nucleon

Phi = 625

Kinetic Energy (MeV/nuc)	Na 11 23	Mg 12 24.4	Al 13 26.93	Si 14 28.17	P 15 31	S 16 32.31	Cl 17 36.14	Ar 18 37.31	K 19 39.79
50.00	1.63E-05	8.14E-05	1.47E-05	5.85E-05	2.75E-06	1.00E-05	2.50E-06	4.39E-06	3.40E-06
62.95	2.03E-05	1.02E-04	1.84E-05	7.31E-05	3.45E-06	1.26E-05	3.14E-06	5.51E-06	4.27E-06
79.24	2.52E-05	1.26E-04	2.28E-05	9.05E-05	4.28E-06	1.56E-05	3.90E-06	6.87E-06	5.32E-06
99.76	3.07E-05	1.54E-04	2.79E-05	1.11E-04	5.26E-06	1.92E-05	4.80E-06	8.47E-06	6.57E-06
125.59	3.69E-05	1.85E-04	3.36E-05	1.33E-04	6.36E-06	2.32E-05	5.83E-06	1.03E-05	8.00E-06
158.11	4.32E-05	2.17E-04	3.95E-05	1.57E-04	7.54E-06	2.75E-05	6.94E-06	1.23E-05	9.57E-06
199.05	4.93E-05	2.47E-04	4.52E-05	1.80E-04	8.72E-06	3.18E-05	8.08E-06	1.43E-05	1.12E-05
250.59	5.43E-05	2.73E-04	5.02E-05	2.00E-04	9.80E-06	3.58E-05	9.13E-06	1.62E-05	1.27E-05
315.48	5.77E-05	2.91E-04	5.36E-05	2.14E-04	1.06E-05	3.88E-05	9.98E-06	1.77E-05	1.39E-05
397.16	5.89E-05	2.98E-04	5.52E-05	2.20E-04	1.11E-05	4.06E-05	1.05E-05	1.87E-05	1.46E-05
500.00	5.76E-05	2.93E-04	5.45E-05	2.18E-04	1.12E-05	4.08E-05	1.06E-05	1.88E-05	1.47E-05
629.46	5.39E-05	2.76E-04	5.15E-05	2.06E-04	1.07E-05	3.92E-05	1.03E-05	1.81E-05	1.41E-05
792.45	4.82E-05	2.48E-04	4.64E-05	1.87E-04	9.81E-06	3.60E-05	9.46E-06	1.66E-05	1.28E-05
997.63	4.11E-05	2.14E-04	4.00E-05	1.63E-04	8.54E-06	3.15E-05	8.27E-06	1.44E-05	1.10E-05
1255.94	3.37E-05	1.77E-04	3.31E-05	1.35E-04	7.11E-06	2.64E-05	6.88E-06	1.19E-05	9.05E-06
1581.14	2.66E-05	1.41E-04	2.64E-05	1.08E-04	5.67E-06	2.11E-05	5.47E-06	9.31E-06	7.05E-06
1990.54	2.01E-05	1.08E-04	2.02E-05	8.30E-05	4.30E-06	1.60E-05	4.11E-06	6.90E-06	5.23E-06
2505.94	1.46E-05	7.92E-05	1.49E-05	6.14E-05	3.11E-06	1.16E-05	2.92E-06	4.82E-06	3.66E-06
3154.79	1.02E-05	5.62E-05	1.06E-05	4.39E-05	2.16E-06	8.12E-06	1.99E-06	3.22E-06	2.45E-06
3971.64	6.90E-06	3.87E-05	7.27E-06	3.05E-05	1.46E-06	5.52E-06	1.33E-06	2.10E-06	1.61E-06
5000.00	4.52E-06	2.59E-05	4.86E-06	2.06E-05	9.61E-07	3.67E-06	8.77E-07	1.35E-06	1.04E-06
6294.63	2.89E-06	1.69E-05	3.16E-06	1.36E-05	6.16E-07	2.38E-06	5.66E-07	8.46E-07	6.60E-07
7924.47	1.80E-06	1.08E-05	2.01E-06	8.75E-06	3.86E-07	1.51E-06	3.57E-07	5.17E-07	4.08E-07
9976.31	1.10E-06	6.78E-06	1.25E-06	5.53E-06	2.37E-07	9.42E-07	2.20E-07	3.08E-07	2.46E-07
12559.43	6.57E-07	4.17E-06	7.63E-07	3.43E-06	1.42E-07	5.73E-07	1.32E-07	1.79E-07	1.44E-07
15811.39	3.85E-07	2.52E-06	4.55E-07	2.09E-06	8.33E-08	3.43E-07	7.73E-08	1.01E-07	8.25E-08
19905.36	2.22E-07	1.50E-06	2.75E-07	1.26E-06	4.81E-08	2.02E-07	4.43E-08	5.64E-08	4.62E-08
25059.36	1.27E-07	8.86E-07	1.55E-07	7.48E-07	2.75E-08	1.18E-07	2.50E-08	3.10E-08	2.55E-08
31547.87	7.13E-08	5.16E-07	8.87E-08	4.39E-07	1.55E-08	6.77E-08	1.39E-08	1.68E-08	1.38E-08
39716.41	4.01E-08	3.01E-07	5.07E-08	2.57E-07	8.76E-09	3.89E-08	7.69E-09	9.08E-09	7.43E-09
50000.00	2.19E-08	1.69E-07	2.80E-08	1.46E-07	4.78E-09	2.17E-08	4.20E-09	4.77E-09	3.88E-09
62946.27	1.31E-08	1.04E-07	1.70E-08	8.98E-08	2.91E-09	1.33E-08	3.58E-09	2.86E-09	2.33E-09

Table 2: Calculated Galactic Cosmic Ray Spectra for Z=1 to 28 and E = 50 to over 60,000 MeV/nucleon

Phi=625

Kinetic Energy (MeV/nuc)	Sc 21 45	Ti 22 47.56	V 23 50.34	Cr 24 52.15	Mn 25 54.07	Fe 26 55.88	Co 27 58.37	Ni 28 58.76
50.00	1.82E-06	6.82E-06	3.05E-06	6.72E-06	3.65E-05	3.75E-05	1.67E-07	1.61E-06
62.95	2.27E-06	8.53E-06	3.80E-06	8.38E-06	4.56E-06	4.68E-05	2.09E-07	2.01E-06
79.24	2.83E-06	1.06E-05	4.70E-06	1.04E-05	5.63E-06	5.79E-05	2.59E-07	2.49E-06
99.76	3.48E-06	1.30E-05	5.74E-06	1.26E-05	6.86E-06	7.06E-05	3.18E-07	3.05E-06
125.59	4.21E-06	1.56E-05	6.89E-06	1.51E-05	8.21E-06	8.47E-05	3.83E-07	3.66E-06
158.11	5.00E-06	1.84E-05	8.07E-06	1.77E-05	9.60E-06	9.93E-05	4.53E-07	4.30E-06
199.05	5.78E-06	2.11E-05	9.18E-06	2.01E-05	1.09E-05	1.13E-04	5.21E-07	4.93E-06
250.59	6.48E-06	2.34E-05	1.01E-05	2.20E-05	1.20E-05	1.25E-04	5.82E-07	5.47E-06
315.48	6.98E-06	2.49E-05	1.06E-05	2.31E-05	1.28E-05	1.33E-04	6.25E-07	5.85E-06
397.16	7.21E-06	2.54E-05	1.07E-05	2.32E-05	1.31E-05	1.37E-04	6.46E-07	6.02E-06
500.00	7.10E-06	2.48E-05	1.03E-05	2.22E-05	1.30E-05	1.34E-04	6.39E-07	5.95E-06
629.46	6.65E-06	2.29E-05	9.32E-06	2.02E-05	1.22E-05	1.27E-04	6.03E-07	5.64E-06
792.45	5.91E-06	2.02E-05	8.00E-06	1.75E-05	1.11E-05	1.14E-04	5.42E-07	5.11E-06
997.63	4.98E-06	1.68E-05	6.52E-06	1.44E-05	9.56E-06	9.88E-06	4.64E-07	4.44E-06
1255.94	3.99E-06	1.34E-05	5.09E-06	1.14E-05	7.93E-06	8.20E-05	3.82E-07	3.70E-06
1581.14	3.03E-06	1.02E-05	3.84E-06	8.67E-06	6.33E-06	6.54E-05	3.04E-07	2.97E-06
1990.54	2.20E-06	7.48E-06	2.84E-06	6.49E-06	4.89E-06	5.03E-05	2.34E-07	2.30E-06
2505.94	1.51E-06	5.29E-06	2.04E-06	4.75E-06	3.64E-06	3.74E-05	1.74E-07	1.72E-06
3154.79	9.84E-07	3.60E-06	1.41E-06	3.37E-06	2.61E-06	2.70E-05	1.25E-07	1.24E-06
3971.64	6.21E-07	2.38E-06	9.45E-07	2.30E-06	1.81E-06	1.89E-05	8.70E-08	8.75E-07
5000.00	3.94E-07	1.55E-06	6.20E-07	1.53E-06	1.22E-06	1.29E-05	5.89E-08	6.00E-07
6294.63	2.49E-07	9.89E-07	3.96E-07	9.86E-07	7.98E-07	8.58E-06	3.88E-08	4.02E-07
7924.47	1.55E-07	6.17E-07	2.48E-07	6.22E-07	5.10E-07	5.61E-06	2.50E-08	2.64E-07
9976.31	9.34E-08	3.75E-07	1.51E-07	3.83E-07	3.17E-07	3.60E-06	1.58E-08	1.70E-07
12559.43	5.48E-08	2.22E-07	8.94E-08	2.30E-07	1.93E-07	2.27E-06	9.79E-09	1.08E-07
15811.39	3.14E-08	1.28E-07	5.18E-07	1.35E-07	1.15E-07	1.41E-06	5.95E-09	6.71E-08
19905.36	1.76E-08	7.26E-08	2.93E-08	7.80E-08	6.66E-08	8.60E-07	3.55E-09	4.12E-08
25059.36	9.70E-09	4.04E-08	1.63E-08	4.43E-08	3.81E-08	5.20E-07	2.09E-09	2.50E-08
31547.87	5.24E-09	2.21E-08	8.90E-09	2.47E-08	2.14E-08	3.10E-07	1.22E-09	1.50E-08
39716.41	2.81E-09	1.20E-08	4.89E-09	1.38E-08	1.20E-08	1.85E-07	7.07E-10	8.97E-09
50000.00	1.46E-09	6.37E-09	2.61E-09	7.44E-09	6.45E-09	1.06E-07	3.95E-10	5.17E-09
62946.27	8.81E-10	4.56E-09	2.99E-09	5.39E-09	3.92E-09	6.60E-08	2.41E-10	3.21E-09

Table 3: Integral LET spectra for aluminum shields of thickness ranging from 50 mils to 1600 mils of aluminum.

6-Sep-91

Integral LET Spectra for August 1990 - March 1991

CRRES Cosmic Ray Model

mg/cm2/micron	Shielding (mils Al)	50	100	200	400	800	1600
0.233	Sensitive region =	1	1	1	1	1	1
Threshold LET(MeV/mg/cm2)	Threshold LET (MeV/m/cm)	Flux (m2s sr)-1	Flux (m2s sr)-1	Flux(m2s sr)-1	Flux(m2s sr)-1	Flux(m2s sr)-1	Flux(m2s sr)-1
4.29E-02	1.00E-02	1.10E+01	2.21E+01	3.31E+01	4.40E+01	5.48E+01	6.52E+01
5.01E-02	1.17E-02	9.91E+00	1.98E+01	2.97E+01	3.95E+01	4.91E+01	5.84E+01
5.85E-02	1.36E-02	8.80E+00	1.76E+01	2.64E+01	3.51E+01	4.36E+01	5.18E+01
6.84E-02	1.59E-02	7.65E+00	1.53E+01	2.29E+01	3.04E+01	3.78E+01	4.49E+01
7.98E-02	1.86E-02	6.51E+00	1.30E+01	1.95E+01	2.59E+01	3.22E+01	3.82E+01
9.32E-02	2.17E-02	5.54E+00	1.11E+01	1.66E+01	2.20E+01	2.73E+01	3.24E+01
1.09E-01	2.54E-02	4.65E+00	9.29E+00	1.39E+01	1.85E+01	2.29E+01	2.71E+01
1.27E-01	2.96E-02	3.79E+00	7.57E+00	1.13E+01	1.50E+01	1.87E+01	2.21E+01
1.48E-01	3.46E-02	3.12E+00	6.24E+00	9.34E+00	1.24E+01	1.54E+01	1.82E+01
1.73E-01	4.04E-02	2.62E+00	5.24E+00	7.84E+00	1.04E+01	1.29E+01	1.52E+01
2.02E-01	4.72E-02	2.19E+00	4.38E+00	6.55E+00	8.69E+00	1.08E+01	1.27E+01
2.36E-01	5.51E-02	1.83E+00	3.66E+00	5.47E+00	7.26E+00	8.98E+00	1.06E+01
2.76E-01	6.43E-02	1.51E+00	3.02E+00	4.51E+00	5.98E+00	7.40E+00	8.72E+00
3.22E-01	7.51E-02	1.24E+00	2.47E+00	3.70E+00	4.90E+00	6.06E+00	7.13E+00
3.77E-01	8.77E-02	1.01E+00	2.02E+00	3.02E+00	4.01E+00	4.95E+00	5.82E+00
4.40E-01	1.02E-01	8.35E-01	1.67E+00	2.50E+00	3.31E+00	4.09E+00	4.80E+00
5.13E-01	1.20E-01	6.99E-01	1.40E+00	2.09E+00	2.77E+00	3.42E+00	4.01E+00
6.00E-01	1.40E-01	5.86E-01	1.17E+00	1.75E+00	2.32E+00	2.86E+00	3.35E+00
7.00E-01	1.63E-01	4.84E-01	9.67E-01	1.45E+00	1.91E+00	2.36E+00	2.76E+00
8.18E-01	1.91E-01	3.88E-01	7.76E-01	1.16E+00	1.53E+00	1.89E+00	2.20E+00
9.55E-01	2.23E-01	3.00E-01	6.00E-01	8.96E-01	1.18E+00	1.45E+00	1.69E+00
1.12E+00	2.60E-01	2.20E-01	4.40E-01	6.57E-01	8.68E-01	1.06E+00	1.24E+00
1.30E+00	3.03E-01	1.46E-01	2.92E-01	4.36E-01	5.75E-01	7.05E-01	8.17E-01
1.52E+00	3.54E-01	9.08E-02	1.82E-01	2.72E-01	3.59E-01	4.39E-01	5.09E-01
1.78E+00	4.14E-01	5.87E-02	1.18E-01	1.76E-01	2.33E-01	2.85E-01	3.30E-01
2.07E+00	4.83E-01	3.89E-02	7.81E-02	1.17E-02	1.55E-01	1.90E-01	2.20E-01
2.42E+00	5.64E-01	2.61E-02	5.26E-02	7.91E-02	1.05E-01	1.29E-01	1.49E-01
2.83E+00	6.59E-01	1.77E-02	3.57E-02	5.39E-02	7.16E-02	8.79E-02	1.02E-01
3.30E+00	7.70E-01	1.21E-02	2.45E-02	3.70E-02	4.93E-02	6.07E-02	7.03E-02
3.86E+00	8.99E-01	8.30E-03	1.69E-02	2.56E-02	3.42E-02	4.22E-02	4.89E-02
4.50E+00	1.05E+00	5.74E-03	1.17E-02	1.78E-02	2.39E-02	2.94E-02	3.42E-02
5.26E+00	1.23E+00	3.98E-03	8.16E-03	1.24E-02	1.67E-02	2.06E-02	2.39E-02
6.14E+00	1.43E+00	2.77E-03	5.69E-03	8.70E-03	1.17E-02	1.44E-02	1.67E-02
7.17E+00	1.67E+00	1.92E-03	3.96E-03	6.06E-03	8.13E-03	1.00E-02	1.17E-02
8.38E+00	1.95E+00	1.32E-03	2.73E-03	4.18E-03	5.61E-03	6.93E-03	8.04E-03
9.78E+00	2.28E+00	9.19E-04	1.90E-03	2.91E-03	3.90E-03	4.82E-03	5.59E-03
1.14E+01	2.66E+00	6.30E-04	1.30E-03	2.00E-03	2.68E-03	3.31E-03	3.84E-03
1.33E+01	3.11E+00	4.19E-04	8.66E-04	1.33E-03	1.78E-03	2.20E-03	2.54E-03
1.56E+01	3.63E+00	2.77E-04	5.72E-04	8.78E-04	1.18E-03	1.45E-03	1.68E-03
1.82E+01	4.24E+00	1.81E-04	3.75E-04	5.76E-04	7.72E-04	9.50E-04	1.10E-03
2.13E+01	4.95E+00	1.08E-04	2.24E-04	3.44E-04	4.61E-04	5.67E-04	6.54E-04
2.48E+01	5.78E+00	5.12E-05	1.06E-04	1.63E-04	2.18E-04	2.68E-04	3.09E-04
2.90E+01	6.75E+00	1.51E-06	3.11E-06	4.74E-06	6.30E-06	7.69E-06	8.80E-06
3.38E+01	7.89E+00	2.56E-07	5.22E-07	7.86E-07	1.03E-06	1.23E-06	1.37E-06
3.95E+01	9.21E+00	1.56E-07	3.19E-07	4.79E-07	6.25E-07	7.46E-07	8.33E-07
4.62E+01	1.08E+01	9.48E-07	1.94E-07	2.92E-07	3.81E-07	4.53E-07	5.05E-07
5.39E+01	1.26E+01	5.91E-08	1.21E-07	1.82E-07	2.38E-07	2.82E-07	3.15E-07
6.29E+01	1.47E+01	3.10E-08	6.37E-08	9.58E-08	1.25E-07	1.48E-07	1.64E-07
7.35E+01	1.71E+01	1.53E-08	3.15E-08	4.74E-08	6.15E-08	7.28E-08	8.07E-08
8.58E+01	2.00E+01	4.12E-09	8.48E-09	1.28E-08	1.66E-08	1.96E-08	2.17E-08

BIBLIOGRAPHY

- Adams, J. H., Jr., Silberberg, R. and Tsao, C. H., (1981), "Cosmic Ray Effects on Microelectronics (CREME), Part I: The Near-Earth Particle Environment," NRL Memorandum Report 4506, Naval Research Laboratory, Washington, DC.
- Adams, J. H., Jr., and Partridge, K., (1982), "Do Trapped Heavy Ions Cause Soft Upsets on Spacecraft?," NRL Memorandum Report 4846, Naval Research Laboratory, Washington, DC.
- Adams, J. H. Jr., Garcia-Munoz, M., Grigoriv, N. L., Klecker, B., Kondratyeva, M. A., Mason, G. M., McGuire, R. E., Mewaldt, R. A., Panasyuk, M. I., Tretyakova, Ch. A., Tylka, A. J. and Zhuravlev, D. A. (1991), "The Charge State of the Anomalous Component of Cosmic Rays," *Ap. J. Letters*, 375, L45.
- Binder, D., Smith, E. C., and Holman, A. B. (1975), "Satellite Anomalies from Galactic Cosmic Rays," *IEEE Trans. Nucl. Sci.*, NS-22, 2675.
- Binns, W. R., Fickle, R. K., Garrard, T. L., Israel, M. H., Klarmann, J., Stone, E. C. and Waddington, C. J. (1981), "Cosmic-ray Abundances of Elements with Atomic Number $26 \leq Z \leq 40$ Measured on HEAO 3," *Ap. J. Letters*, 247, L115.
- Breneman, H. H., and Stone, E. C. (1985), "Solar Coronal and Photospheric Abundances from Solar Energetic Particle Measurements," *Ap. J. Letters*, 299, L57.
- Cook, W. R., Stone, E. C. and Vogt, R. E. (1984), "Elemental Composition of Solar Energetic Particles," *Ap. J.*, 279, 827.
- Dietrich, W. F. and Simpson, J. A. (1978), "Preferential Enhancements of the Solar Flare-Accelerated Nuclei Carbon to Zinc from ~ 20 -300 MeV/nucleon," *Ap. J. Letters*, 225, L41.
- Durgaprasad, N., Mitra, B., Singh, R. K., Biswas, S., Dutta, A. and Goswami, J. N. (1990), "Spacelab-3 Observations of Enhanced Sub-iron (Sc-Cr) to Iron Abundance Ratios in the Low Energy (30-100 MeV/n) Galactic Cosmic Rays," in 21st ICR Conference Papers, ed. R. J. Protheroe, (Australia, 1990, University of Adelaide), Vol. 3, p. 389.
- Engelmann, J. J., Ferrando, P., Soutoul, A., Goret, P., Juliusson, E., Koch-Miramond, L., Lund, N., Masse, P., Peters, B., Petrou, N. and Rasmusen, I. L. (1990), "Charge Composition and Energy Spectra of Cosmic-Ray Nuclei for Elements from Be to Ni. Results from HEAO-3-C2," *Astron. and Astrophys.*, 233, 96.

- Evenson, P., Garcia-Munoz, M., Meyer, P., Pyle, K. R. and Simpson, J. A. (1983), "A Quantitative Test of Solar Modulation Theory: The Proton, Helium, and Electron Spectra from 1965 through 1979," *Ap. J. Letters*, 275, L15.
- Ferrando, P., Lal, N., McDonald, F. B. and Webber, W. R. (1991), "Studies of Low-Energy Galactic Cosmic-Ray Composition at 22 AU: I. Secondary/Primary Ratios," *Astronomy and Astrophysics*, 247, 163.
- Fichtel, C. E. and Reames, D. V. (1968), "Cosmic-ray Propagation," *Phys. Rev.*, 175, 1564
- Fisk, L. A. (1979), "The Interactions of Energetic Particles With the Solar Wind," in *Solar System Plasma Physics*, Vol. 1, ed. E. N. Parker, C. F. Kennel, and L. J. Lanzerotti (Amsterdam: North Holland), p. 179.
- Freier, P. S. and Webber, W. R. (1963), "Exponential Rigidity Spectrum for Solar-Flare Cosmic Rays," *JGR*, 68, 1605.
- Garcia-Munoz, M., Mason, G. M., Simpson, J. A. and Wefel, J. P. (1977), "Charge and Energy Spectra of Heavy Cosmic Rays at Intermediate Energies," in *15th ICR Conference Papers*, (Plovdiv, Bulgaria; Bulgaria Academy of Sciences), Vol.1, p. 230.
- Garcia-Munoz, M., Margolis, S. H., Simpson, J. A. and Wefel, J. P. (1979), "The Energy Dependence of the Ratios of Secondary to Primary Elements in the Cosmic Radiation," in *16th ICR Conference Papers*, (Kyoto, Japan; Physical Society of Japan), Vol.1, p. 310.
- Garcia-Munoz, M., Meyer, P., Pyle, K. R., Simpson, J. A., and Evenson, P. A. (1986), "The Dependence of Solar Modulation on the Sign of the Cosmic Ray Particle Charge," *J. Geophys. Res.*, 91, 2858.
- Garcia-Munoz, M., Simpson, J. A., Guzik, T. G., Wefel, J. P. and Margolis, S. H. (1987), "Cosmic-Ray Propagation in the Galaxy and in the Heliosphere: The Pathlength Distribution at Low Energy," *Ap. J. Suppl.*, 64, 269.
- Gleeson, L. J. and Axford, W. I. (1968), "Solar Modulation of Galactic Cosmic Rays," *Ap. J.*, 154, 1011.
- Guzik, T. G. (1988), "The SEP Matter Sample and its Correlation with Gamma-ray Observations," *Solar Physics*, 118, 185.
- Guzik, T. G. (1990), "Current and Future Uses of Accelerators in Particle Astrophysics," in *Particle Astrophysics: The NASA Cosmic Ray Program for the 1990's and Beyond*, eds. W. V. Jones, F. J. Kerr, J. F. Ormes, (AIP Conference Proceedings 203: American Institute of Physics, New York, NY), p. 275.

- Iverson, W. R. (1979), "Do Cosmic Rays Spell Death for VLSI?," *Electronics* (November), p. 44.
- Jokipii, J. R. (1971), "Propagation of Cosmic Rays in the Solar Wind," *Rev. Geophys. Space Phys.*, 9, 27.
- Kolasinski, W. A., Blake, J. B., Anthony, J. K., Price, W. E. and Smith, E. C. (1979), "Simulation of Cosmic-ray Induced Soft Errors and Latchup in Integrated-Circuit Computer Memories," *IEEE Trans. Nucl. Sci.*, NS-26, p. 5087.
- Lamport, J. E., Mason, G. M., Perkins, M. A. and Tuzzolino, A. J. (1976), "A Large Area Circular Position Sensitive Si Detector," *Nucl. Instr. and Methods*, 134, 71.
- Lezniak, J. A. and Webber, W. R. (1978), "The Charge Composition and Energy Spectra of Cosmic-ray Nuclei from 3000 MeV per Nucleon to 50 GeV per Nucleon," *Ap. J.*, 223, 676.
- Maehl, R. C., Ormes, J. F., Fisher, A. J. and Hagen, F. A. (1977), "Energy Spectra of Cosmic Ray Nuclei: $4 \leq Z \leq 26$ and $0.3 \leq E \leq 2 \text{ GeV amu}^{-1}$," *Astrophysics and Space Sci.*, 47, 163.
- Mason, G. M., Reames, D. V., Klecker, B., Hovestadt, D. and von Rosenvinge, T. T. (1986), "The Heavy-Ion Compositional Signature in ^3He -rich Solar Particle Events," *Ap. J.*, 303, 849.
- McDonald, F. B., Teegarden, B. J., Trainor, J. H. and Webber, W. R. (1974), "The Anomalous Abundance of Cosmic-ray Nitrogen and Oxygen Nuclei at Low Energies," *Ap. J. Letters*, 187, L105.
- McKibben, R. B. (1986), "Modulation of Galactic Cosmic Rays in the Heliosphere," in The Sun and the Heliosphere in Three dimensions, ed. R. G. Marsden, (Dordrecht, The Netherlands; D. Reidel Publ. Co.), p. 361.
- McGuire, R. E., von Rosenvinge, T. T. and Reames, D. V. (1985), "Variations in Elemental Composition of Several MeV/nucleon Ions Observed in Interplanetary Space," in 19th ICR Conference Papers, (LaJolla, CA; NASA), Vol. 4, p. 225.
- McGuire, R. E. and von Rosenvinge, T. T. (1984), "The Energy Spectra of Solar Energetic Particles," *Adv. in Space Res.*, 4, 117.
- Mewaldt, R. A., Spalding, J. D. and Stone, E. C. (1984), "A High-Resolution Study of the Isotopes of Solar Flare Nuclei," *Ap. J.*, 280, 892.

- Meyer, J. P. (1985a), "The Baseline Composition of Solar Energetic Particles," Ap. J. Supplement, 57, 151.
- Meyer, J. P. (1985b), "Solar-Stellar Outer Atmospheres and Energetic Particles and Galactic Cosmic Rays," Ap. J. Supplement, 57, 173.
- Orth, C. D., Buffington, A., Smoot, G. F. and Mast, T. S. (1978), "Abundances and Spectra for Cosmic-ray Nuclei from Lithium to Iron for 2 to 150 GeV per Nucleon," Ap. J., 226, 1147.
- Oschlies, K., Beaujean, R. and Enge, W. (1989), "On the Charge State of Anomalous Oxygen," Ap. J., 345, 776.
- Parker, E. N. (1965), "The Passage of Energetic Charged Particles Through Interplanetary Space," Planet. Space Sci., 13, 9.
- Seo, E. S., Ormes, J. F., Streitmatter, R. E., Stochaj, S. J., Jones, W. V., Stephens, S. A. and Bowen, T. (1991), "Measurement of Cosmic-ray Proton and Helium Spectra During the 1987 Solar Minimum," Ap. J., 378, 763.
- Silberberg, R. and Tsao, C. H., (1990), "Spallation Processes and Nuclear Interaction Products of Cosmic Rays," Phys. Reports, 191, (b), 351.
- Simpson, J. A. (1983), "Elemental and Isotopic Composition of the Galactic Cosmic Rays," in Ann. Rev. Nucl. Part. Sci., Vol. 33, p. 323.
- Simpson, J. A., Munoz, M. G., Perkins, M. and Wefel, J. P. (1985), "The Experiment for High Energy, Heavy Nuclei Composition (ONR-604)," in CRRES/SPACERAD Experiment Descriptions, eds. M. S. Gussenhoven, E. G. Mullen and R. C. Sagalyn, Air Force Geophysics Laboratory Report AFGL-TR-85-0017 (Hanscom AFB, MA, ADA160504) p. 163.
- Urch, I. H. and Gleeson, L. J. (1972), "Galactic Cosmic Ray Modulation from 1965-1970," Astrophys. Space Sci., 17, 426.
- Webber, W. R., Kish, J. C. and Schrier, D. A. (1990), "Formula for Calculating Partial Cross Sections for Nuclear Reactions of Nuclei with $E \geq 200$ MeV/nucleon in Hydrogen Targets," Phys. Rev. C, 41, 566.